12

Power Transformers

12.1 Introduction

Power transformers have been introduced since the early days of power transmission. Its development combined with the development of circuit interrupting devices, interrupters, and circuit breakers has contributed to the establishment of ac power transmission as the principal mode of transmitting electric power over long distances as well as distributing it to the consumer. However, while the demand for higher interrupting capacity and the high risk of fire hazards have favored the diversification of circuit interrupting devices from bulk oil breakers into new technologies using nonflammable air and SF_6 as the arc quenching medium, the basic design of power transformers did not change significantly during the last hundred years while progressing to meet the ever-increasing needs of modern power transmission system. It reached the voltage level of 735 kV in the 1960s and then crossed the 1000 kV level in the 1990s. Its power rating has progressed from an initial few kVA to reach several hundreds of MVA in today's transformer units. Such a performance of power transformers is the result of the continuous improvement in material application and technology.

Power transformers are built around a magnetic core, which confines the magnetic flux and provides an effective means of transferring the electric energy from one winding to the other. The windings operating at different voltages are built closely around the magnetic circuit, on an insulating structure, usually pressboard cylinders, to minimize straying magnetic field and assure maximum efficiency in energy transfer. The whole assembly is located within a metallic tank, which provides a contained insulating environment to the transformer assembly with accesses to the external circuit via bushings connecting the winding ends to appropriate nodes of the external circuit.

Core: The vast majority of power transformers is of core-type design. A transformer core is assembled from laminations, 0.025–0.05 cm thick, containing approximately 3% silicon and 97% steel. One of the greatest contributions to transformer efficiency and low cost was the introduction of grain-oriented iron in the 1940s. Its higher permittivity and lower cost increased the working flux density by approximately 30%. The silicon content reduces the viscous resistance to magnetization or hysteresis and prevents increased loss with age. Most lamination materials are cold rolled and specially annealed to orient the grains, or iron crystals, to obtain very high permeability and low hysteresis to flux in the direction of rolling. Most lamination materials are treated in one or several ways to develop a chemical coating to insulate the laminations from each other. The core construction may be built up from separated laminations, with layers of lamination placed so that the gap between lamination ends of one layer is overlapped by the lamination in the next layer. It may also be wound from a long continuous strip so that the flux will always flow along the grain of the strip. The resulting cylindrical core does not lend itself to the winding of the coils on the transformer core, especially for large HV coils, which are easier to wound separately from the core (Bean et al., 1959).

Windings: Are the other elements of power transformers. They allow the transfer of energy from one winding to the other according to their turn ratio, which regulates the output voltage and current:

$$\frac{U_s}{U_p} = \frac{N_s}{N_p} = \frac{I_p}{I_s}$$

where N_s and N_p are the number of turns in the secondary and primary windings, respectively.

Windings are wound from insulated conductors to form either cylindrical or layer coils or continuous-wound or interleaved disc-type coils. The selection of a specific coil arrangement is a matter of finding the optimal arrangement with respect to

- Adequate dielectric strength against the various types of stresses subjected to power transformers: operating ac voltage, switching and lightning impulses, and fault and test conditions
- Adequate coil ventilation
- Adequate mechanical strength
- Minimum cost

The construction of the windings must permit bringing out properly insulated leads and taps. It must further allow multiwinding arrangements and practical schemes to minimize eddy current losses, for example, transposition of subdivided conductors (Bean et al., 1959). Figure 12.1 illustrates the arrangement of windings of an HV transformer: the low-voltage winding is next to the core, inside the HV winding. Insulating barriers are located in the interwinding space to improve the field distribution and hence the dielectric performance of the insulation in the region around the HV end of the coils. Figure 12.1 also shows a typical potential distribution around the insulation of a power transformer (Okubo et al., 1987).

Transformer insulation: Is the single factor, which accounts for the development of power transformers into higher voltages, up to the 1000 kV level at present. This is attributed to the excellent ability of oil–paper insulation to meet the specific requirements of power transformers: to have an excellent dielectric performance and heat transfer properties. In the oil–paper insulation system, the main component is the mineral oil, which serves as the insulating material and at the same time as a cooling fluid. The cellulose paper, principally in the form of pressboard, made of paper, upgraded Kraft papers and polymer-based paper (Nomex), is required to provide a mechanical support to the windings and to allow adequate oil circulation for removal of the heat generated from the windings to low-temperature regions within the transformer.
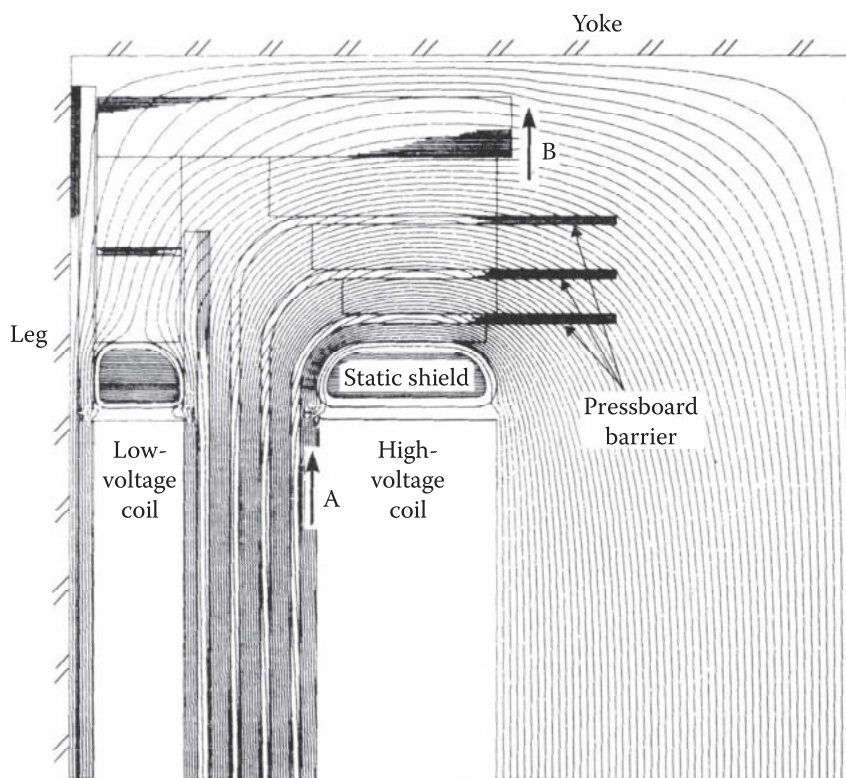

FIGURE 12.1   Field distribution in a typical transformer insulation. (From Okubo, H. et al., *IEEE Trans. Power Deliv.*, PWRD-2(1), 126, January 1987.)

For large power apparatus, the risk of fire hazards inherent to mineral oil is of most concern. The efforts to improve the insulation performances aim primarily at insulating fluids with low flammability: aliphatic hydrocarbons, silicon oils, the perfluorocarbons, and esters (Bartnikas and Srivastava, 1980). Upgraded Kraft papers and polymer-based paper (Nomex), with better thermal properties, are introduced in the insulation of power transformer to allow a higher operating temperature. Their utilization prevents solid particle contamination from bridging the oil gap. The dielectric stresses of power transformers remain relatively low, 2–5 kV/mm (Wilson, 1980; Rouse, 1987). This is explained by the fact that the ac dielectric performance of the oil–paper insulation is determined principally by the insulating fluid, and the different fluids have dielectric strength comparable to that of mineral oil. The presence of large volumes of oil combined with the distribution of the electric field (nonuniform and variable from one place to the other within the apparatus) and the unavoidable presence of particle contamination in the oil require an adequate operating margin and, hence, relatively low operating stresses. To improve the withstand characteristics and counter the effect of protrusions at the conductor surface, the winding conductors are varnished (for low-voltage windings) or taped with paper. The HV connections are also wrapped with paper tape; the thickness of the paper tape layer varies with the local stress.

Impregnation and preservation: Following the assembly of the transformer core and windings within the containing tank, the latter is cleaned and the paper vacuum dried before being filled with insulating oil for impregnation of the dry paper. Vacuum filling of the oil ensures that no gas pockets remain within the transformer tank. Drying the paper to remove the moisture is a delicate process, since water is also produced by the decomposition of paper and overdrying the paper will decompose it. In transformer, however, it is not necessary to carry the drying process near to the danger limit of 0.1% apparent moisture (Norris, 1963). The impregnation process is basically simple: it occurs naturally in time by simple immersion. However, to accelerate the process, heat, vacuum, and pressure are employed in industrial impregnation processes (Norris, 1963). To account for the expansion of the oil during load cycles, a conservator is added to the tank, usually located above the latter, and the oil is topped up within the conservator, thus keeping the whole insulation immersed within the insulating oil.

The dominant weakness of oil-impregnated paper insulation is its being easily contaminated, by solid particles, fibers, carbons, sand, etc., and, particularly, moisture. This emphasizes the need for preservation of the original state of the insulation throughout its service life if its initial strength is to be maintained. Since solid particles are most likely introduced during the manufacturing of the transformer, the preservation of the insulation simplifies to that of preventing moisture from entering the oil-impregnated paper via the oil. The current method using a conservator vessel with dehydrating breather plus an oil seal between the breather and the atmosphere has proved its efficiency and has been the standard practice for large HV transformers.

Hermetic sealing of the transformer tank with flexible metallic bellow or plastic diaphragm to take care of the oil expansion offers the possibility of preventing moisture from entering the impregnated paper insulation and further improving the dielectric performance of the oil-impregnated paper insulation by using degassed oil. Various methods of semisealing, often with nitrogen to eliminate possible oxidation effect as well as moisture, have been suggested. However, the question is far from settled since such an effective seal will also trap gas and moisture coming from the aging of impregnated paper insulation within the transformer and further accelerates the aging process.

SF_6 insulation: The introduction of SF_6 insulation in power apparatus also triggered the development of SF_6-insulated transformers as a solution to the fire hazard. However, while the gas insulation can handle the relatively moderate insulating stresses of power transformers, the problem remains regarding an efficient and economical solution to the removal of their heat losses. At present, their development is limited to units of moderate power ratings, 275 kV and 300 MVA, for use in urban areas where the land cost is high and severe control regarding the environmental impact of substations (Tokoro et al., 1982; Mukaiyama et al., 1991).

Design considerations: Design of power transformers obviously remains the property of manufacturers; we review in the following the main design aspects of interest to utility engineers, in particular the basic parameters that determine the size of power transformers.

The basic relationship between the flux in the core and the winding voltage is

$$u(t) = N \frac{d f}{dt} \tag{12.1}$$

where

$u(t)$ is the voltage developing across the winding
N is the number of turns
S is the core section
ϕ is the magnetic flux within the core

Under ac voltage, the earlier relation becomes

$$u(t) = U \sin wt = N \frac{d f}{dt} \tag{12.2}$$

where

U is the magnitude of the ac voltage
$\omega = 2\pi f$ the angular frequency

Integrating Equation 12.2 yields

$$f(t) = \frac{U}{wN} \cos wt = f_{max} \cos wt \tag{12.3}$$

Equation 12.3 determines the maximum flux in the core for a given maximum voltage U across the winding. On the other hand, the maximum flux density in low-loss iron core is selected to provide a margin below the saturation density of the iron to limit the exciting current under event of TOVs. This allows the determination of the core cross section as a function of N, the number of turns. The kVA rating of the transformer fixes the nominal current I that, together with the number of turns N, determines the cost of copper for the winding. Some optimization is then possible to reach a design value for the core cross section and its cost, the number of turns N, and the copper cross section and its cost.

The voltage at the HV winding is the main parameter for the dimensioning of the transformer insulation: turn-to-turn and layer-to-layer insulation, insulation between windings, and between winding and the transformer tank. These aspects will be discussed further in the chapter.

In addition to the earlier two fundamental aspects, transformer design must take into account the following:

- The removal of heat generated in the windings. This is a two-stage process, where the generated heat is first transferred to the oil volume and, subsequently, to the heat exchanger to evacuate the generated heat into an ambient environment. In cylindrical wound coils, vertical spacers are placed around the insulating cylinder, over which the winding is wound, to form ducts for oil circulation between the cylinder and the inside of the coil. Spacers and washers are used in disc-type coils to separate the sections. Insulating spacers are also placed at the ends of the coil for mechanical support.

  In natural oil natural air (ONAN) transformers, the generated heat is transferred to the oil via the thermosiphon effect: the expansion of the oil volume in the region of high temperature initiates the oil circulation, which is sustained by the temperature difference between the hot winding and the cooler surrounding oil. When the heat removal efficiency exceeds 0.14 W/cm² (0.9 W/in.²) (Bean et al., 1959), the surface temperature drop through the insulation may exceed 20°C, reducing the heat transfer efficiency due to the usual 55°C allowance for temperature rise in power transformers. Forced oil flow may be necessary. The heat transfer from the oil to the surrounding ambient is made via the transformer tank. For small transformers, this is sufficient; in large transformer units, the oil is circulated through radiators that are adequately dimensioned.
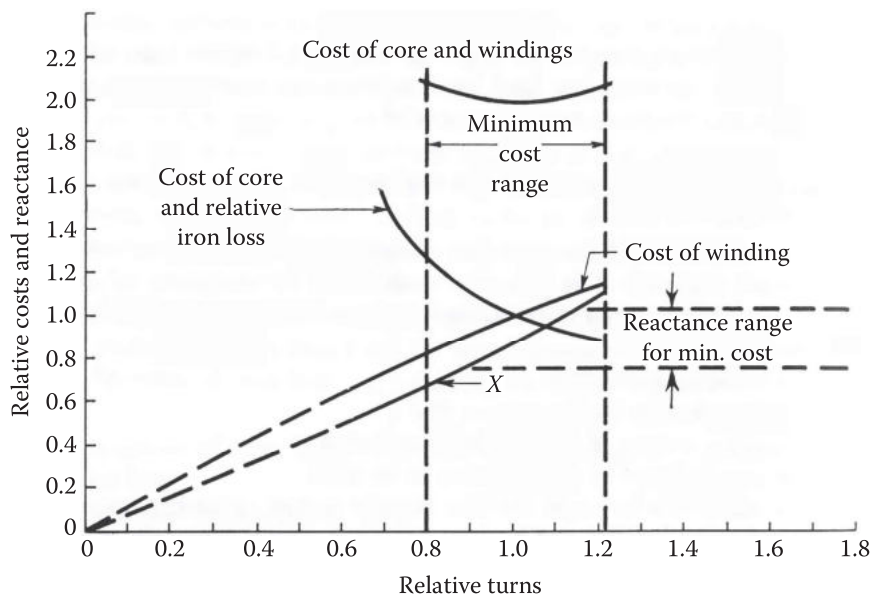
FIGURE 12.2 Cost-effective approach to power transformer design. (From Bean, R.L. et al., *Transformers for the Electric Power Industry*, McGraw-Hill Book Co., New York, 1959.)

- The mechanical stresses are related to load and short-circuit currents. Cylindrical coils are subjected mainly to radial forces. Axial forces can, however, develop as a result of imperfect coil alignment or by the presence of taps. Disc-type coils are subjected to axial forces. To counter these mechanical forces, collars are used to support the end turns, and the end of the windings is rigidly held in place by properly anchoring the leads.

Both these aspects, which involve specific manufacturer's experiences, are out of the scope for the present book. The readers can find a comprehensive discussion on the subject in the reference (Bean et al., 1959). Because of the large number of parameters involved, manufacturers usually take a cost-effective approach to design power transformers, where their in-house experience plays a significant role. Figure 12.2 illustrates such a cost-effective design approach, where the variations of the relative cost associated with various design parameters are presented in terms of the relative number of turns in the winding. It is shown that the winding cost goes up with the number of turns while the cost of the core decreases. A range of minimum cost of core and windings can be defined, from which the final design parameters are optimized.

This chapter reviews the main insulating properties of transformer insulation, practical approaches to its dimensioning, improvements to the insulating materials, the control of humidity and particle contamination, and the environmental impact, mainly generation of AN, of power transformers.

12.2 Transformer Insulation

12.2.1 Operating Stresses

Evolution of operating stresses in electric equipment follows closely improvements in the insulation system. A better dielectric performance improves the characteristics of related equipment, in voltage and power ratings, while enhancing their reliability and reducing the physical dimensions and sometimes their cost. Considerable improvements have been achieved since the introduction at the beginning of the twentieth century of oil–paper insulation, namely, with the development in material technology, which provides better basic components, polymer film and paper base, and impregnating fluid.

However, because of the specific needs and different operating conditions, the operating stresses vary considerably with each type of equipment. Generally speaking, the less severe stresses are found in large power apparatus, transformers, and shunt reactors. The most severe stresses are found in the small components,

TABLE 12.1

Typical Operating Stresses for Oil–Paper Insulation in Power Transformers

	Symbol	Notes	Units	Values
Dielectric stresses				
Nominal stress[a]	En	AC	kV_{rms}/mm	1–3
Maximal stress[b]	Em			2–5
Test stress[c]		AC		3–6
Lightning impulse			kV/mm	
Switching impulse				
Breakdown field[d]		AC	kV_{rms}/mm	30–40
Lightning impulse			kV/mm	80
Thermal constraints				
Operating temperature			C	85
Overloading temperature			C	95
Temperature rise			C	65
Hot spot temperature			C	100
Environmental stresses				
Minimal ambient temperature			C	−50
Maximal ambient temperature			C	40

[a] Stresses under normal operating conditions.
[b] Stresses under maximal operating conditions, typically 1.5–2 times the in-service stresses.
[c] Stresses defined by test conditions, typically 2 times the maximal stresses.
[d] Limit withstand of the insulation, established from laboratory tests on samples, models, or prototype.

condensers, where the need of storing large amounts of energy in the smallest volume possible contributes to favor a uniform field configuration operating at high stresses. Table 12.1 summarizes the typical operating stresses for power transformers. Withstand levels for lightning impulse, switching impulse and power frequency as a function of highest operating voltage are given in IEC Standard (IEC 600-71-1, 1993).

12.2.2 Oil–Paper Insulation in Power Transformers

The oil-impregnated paper insulation used in power transformers has a dielectric strength much higher than that of the oil and paper taken separately. However, it is sensitive to absorption of moisture and gases. As a result, adequate operation of power transformers depends on both its design and on the preservation of the initial state of the insulation. These aspects will be discussed in the following.

12.2.2.1 Winding Arrangement

As already mentioned, power transformers use one of the two types of winding: the cylindrical coil and the interleaved disc-type coil.

The cylindrical wound coil consists of one or more concentric layers of insulated conductors, wound on insulating cylinders. Each layer has several turns adjacent to each other. Generally, the coils have an even number of layers, so that both start and finish lead can be brought out at the same end of the coil. Figure 12.3 illustrates such an arrangement of a four-layer HV winding, with one end solidly grounded. The insulation to ground gradually increases from the layer next to the low-voltage coil out to the last layer connected to the HV line in step of approximately *U/m*, where *U* is the ac winding voltage and *m* the number of layers in the coil, and can be graded accordingly. The cylindrical wound coil suffers from the poor impulse voltage distribution between turns in the last layer connected to the HV line, due to the high ground capacitance and the low series capacitance between turns.

In the continuous-wound disc coil illustrated in Figure 12.4, the turns are wound in sections or discs, with the first (start) turn on the insulating cylinder and the subsequent turns wound over it to form a disc
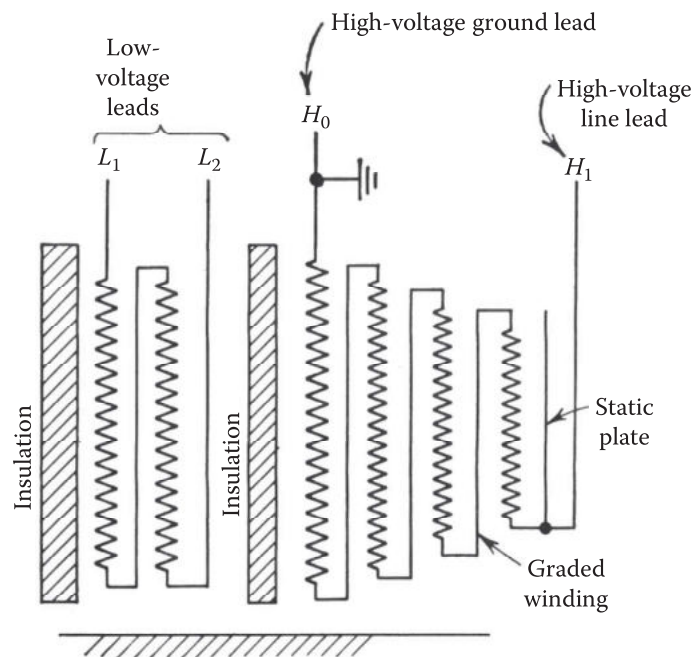
FIGURE 12.3 Arrangement of a four-layer winding. (From Bean, R.L. et al., *Transformers for the Electric Power Industry*, McGraw-Hill Book Co., New York, 1959.)
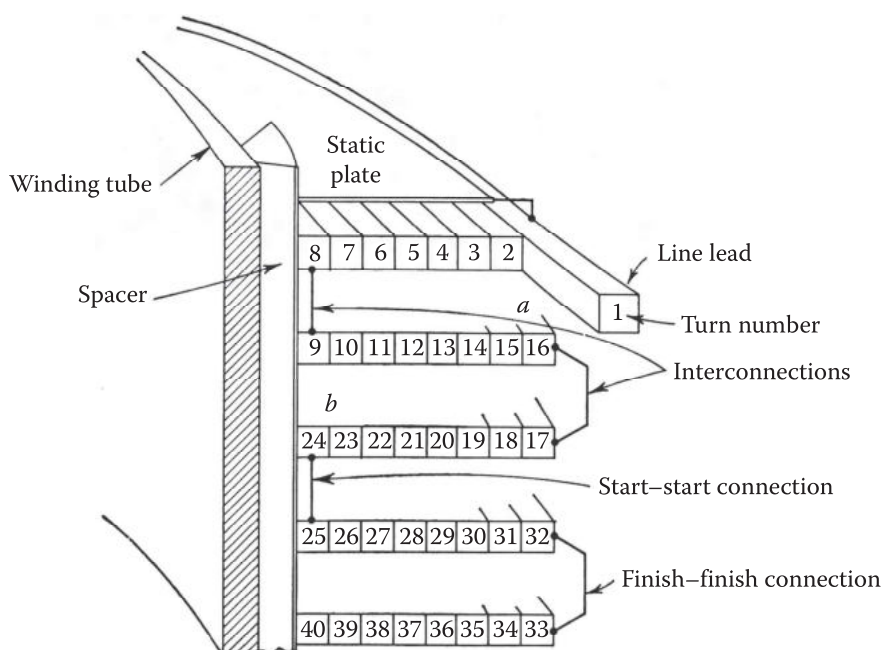

FIGURE 12.4 Illustration of a disc-type coil. (From Bean, R.L. et al., *Transformers for the Electric Power Industry*, McGraw-Hill Book Co., New York, 1959.)

section, whose thickness is equal to the turn width. The connection between adjacent discs is illustrated in Figure 12.4. The ac voltage distribution is graded among the series-connected disc sections, which are subjected to a stress of 2 *U/m*, where *m* is the number of disc sections. Figure 12.5 illustrates a winding arrangement of disc sections with the ends at ground potential and the center at the line potential.

12.2.2.2 Transformer Insulation Characteristics

It is obvious from the earlier discussion that transformer insulation is complex and cannot be described as a single uniform system. At best, one can subdivide the transformer insulation into a few subsystems,
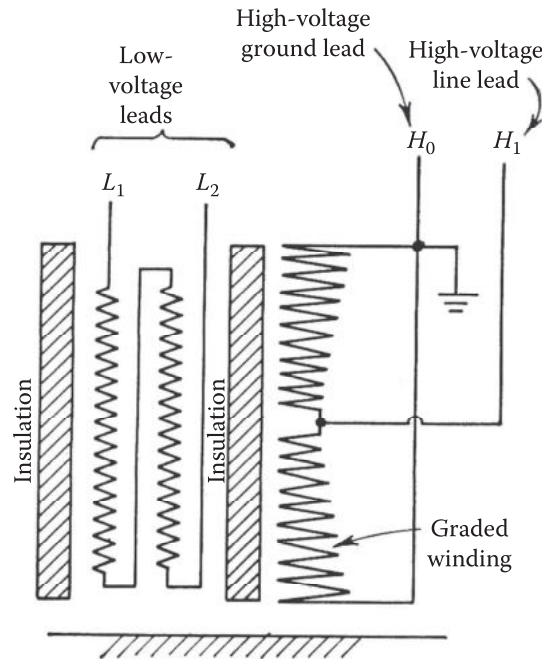
FIGURE 12.5 Arrangement of a disc–type coil winding. (From Bean, R.L. et al., *Transformers for the Electric Power Industry*, McGraw-Hill Book Co., New York, 1959.)

related to the individual windings, the interwinding insulation, the winding-to-ground insulation, and the insulation of the bushing and HV leads.

Insulation of the individual winding: Is essentially assured by the insulation of the conductor, filling most of the space between two adjacent conductors. Since the voltage is distributed over the whole length of the winding, the ac stress seen by the turn-to-turn gap is approximately U/N, where U is the voltage across the winding and N the number of turns. When the winding is made up of several layers or separate sections, the adjacent layers or sections are subjected to an ac stress of U/m or $2U/m$, where m is the number of layers or sections, depending on how the layers or sections are connected. Usually, there is no difficulty to design appropriate insulation for the ac stresses.

The problem is different under impulse voltage stresses, due to the unequal voltage distribution along the winding. Figure 12.6 illustrates the circuit representation of a winding, taking into account the capacitances to ground and series capacitances between turns. During impulse voltage, the voltage distribution is dictated mainly by the capacitances, resulting in a generally nonuniform distribution, with a large proportion of the impulse stress applied to the line end turns of the winding, as shown in Figure 12.6b. This has been identified as a cause for failure of power transformers under switching and lightning impulse conditions (Freyhult and Carlson, 1991).

Several possibilities exist to improve the transient voltage distribution along the winding. They generally aim at increasing the ratio of distributed series capacitance to ground capacitance, namely, by the use of disc windings, which have a naturally high ratio of series-to-ground capacitances. This practice is usually followed in EHV power transformers (Freyhult and Carlson, 1991).

The series capacitances between turns can be increased by the addition of an electrostatic shield to the line end winding, as illustrated in Figure 12.7. It can be further improved by the Hisercap design illustrated in Figure 12.8 (Grimmer and Teague, 1951): the disc-type coil is wound as a double conductor, with the second set of turns connected back in series with the first. The capacitance between the two sets of turns is increased many times the normal turn–turn capacitance. However, this design subjects the insulation of the coil conductor to half of the coil voltage.

Interwinding insulation: The space between the low- and HV windings is basically an oil space. The presence of large sheets of pressboard, subjected to the full potential difference across the windings, tends to favor the development of creep discharge over its surface, a recognized mode of failure of power transformer insulation. The phenomenon may also be enhanced by the gradual accumulation of carbon
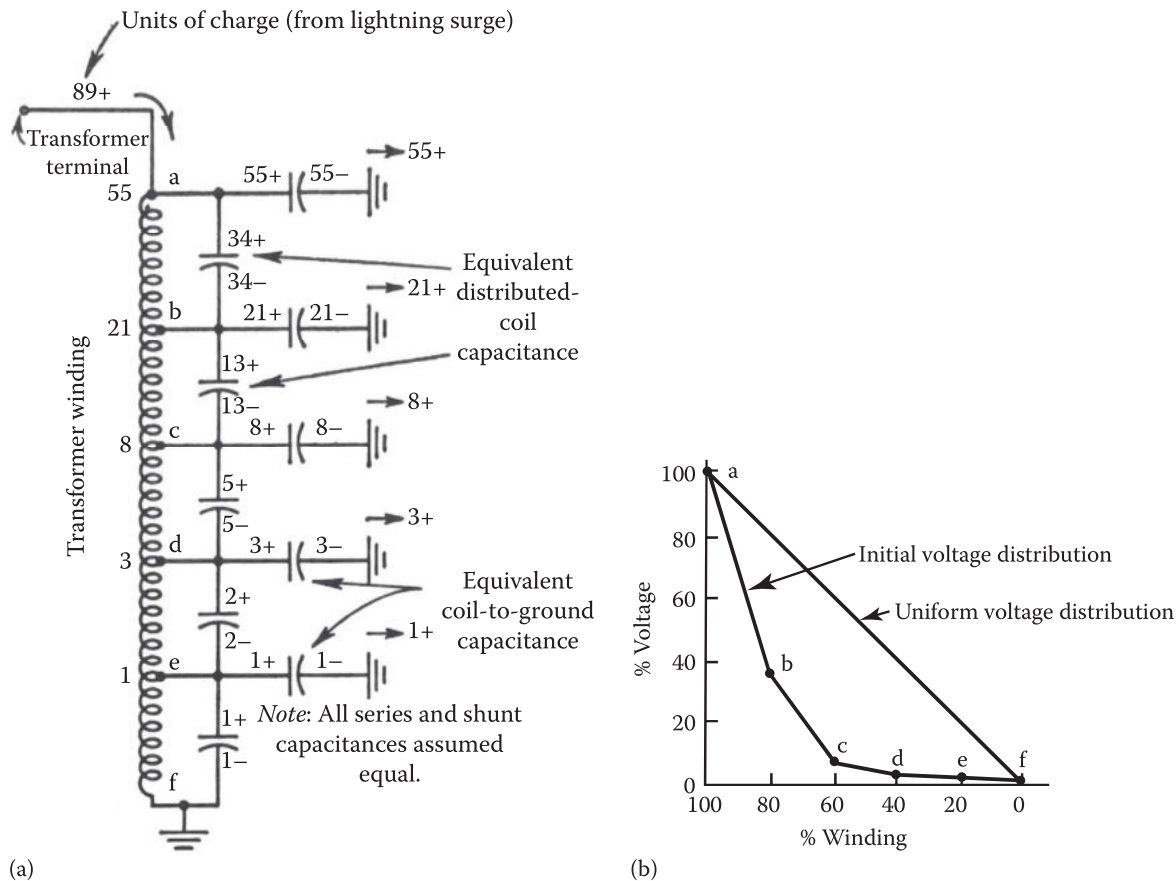
FIGURE 12.6 Circuit representation of a winding and its initial voltage distribution under impulse voltage. (a) Equivalent winding capacitance distribution. (b) Initial and steady state voltage distributions. (From Bean, R.L. et al., *Transformers for the Electric Power Industry*, McGraw-Hill Book Co., New York, 1959.)

particles at the pressboard interface. The problem is dealt with by installing several pressboard barriers, which extend above the winding end and are shaped to improve the field distribution and prevent bridging of the oil space by solid particles and, hence, the dielectric performance of the interwinding gap.

Winding to earth: The space between winding and the ground tank is essentially oil-filled. This oil gap usually has a considerable stress volume, and their design aims at minimizing the stress volume and the actual stresses as much as possible. Large oil volume breakdown is affected by particle contamination, discussed in more detail in Chapter 6, which, however, is unavoidable, but can be minimized by adequate filtering of the oil during the commissioning of power transformers (Palmer and Sharpley, 1969) and follow-up in service.

Bushing: Is necessary to connect the transformer winding to the overhead lines. Generally, bushing forms a separate component of the transformer, with its own insulation system, typically of the same type as the equipment it is connected to. Detailed discussions of bushing are presented in Chapter 11. Connections of the HV leads to the bushing terminal often produce local field enhancement, which can be countered by the use of bushing shield electrode. The bushing shield to ground forms a simple oil gap, subjected to volume effect that is treated in the following.

12.2.2.3 Physical–Chemical Properties of Oil-Impregnated Paper

Oils: Have a petroleum base and are complex mixtures of aromatic, alkane, and cycloalkane hydrocarbons, containing hundreds and possibly thousands of individual compounds, although the exact number has never been reported. The typical Voltesso 35 oil contains 12.9% of aromatic, 42.9% of naphthalene, and 44.2% of paraffin. Oil shows a variety of molecular sizes and structures. Its molecular weight is an average value of the molecular weight distribution. Aromatics tend to increase the dielectric losses of the oils, but their presence is necessary to inhibit gas evolution in the oil under electrical stress.
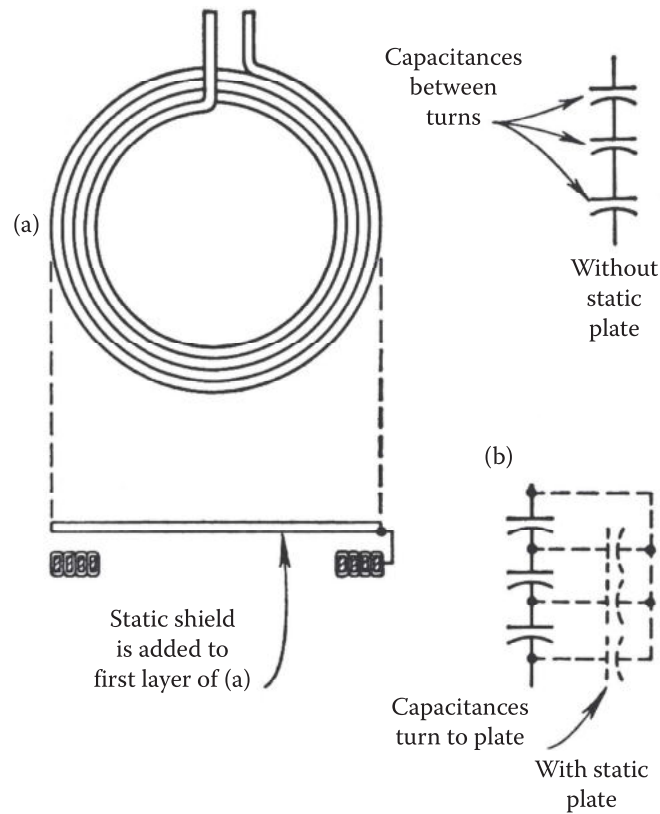
FIGURE 12.7 Improvement of the series capacitance between turns by an electrostatic shield. (a) Schematic diagram of added static shield. (b) Equivalent capacitive circuit. (From Bean, R.L. et al., *Transformers for the Electric Power Industry*, McGraw-Hill Book Co., New York, 1959.)
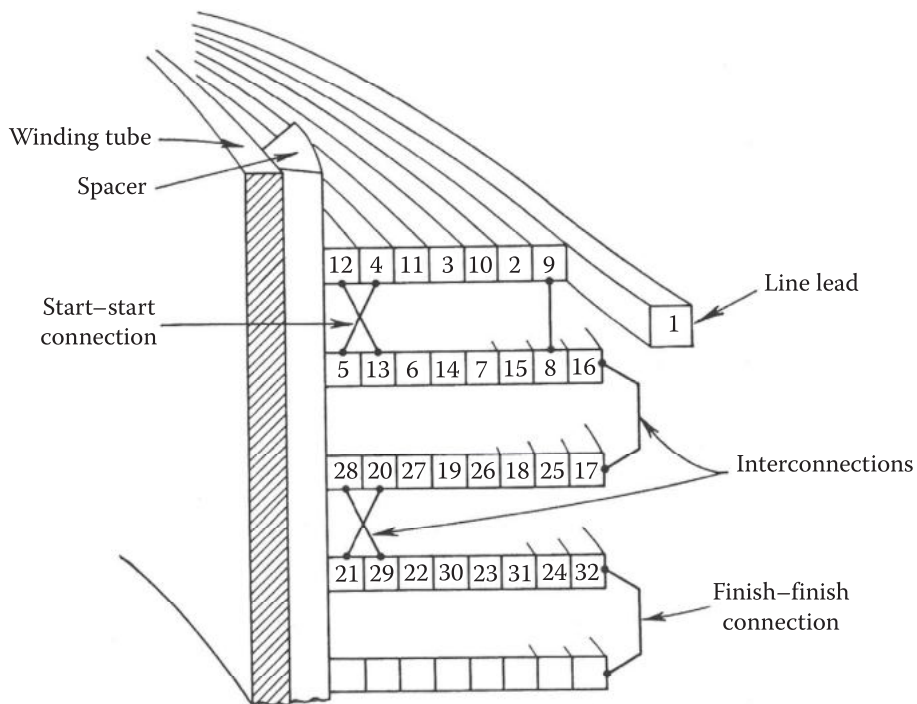

FIGURE 12.8 Illustration of Hisercap coil. (From Bean, R.L. et al., *Transformers for the Electric Power Industry*, McGraw-Hill Book Co., New York, 1959.)

Other additives are also used to delay oxidation. The dielectric losses in new purified oils are very low and attributed to the small permanent dipole moment or the polarity of the aromatic molecules.

Table 12.2 summarizes some of the properties of new transformer oils (Shroff and Stannett, 1985). Their viscosity can vary from 10 to 2500 cSt over the temperature range from 40°C to −40°C. The adequacy of the oil for service is determined by the extent to which it forms sludge and corrosive acidity compounds in the presence of oxygen. To reduce corrosiveness, oils should be free from sulfur, inorganic chlorides, and sulfates, usually introduced by direct contamination or inadequate refining.

Paper: Kraft papers consist of cellulose fibers felted together to form mechanically strong sheets. When properly dried and impregnated with dielectric liquids, they have good dielectric strength, have acceptable loss characteristics, and are suitable for use in the electrical insulation of power equipment. Table 12.3 summarizes some of the properties of Kraft paper. The porosity determines the ease

TABLE 12.2

Properties of Oil Used in Power Transformers

Parameters	Symbol	Unity	Value	Condition
Aromatic content		%	12.8	
AC dielectric strength		kV/mm	30	
Impulse dielectric strength		kV/mm	166–192	
Dielectric constant	ε_r		2.2–2.3	100°C
Dissipation factor	$\tan\delta$	%	0.05	25°C
			0.5	100°C
Density		g/mL	0.906	15°C
AC design electric field		kV/mm	3–5	
Interfacial tension		N-m	40.8×10^{-3}	
Neutralization number			0.01	
Design temperature		C	95–100	
Water content in oil		ppm	10	
Cloud point		C	−36	
Pour point		C	−46	
Flash point		C	150–160	
Fire point		C	177–180	
Viscosity		mm²/s	10	40°C
			85	0°C
			6000–2500	−40°C
Coefficient of thermal expansion		cm³/cm³/C	$7–8 \times 10^{-4}$	
Gassing		μL/min	13	
Acidity index		mg KOH/g	0.03	
Thermal conductivity		cal./cm·s·C	$3–4 \times 10^{-4}$	

TABLE 12.3

Properties of Kraft Paper

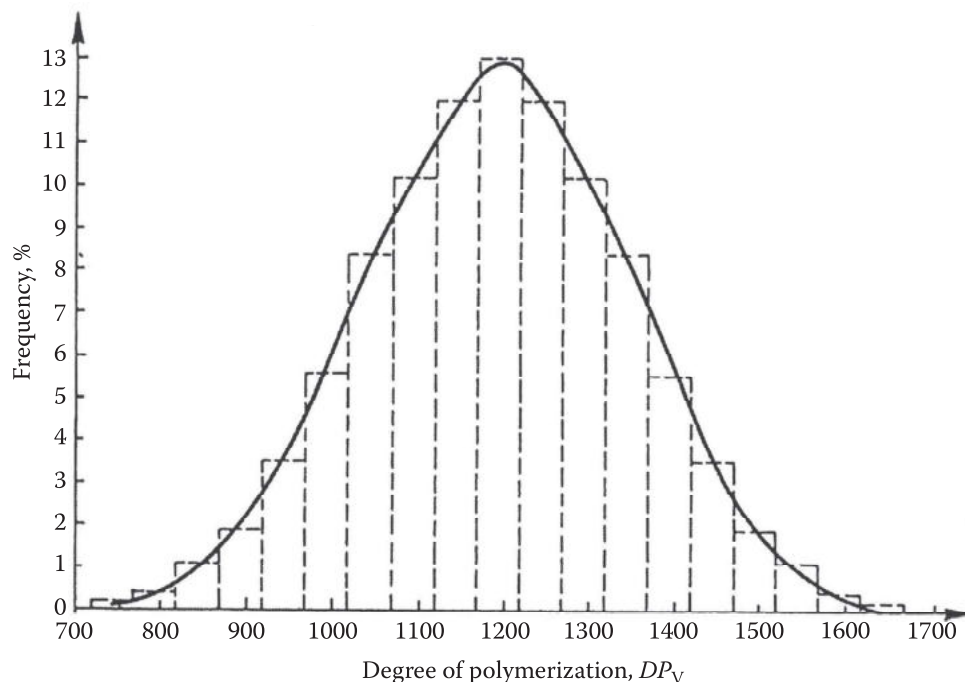| Parameters	Symbol	Unit	Values
Dielectric constant	ε_r		2.4
Dissipation factor	$\tan\delta$	%	0.3
Density		g/ml	0.8
Electrical strength		kV/mm	18
Design temperature		C	95–100
Moisture in paper		%	1–5
Tensile strength of paper		kg/m²	1300

FIGURE 12.9 Typical distribution of the *DP* of Kraft paper. (From Bouvier, B., *Papier et papier imprégné*, Techniques de l'ingénieur, D-280, 1, 1977.)

with which the paper may be dried and impregnated. The density varies with the arrangement of the individual fibers but is usually around 0.8 g/cm³. Higher-density papers are less porous and, therefore, possess higher tensile strength so that when impregnated with oil, they exhibit higher dielectric break-down strength.

The cellulose paper is defined by the general chemical formula $C_{12}H_{20}O_{10}$. The paper fibers consist of a chain of *glucose repeating* units arranged in cellobiose pairs (Bartnikas and Srivastava, 1980). The number of glucose units in the chain is referred to as the *degree of polymerization* (*DP*) of the paper. Figure 12.9 illustrates a typical distribution of *DP* in Kraft paper, which varies from 700 to 1600, with an average value around 1200 (Bouvier, 1977). The polymolecular nature of the paper fibers prevents the determination of the exact molecular mass and the total length of the molecular chain. One estimates that the paper fibers can have a molecular mass of 10^5 and a length of 10^3 A.

Exposed to ambient air, the paper absorbs humidity in the air via capillary action of the fibers. Under normal conditions, the paper can contain up to 12% by weight of water (Bartnikas and Srivastava, 1980; Oommen et al., 1982). Most of this water can be removed by heating under vacuum. In regions where the cellulose molecules exhibit an orderly arrangement (crystallites), water is retained by absorption forces. This colloidal or bound water is believed to be held by hydrogen bonds that exist between the H_2O dipoles and the hydroxyl groups of the cellulose molecules. The strength of these dipole bonds prevents the removal under vacuum of the colloidal water that will contribute to the overall ionic conduction losses if dissociated.

12.2.2.4 Control of Humidity

Moisture can be absorbed readily by paper exposed to ambient air. The amounts vary with the relative humidity, as illustrated in Figure 12.10 (Fabre and Pichon, 1960; Bouvier, 1977), which shows the variations in the water content of Kraft paper as a function of the partial water vapor pressure in the ambient air, at different temperatures. It can be seen that the water absorption by the paper increases with the partial vapor pressure and decreases with the temperature.

Water is also absorbed by the oil in power transformers. Furthermore, in the presence of cellulose, paper, pressboard, etc., which have a higher affinity for water, a continuous exchange of humidity occurs
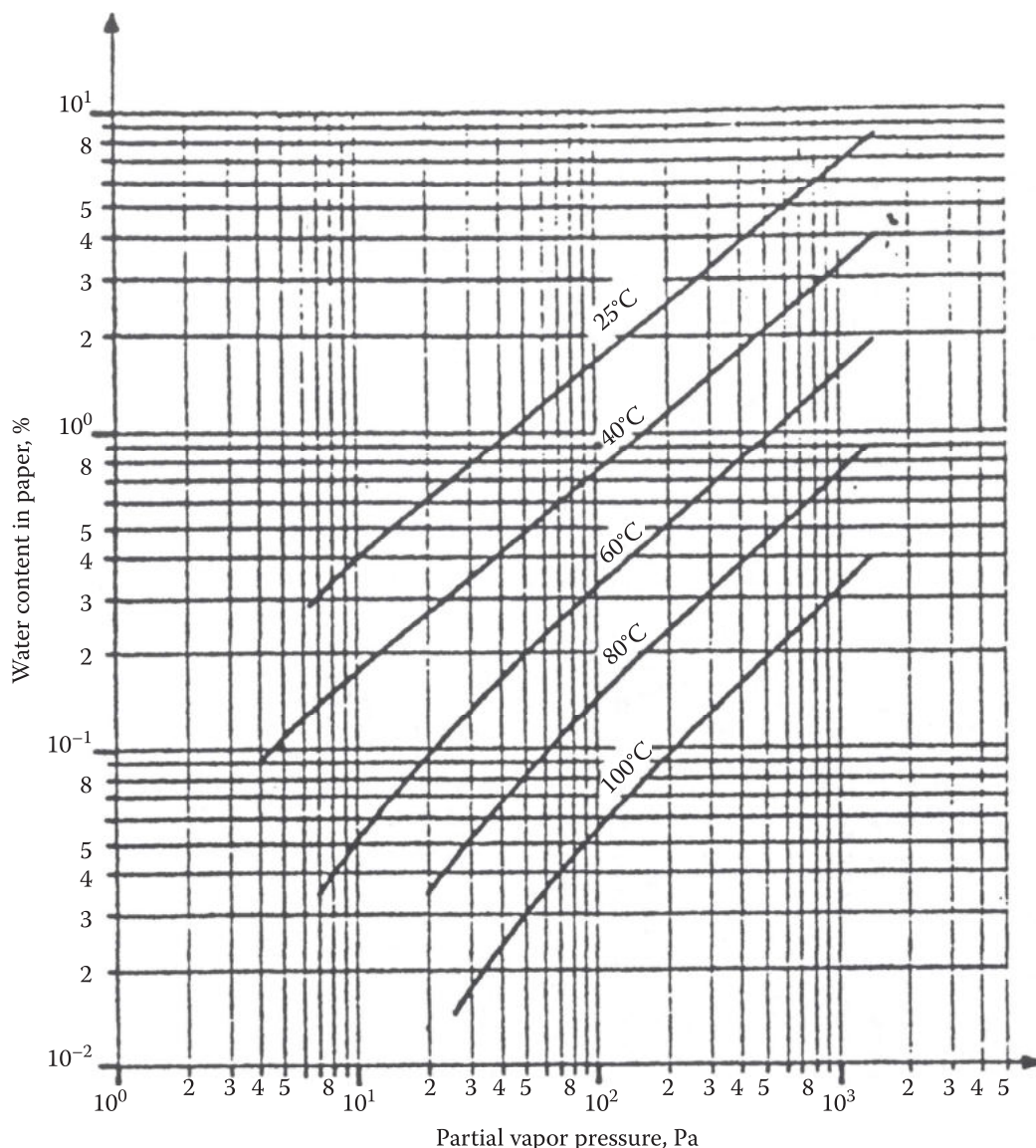
FIGURE 12.10 Variations of the water content in nonimpregnated Kraft paper with the partial pressure of water vapor and for different temperatures. (From Bouvier, B., *Papier et papier imprégné*, Techniques de l'ingénieur, D-280, 1, 1977.)

between the oil and the cellulose to maintain an equilibrium state. Figure 12.11 shows the variations of the water content in the oil and Kraft paper at equilibrium (Oommen et al., 1982). It can be seen that even with a relatively dry oil, containing 10–20 ppm of water, moisture in the paper can be several orders of magnitude higher, reaching 5%–8%. However, over the normal operating temperature range in power transformers, typically 70°C–90°C, water content in the paper is less than 1% for humidity in the oil of 10 ppm or lower.

The effect of humidity on oil and oil–paper insulation is a reduction of the breakdown voltage and increases electrical conductivity and dissipation factor tan δ (Fallou, 1970). The dielectric strength of mineral oil measured with *VDE* electrodes shows a slight reduction, about 15%, at a water content of 10 ppm. It passes by a plateau at 70% at a water content of 20 ppm before it reduces notably at water contents higher than 20 ppm (Miners, 1982). However, its estimation in a practical system is more difficult, and its effect on dielectric performance consequently less predictable than in laboratory tests.

With today's proper control of humidity in power transformers, its influence on the insulation performance does not present a problem. Typical water content in power transformers is of the order of 10 ppm (Norris, 1963). Two approaches are currently used to control the humidity:
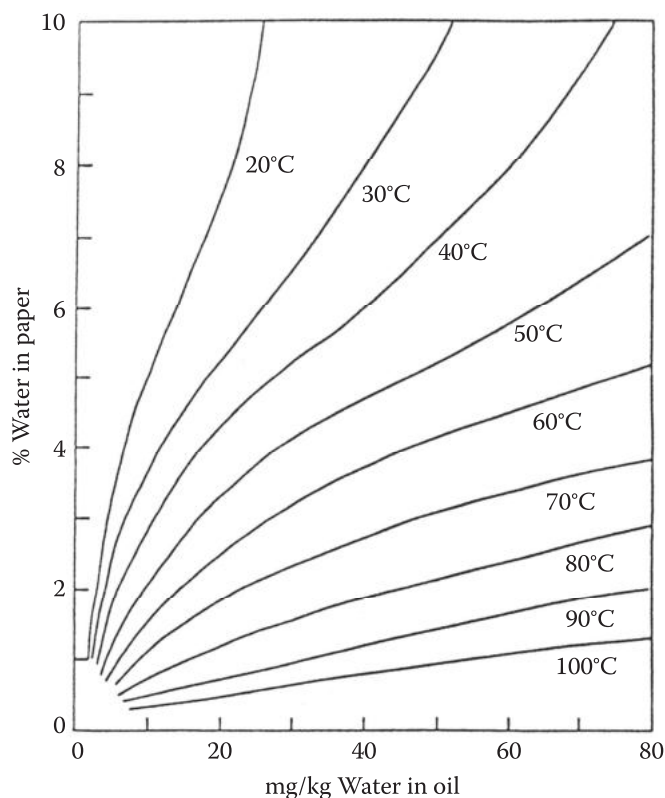
FIGURE 12.11   Variations of the water content in paper (in %) as a function of the water content (in ppm) on oil at equilibrium. (From Oommen, T.V. et al., *IEEE Trans. Power Appar. Syst.*, PAS-101, 1048, May 1982.)

In one approach, a hermetic tank is used to completely separate the oil–paper insulation from the ambient environment. A cushion filled with neutral gas, usually nitrogen, compensates for the fluctuations in the oil volume during load cycles. In this approach, the gaseous decomposition by-product of the oil and cellulose by PDs or in the presence of hot spots is contained in the tank, and tends to increase with time, with the risk of forming gas bubbles when the dissolved gases in the oil exceed the equilibrium level.

In North America, the tendency is to allow open contact between the oil and ambient air, with humidity removed by silica gel, within the conservator. In this approach, the gaseous decomposition by-products of oil and cellulose are dispersed to the ambient air and do not accumulate. The oil is in constant equilibrium with the ambient air, and the risks of forming gas bubbles are minimized. Noting that dissolved gases in oil constitute one of the practical methods to monitor the insulating state of the oil–paper insulation, its analysis should take into account the method used by the manufacturer to control humidity ingress to oil discussed earlier.

12.2.2.5 Control of Particle Contamination

Particle contamination is another factor affecting the dielectric performances of oil–paper insulation. It is now recognized that solid particle contamination is unavoidable in power transformers and reactors under practical conditions.

Nature of particles: The nature of particles found in power transformers can be evaluated by *ferrography*. It varies significantly, but the most common are cellulose fibers, sand, carbon, copper, aluminum, and ion particles. Obviously, the particles found are related to materials used in the manufacture of the transformer, namely, cellulose fibers, sand, carbon, copper, aluminum, and iron. Figure 12.12 shows the result obtained from ferrographic analysis of oil samples taken from operating transformers. The ferromagnetic particles are aligned, while nonmagnetic particles are deposed in disorder on the glass plate.
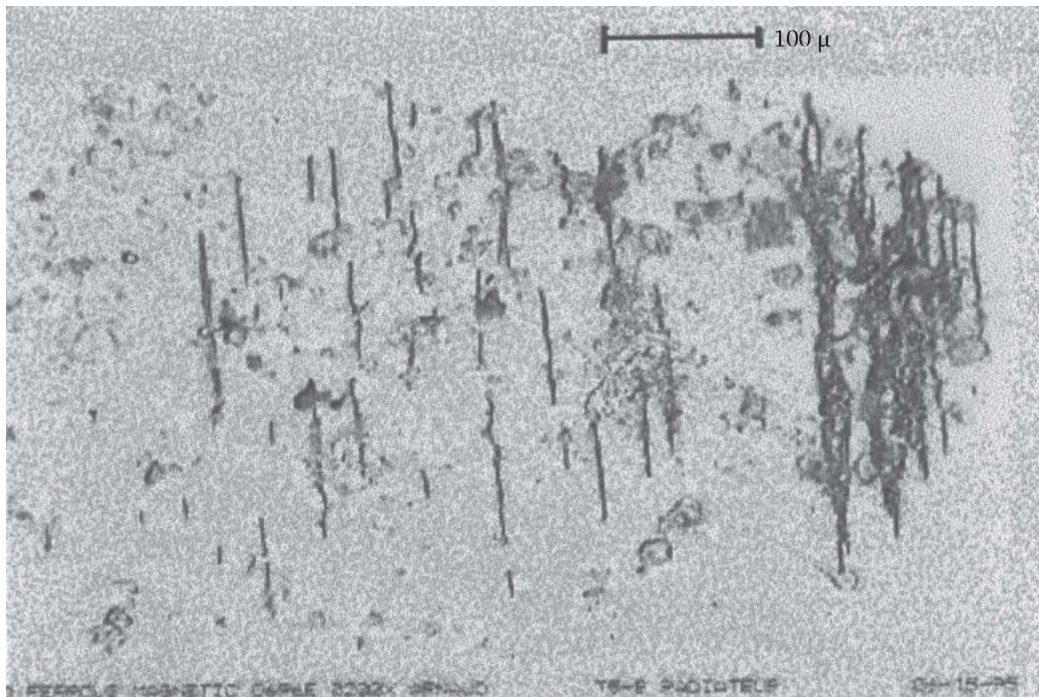
FIGURE 12.12 Result of a ferrographic analysis of an oil sample of an in-service power transformer.

It is generally accepted that particle contamination of power transformers is introduced during manufacturing, commissioning, and during major repairs, when the oil must be removed and the transformer refilled after repair work. Cellulose fibers come from paper and pressboard used in the insulation. They can have considerable dimensions and are sensitive to humidity: humid fibers become more conducting, with detrimental effects on dielectric performances of the insulation. Sand particles are probably introduced during the manufacturing process. Metallic particles from transformer core, conductors, windings, and metallic connections are also introduced during manufacturing.

In transformers equipped with automatic tap changers, carbon particles are produced due to arcing during operations of the tap changers and must be prevented from contaminating the bulk oil volume. This is done by separating the tap changers compartment, including its oil, from the main transformer tank. Monitoring the particle content in oil constitutes one of the practical methods to monitor the actual state of the insulation system for adequate use in power transformers. Any sudden change in the particle content in the oil is indicative of contamination and its source should be identified.

The particle content in power transformers may, therefore, vary significantly. Following the commissioning of power transformers, the particle content shows an initial sharp increase and gradually stabilizes afterwards and may even slightly improve with time (Palmer and Sharpley, 1969). The initial increase of particle content is attributed to the mechanical vibrations during operation, which liberates the particles from the core and insulation, while improvement in the particle content with time may be explained by the settling of the particles in natural particle traps within the transformer tank where the oil flow is minimal.

It may be expected that deterioration in the oil insulation strength occurs with increase in particle contamination, especially when the particles are conducting; carbon; metallic particles; and/or moisture-saturated cellulose fibers. In power transformers, the breakdown process of an oil gap can be divided into two stages: initiation and development of the breakdown. In uniform and quasi-uniform field gaps, breakdown initiation is greatly affected by the electrode surface condition and by the oil quality, which results in the well-known electrode area and stressed oil volume effects (Wilson, 1953; Weber and Endicott, 1956). The phenomenon is directly related to the statistical nature of discharge initiation and can be evaluated from the experimental distribution of the probability to initiate the breakdown from an elementary surface or volume (Trinh et al., 1982a,b) discussed in Chapter 6 and in Section 12.3.2.

Particle content: Measuring particle content is, at present, a useful and nonintrusive means to control and monitor the quality of the oil in operating power transformers. Oil samples are taken from operating transformers for laboratory analysis for their gas and particle content and dielectric strength. It should be borne in mind that oil sampling does require due precautions regarding cleanliness of the sampling bottles but also in the measurement of the particle contents and hence the dielectric strength. The last two parameters are affected by the time the oil remains in the sampling bottles due to the sedimentation of the particles. Figure 12.13 shows the variations in time of the particle contents in oil, represented by the number of particles having a diameter greater than the values in the *x*-axis (Trinh et al., 1980). One can see that the particle count varies with the size of the particles following approximately a power law.

However, particle content also changes in time due to sedimentation of the particles, as shown by the distributions obtained for different times at rest before the particle count. The particle content improves and with it, the dielectric strength of the oil sample being analyzed. This is the main cause of the significant differences observed in the early investigation of particle contamination, between the laboratory and measurements made on-site. The problem is settled by the introduction of the ultrasonic homogenization of the oil sample prior to analysis (Crine and Vincent 1988; Samat and Lacase, 1988).

Figure 12.14 illustrates the improvement in the particle count obtained with the ultrasonic homogenization: a stable particle content after a minimal homogenization time. On the other hand, Figure 12.15
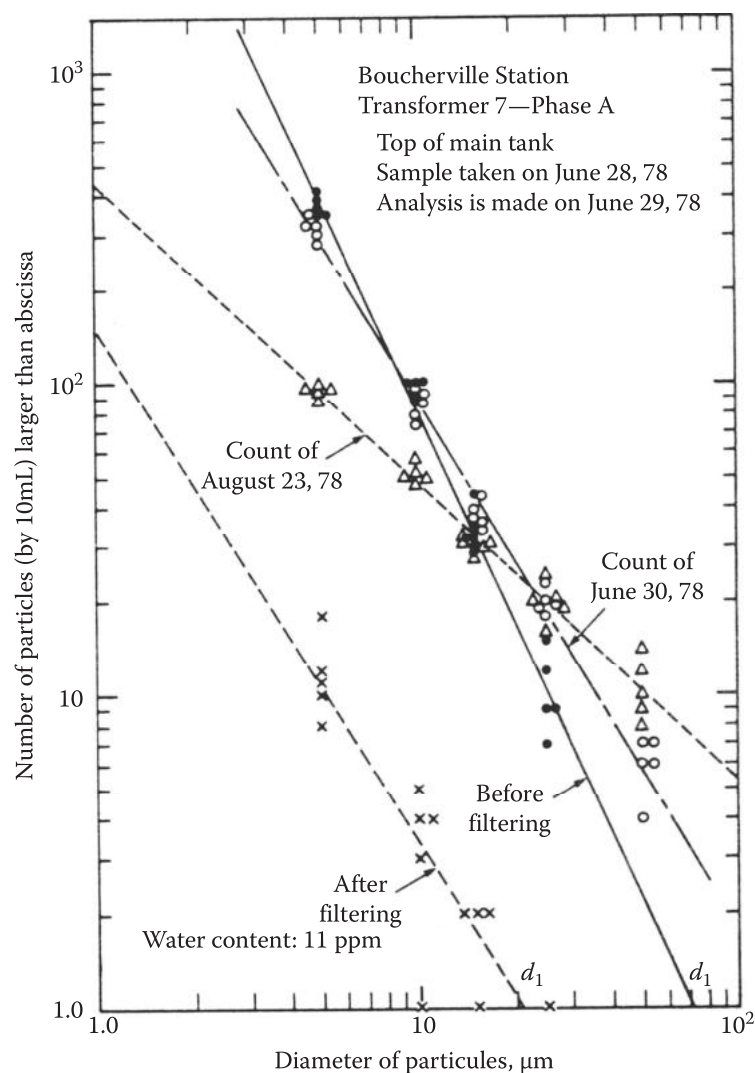

FIGURE 12.13   Variations in the distribution of particle content with time. (From Trinh et al., 1980.)
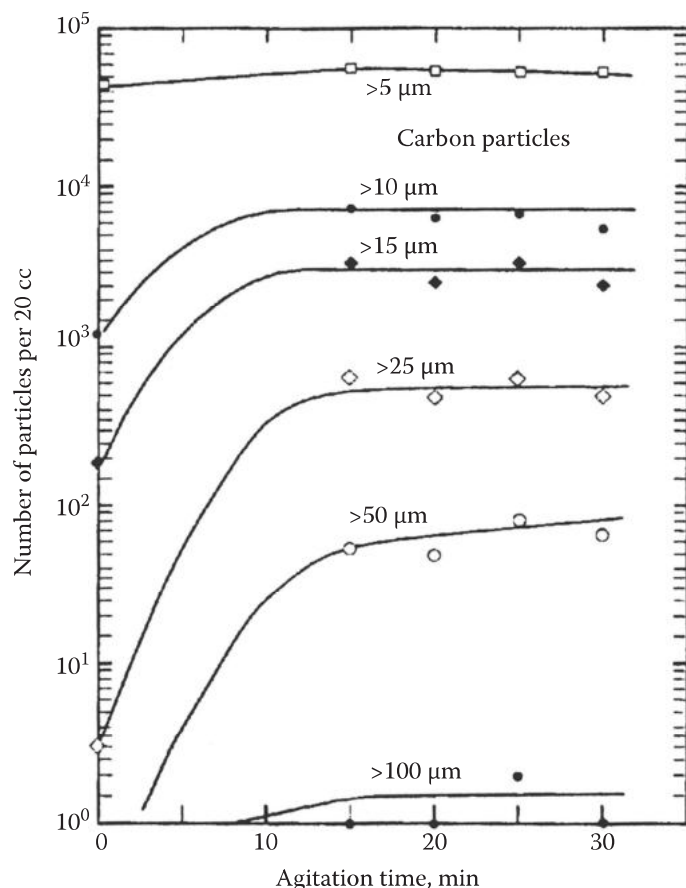
FIGURE 12.14   Influence of the ultrasonic homogenization on the measured particle content. (From Crine, J.P. and Vincent, C., *IEEE Trans. Electr. Insul*., EI-23(4), 751, August 1988.)
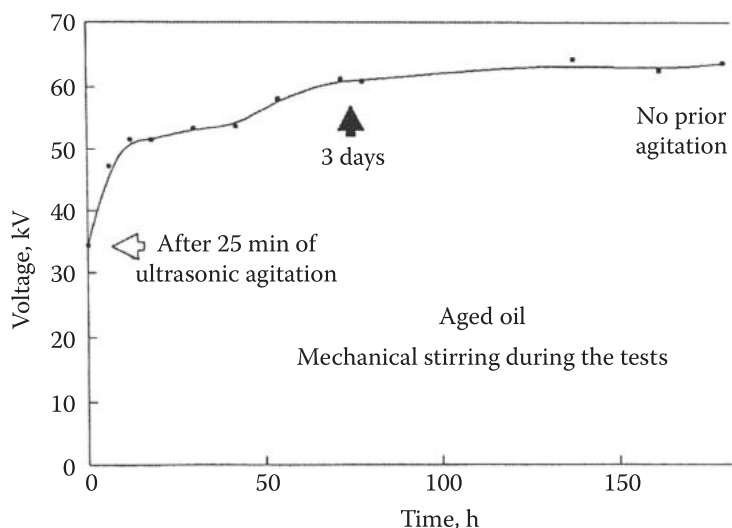

FIGURE 12.15   Influence of the sedimentation of particles on the measured dielectric strength of the oil sample. (From From Crine, J.P. and Vincent, C., *IEEE Trans. Electr. Insul*., EI-23(4), 751, August 1988.)

shows the effect of sedimentation of solid particles on the measured dielectric strength of the oil sample: a steady improvement during the first 100 h of rest time for the oil sample.

Adequacy of oil quality: Filtering the oil to remove solid particles is the logical answer to particle contamination, as illustrated by the results in Figure 12.13 comparing the particle content before and after filtering of the oil sample. However, super-clean oil is not necessarily the ultimate solution,

since it is sensitive to electrostatic charge accumulation resulting in flashover of the oil gap. As a result, utilities tend to establish criteria for an acceptable oil quality based on the measured particle content. The best way to present particle contamination in the oil is by a distribution of the measured particle content. A graphic paper with limit distributions defining the range of acceptable particle contents can be used to present the measurement (Figure 12.16): region A corresponds to severe particle contamination, region B to acceptable level of particle contamination, and region C to clean oil with little particle contamination. It allows a rapid evaluation of the adequacy of the oil sample regarding its particle content.

Index of particle content: An index of particle content δp (Trinh et al., 1982b) may also be defined as

$$d_p = \ln \left(n_0 * d_1 \right) \tag{12.4}$$

where

n_0 is the number of particles larger than 1 μm per unit volume (100 mL)

d_1 the maximal diameter in μm of the particles in the sample

Typical distribution of particle content has $n_0 = 1 \times 10^4$ and $d_1 = 100$ μm, corresponding to an index of $\delta_p = 13.8$. Practical transformer oils have a particle content index between 13 and 15, a contaminated oil has an index higher than 15, while a well-filtered oil has an index below 13.

12.2.3 SF₆ Insulation

This constitutes an adequate answer to the fire hazard problem related to the presence of mineral oil in power transformers. The relatively low dielectric stresses in power transformers, between 3 and
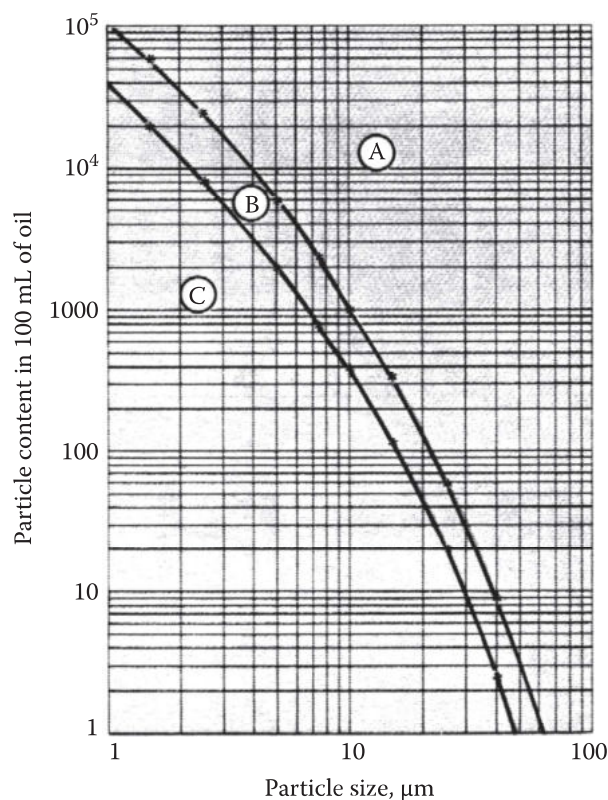

FIGURE 12.16 Representation of acceptable particle contents in transformer oil. A: Region of severe particle contamination. B: Region of acceptable particle contamination. C: Region of clean oil. (From Samat, J. and Lacasse, D., *Revue Alsthom*, (11), 47, 1988.)

5 kV$_{rms}$/mm, allow the use of SF$_6$ at relatively low pressure and do not present a particular difficulty. However, the relatively poor heat transfer characteristics of SF$_6$ present a serious problem to evacuate the heat generated by the power transformers. Two approaches are considered; both use perfluorocarbons as the cooling medium.

In the first approach illustrated in Figure 12.17, the perfluorocarbon liquid is dripping on the hot windings. The cooling by vaporization of the liquid is efficient; the vaporized liquid eventually condenses and is collected to recirculate. The main drawbacks of this solution reside in the difficulty to assure a uniform cooling over the whole winding, with the risk of forming hot spots in the winding insulation (Narbut et al., 1959; Tokoro et al., 1982).
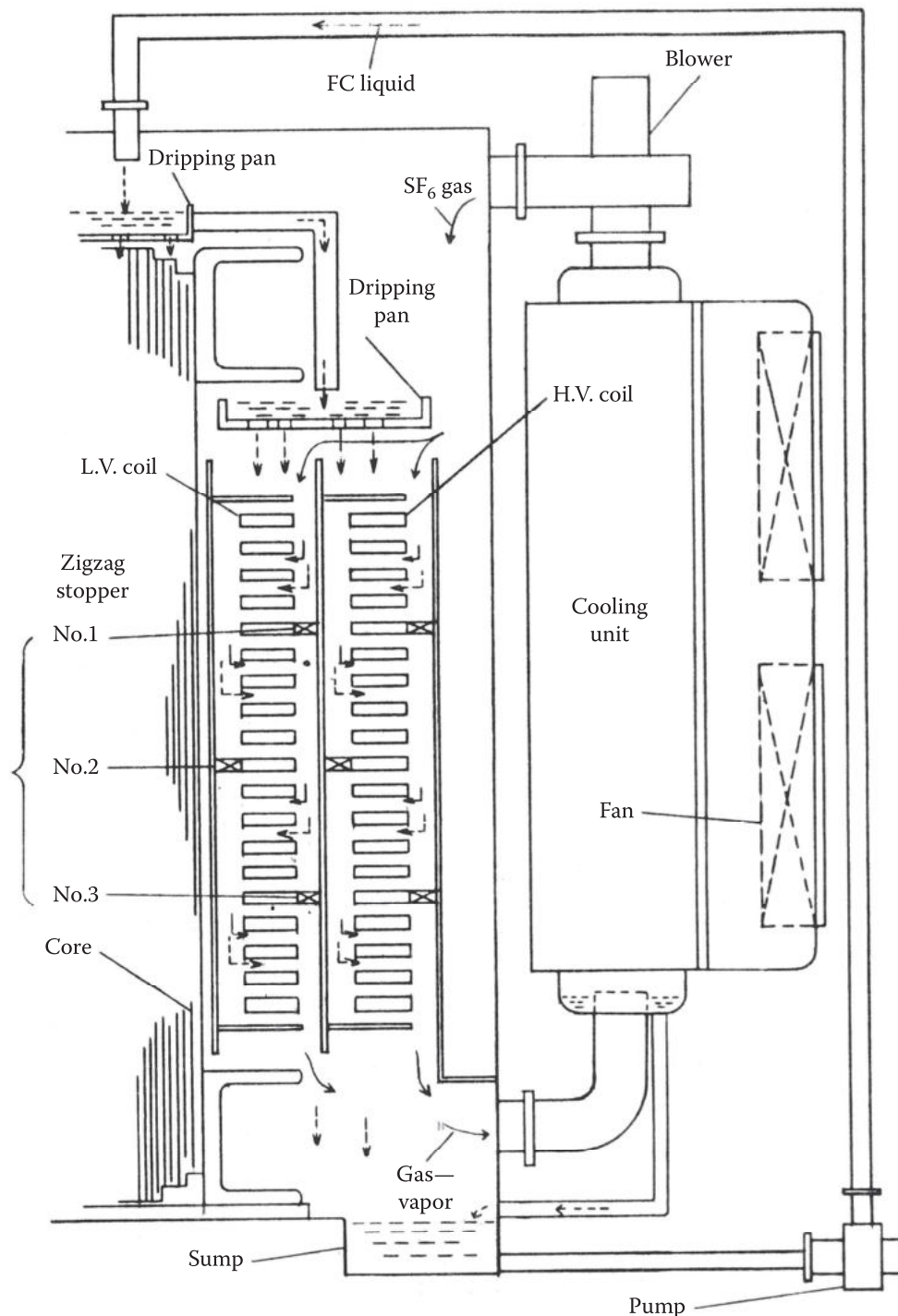

FIGURE 12.17 Perfluorocarbon vapor cooled gas-insulated power transformer. (From Tokoro, K. et al., *IEEE Trans. Power Appar. Syst.*, PAS-101(11), 4341, 4349, November 1982.)
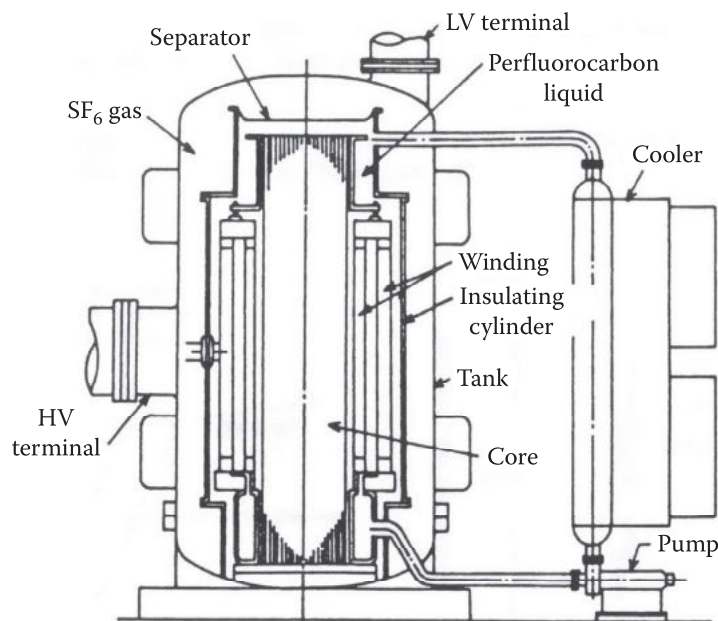
FIGURE 12.18 Liquid perfluorocarbon cooled gas-insulated transformer. (From Mukaiyama, Y. et al., *IEEE Trans. Power Deliv.*, PWRD-6(3), 1108, 1991.)

In the second approach shown in Figure 12.18, the windings are immersed in liquid perfluorocarbons, which literally replace the mineral oil. The principal drawback of this approach is the high cost of perfluorocarbons (Mukaiyama et al., 1991). Up to present, the development of SF_6-insulated power transformers has been modest; units of 275 kV, 300 MVA have been in operation in Japan since 1990s (Mori, 1990).

12.3 Considerations on the Dimensioning of Oil–Paper Insulation

Adequate dimensioning of the insulation is a principal aim in the design of power equipment. In power transformers, several causes have been identified for their failures (Freyhult and Carlson, 1991): failure of the bushing shield electrode, tracking of insulating surfaces, and turn-to-turn and interdisc insulation failures close to the line entrance. However, partial failures between turns or winding layers and sections do not always result in immediate failure of the insulation, which occur either across the oil space or along an insulating surface, between the windings to ground. The adequacy of the clearance distance in oil or along an insulating surface becomes essential to insulation of power transformer and can be evaluated in two different ways, namely:

- Evaluation of the cumulative stress
- Evaluation of the breakdown probability of the oil gap, using the stressed area or volume effect

12.3.1 Cumulative Stress

Evaluation of the cumulative stress provides a straightforward means to verify the adequacy of the clearance distances by making sure that the cumulative stress remains below a critical level, usually obtained from experimental data. It is defined as the average field E_b evaluated along a hypothetical breakdown path in the oil insulation, starting from an initial point located in the highly stressed region (Moser, 1979; Nelson, 1989), according to

TABLE 12.4

Moser Criterion, with $d_0 = 1$ cm

Parameters	Breakdown in Oil	Along Oil–Paper Interface
Exponent α	−0.38423	−0.46015
Maximal field, E_0 (kV/mm)	4.3468	4.0644

$$E_b = \frac{U_{max} - U}{\mathrm{D}l} \tag{12.5}$$

where

U_{max} is the potential at the initial point

U is the potential at a point P on the evaluation path

Δl the distance measured along the evaluation path from the initial point to P

In this manner, the cumulative stress is maximal at the initial point and is effectively equal to the local field; it decreases gradually along the evaluation path.

Moser criterion: Is essentially empirical, as established from the experimental data gathered on the cumulative breakdown field, E_b (kV/mm). Moser has shown that E_b varies with the distance d (mm) covered by the breakdown, according to the empirical relation (Nelson, 1989)

$$E_b = E_0 \left(\frac{d}{d_0} \right)^a \tag{12.6}$$

where E_0 and α are experimental parameters obtained in the reference gap of length d_0.

Taking the logarithm of both sides of Equation 12.6, one gets

$$\ln\left(E_b\right) = a * \ln d + A_0 \quad \text{with } A_0 = \ln E_0 - a \ln d_0 \tag{12.7}$$

The experimental values of α and E_0 are given in Table 12.4 for the cases of breakdown in the bulk oil and along an oil–paper interface. Equation 12.7 implies that the Moser criterion can be represented by a straight line, when one presents the variations of cumulative stress in a *log–log* graphic paper, which should not be crossed by the design stress curves. Examples of the application of the Moser criterion in the dimensioning of transformer insulation are shown in Figure 12.19, which compare different cumulative stress curves in oil and along an oil–paper interface with the Moser straight line (Nelson, 1989). The cumulative stress curves, which intercept the Moser straight line, are considered as having insufficient clearance.

12.3.2 Breakdown Probability

Another approach to assess the adequacy of clearance distances in oil insulation comprises subdividing the oil gap in elementary surfaces and volumes, as illustrated in Figure 12.20, and evaluating the breakdown probability associated with a path, a surface, or a volume around an HV electrode. Proper design limits this breakdown probability below a threshold value generally defined from field experiences. Noting that the evaluation of the breakdown probability along a specific path is similar to the notion of cumulative stress of Moser, a comparative evaluation of the two approaches allows definition of the threshold probability to be respected in the dimensioning of oil–paper insulation. The evaluation of the breakdown probability consists, in general, in subdividing the oil insulation gap in N_s elementary
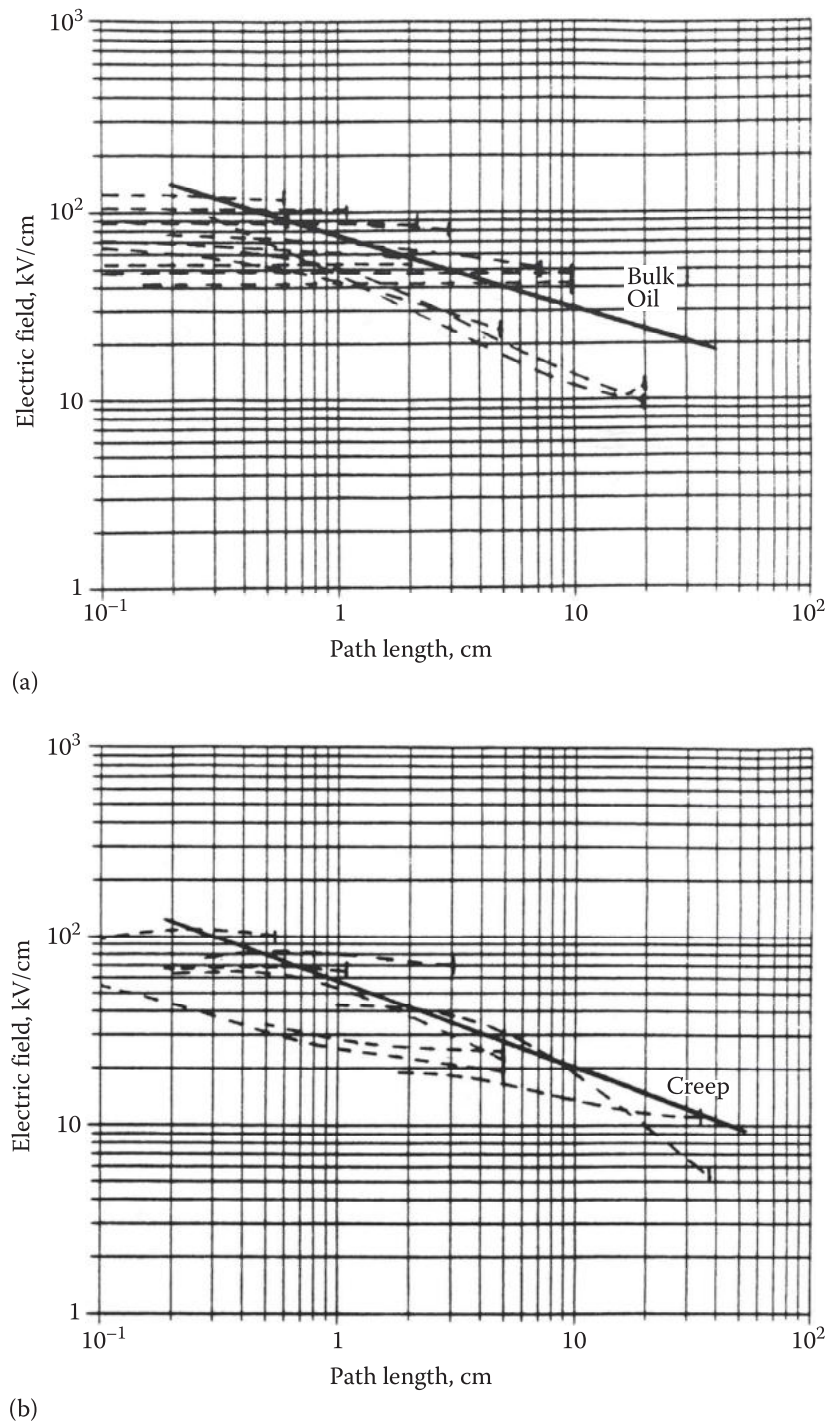
(a)

(b)

FIGURE 12.19 Illustration of the application of Moser criterion in the dimensioning of oil–paper insulation. (a) Cumulative stress in bulk oil. (b) Cumulative stress along an oil-paper interface. (From Nelson, J.K., *IEEE Trans. Electr. Insul.*, EI-24, 835, October 1989.)

surfaces and N_v elementary volumes, of which the probability to initiate a breakdown is known, and then evaluating the breakdown probability, according to the general expression

$$P_n\left(u\right)=1-\prod_{N_s}\left[1-p_s\left(u\right)\right]\prod_{N_v}\left[1-p_v\left(u\right)\right] \qquad (12.8)$$

where $p_s(u)$ and $p_v(u)$ are, respectively, the probabilities to initiate the breakdown of the oil gap from an elementary surface or volume at the voltage u.
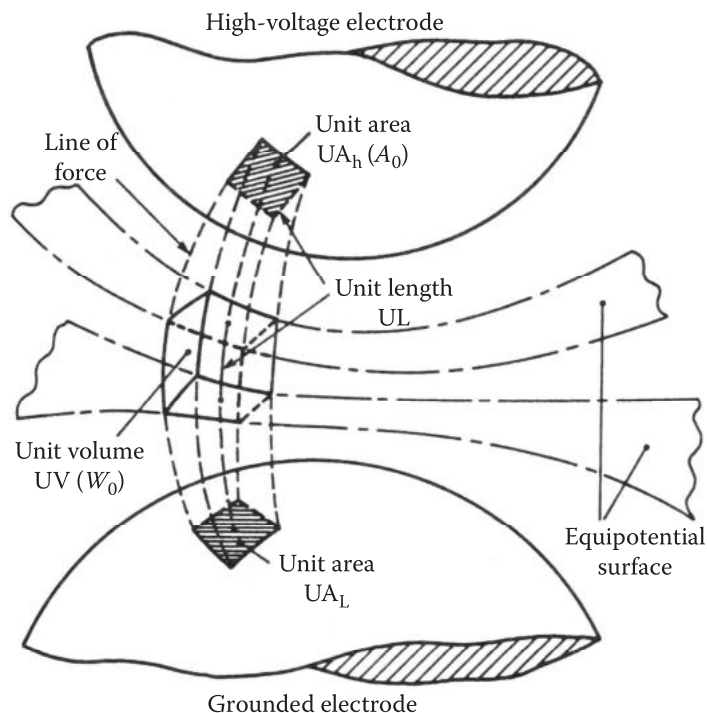
FIGURE 12.20 Illustration of elementary surfaces and volumes in an oil gap. (From Trinh, N.G. et al., Electrode area, stressed-volume: Two apparent effects of large-volume oil-insulation, in *IEEE International Symposium on Electrical Insulation*, Philadelphia, PA, June 6–9, 1982a, pp. 115–118; Trinh, N.G. et al., *IEEE Trans. Power Appar. Syst.*, PAS-101(10), 3712, October 1982b.)

Distribution probability to initiate breakdown from an elementary surface or volume: As discussed in Chapter 6, the breakdown of an oil gap can be evaluated in terms of an effect of the surface and/or volume, from the distribution function of the probability to initiate breakdown from an elementary surface or volume. Their predominance is related to surface condition of the electrode and cleanliness of the oil. For a well-filtered oil, the effect of the electrode surface predominates over the volume effect, while the reverse is true for a solid particle-contaminated oil.

Tables 12.5 and 12.6 give the defining parameters for the probability distribution function to initiate breakdown from an elementary surface A_0 and volume W_0, taken arbitrarily as $A_0 = 0.1$ cm^2 and volume $W_0 = 2 \times 10^{-2}$ cm^3 for a typical transformer oil. The distribution function can be assumed to be of the *normal*, *extreme value*, *or* Weibull type (Trinh et al., 1982).

TABLE 12.5

Probability Distribution Parameters for Initiating Breakdown from an Elementary Surface, $A_0 = 0.1$ cm^2

Parameters	Units	Normal	Extreme Values	Weibull CIGRE Procedure
Impulse voltage				
Mean E_m, position parameter E_0	kV/mm	108.7	86.48	46.38
Sigma σ, scale parameter α	kV/mm	20.54	5.69	67.78
Form factor β				3.4
AC voltage				
Mean E_m, position parameter E_0	kV/mm	36.31	30.36	16.21
Sigma σ, scale parameter α	kV/mm	6.7	2.01	22.11
Form factor β				3.4

Source: Trinh, N.G. et al., *IEEE Trans. Power Appar. Syst.*, PAS-101(10), 3712, October 1982b.

TABLE 12.6

Probability Distribution Parameters for Initiating Breakdown from an Elementary
Volume, $W_0 = 2 \times 10^{-2}$ cm^3

Parameters	Units	Normal	Extreme Values	Weibull CIGRE Procedure
Impulse voltage				
Mean E_m, position parameter E_0	kV/mm	94.25	76.83	47.57
Sigma σ, scale parameter α	kV/mm	15.56	4.1	51.35
Form factor β				3.4
AC voltage				
Mean E_m, position parameter E_0	kV/mm	31.48	26.67	16.15
Sigma σ, scale parameter α	kV/mm	5.11	1.44	16.86
Form factor β				3.4

Source: Trinh, N.G. et al., *IEEE Trans. Power Appar. Syst.*, PAS-101(10), 3712, October 1982b.

TABLE 12.7

Dimensions of the Test Cell

Parameters	Dimensions (cm)	Remarks and Values
Main tank		
Radius	100	
Height	250	
Turret		
Radius	50	
Length	250	275 cm to the base of the bushing
HV electrode		
Bushing shield electrode	40	
Length of connector	205	
Test electrode, length	40	Baril type Electrode $r_e = 20$ cm
Height above ground	100	

12.3.3 Example of Assessment for Adequacy of a Test Cell

As an application of the earlier approaches to dimensioning of oil insulation, they will be used to assess the adequacy of a test cell to evaluate the dielectric performances of a bushing shield in turret assembly. Figure 12.20 shows the general arrangement of the test cell: a main cylindrical tank of 100 cm radius, surmounted by a cylindrical turret of 50 cm radius, which provides access to the HV source, via the bushing. Detailed dimensions are given in Table 12.7. Two standard bushing shield electrodes are used, one at the bushing end as part of the test bushing shield–turret assembly and the other bushing shield terminated with a hemispherical cap, at the end conductor connection, which completes the test assembly.

12.3.3.1 Field Calculation

Field calculations are made using the method of charge simulation (Singer et al., 1974; Trinh, 1980) discussed in Chapter 2. The results are summarized in Table 12.8 for different locations where the field is high, identified in Figure 12.21. The calculation of the normalized field is made with an applied voltage of 1 kV. To obtain the actual field at the test voltage, it suffices to multiply the normalized gradient (kV/cm) by the test voltage. Specific values of the electric field corresponding to the three voltage levels of 425, 700, and 960 kV are also given in Table 12.8 for different points of calculation: 1–9.

TABLE 12.8

Normalized and Actual Gradients at Calculation Points

Gradient (kV/cm) at	1 kV—Normalized	425 kV	700 kV	960 kV
Bushing shield				
Point of calculation 1	7.1737×10^{-3}	3.0488	5.0215	6.8867
Point of calculation 2	6.4914×10^{-3}	2.7588	4.5439	6.2317
At the turret	1.1906×10^{-3}	0.7570	1.2469	1.7101
Point of calculation 3	7.4111×10^{-3}	3.1497	5.1877	7.1146
HV connection				
Point of calculation 4	5.7432×10^{-3}	1.8175	2.9936	4.1055
Point of calculation 9	6.6771×10^{-3}	0.2795	4.6039	6.3140
Termination electrode				
Point of calculation 5	4.9529×10^{-3}	2.1049	3.4670	4.7547
Point of calculation 6	5.1586×10^{-3}	2.1924	3.6110	4.9522
At the surface of the tank	0.4084×10^{-3}	0.1791	0.2950	0.4046
Point of calculation 7	5.9747×10^{-3}	2.5392	4.1822	5.7357
At the bottom of the tank	0.2268×10^{-3}	0.0964	0.1587	0.2177
Point of calculation 8	2.5695×10^{-3}	1.0920	1.7986	2.4667

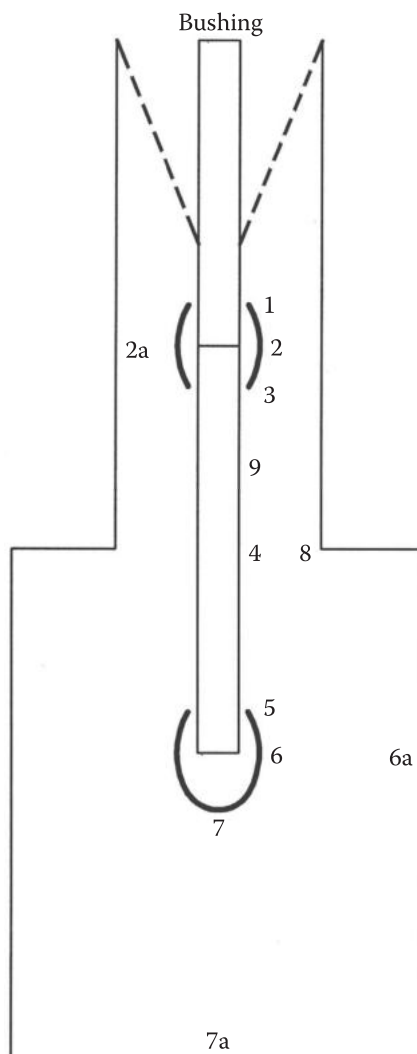*Note:* The normalized gradient is calculated with a radius of curvature of 5 cm.

FIGURE 12.21 Arrangement of the test cell. Numbers refer to field calculation sites, with results provided in Table 12.8.
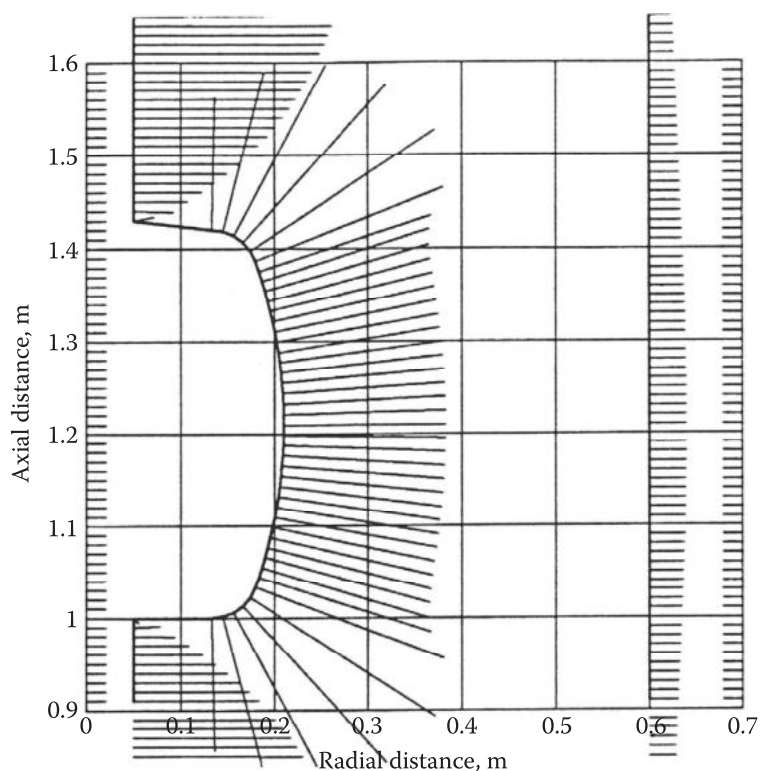
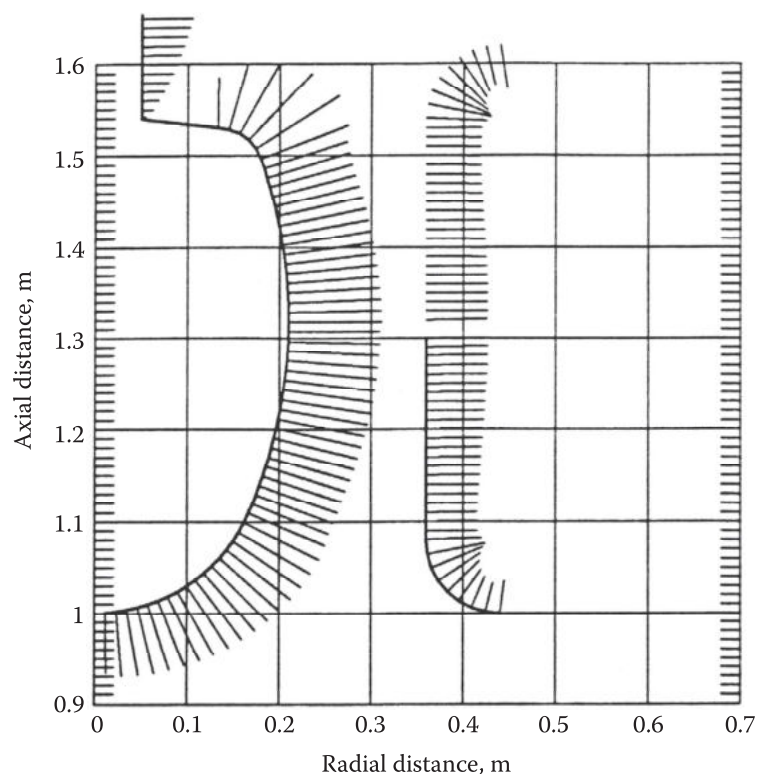**FIGURE 12.22** Calculated field distribution around the bushing shield.

FIGURE 12.23 Calculated field distribution at the termination electrode.

Figures 12.22 and 12.23 show the field distribution at the bushing shield and termination electrode, represented by the local field vectors at the electrode surface. One notices that the maximum field occurs at the edges of the bushing shield, while a local maximum occurs at its central portion (points of calculation 1–3). This would ensure that breakdown would occur at the bushing shield electrode under test.

On the other hand, the termination electrode effectively controls the field distribution to relatively low values over its whole surface (points of calculation 5–7) to avoid undesirable breakdown initiated from the termination electrode.

The adequacy of the test cell for evaluating bushing shield electrodes will be evaluated using the approaches of cumulative stress and breakdown probability in the following.

12.3.3.2 Cumulative Stress

The cumulative stress is calculated along a probable breakdown path, typically along the radial path originating from a highly stressed point to the ground tank (or turret), and for the three voltage levels. The results are presented in Figures 12.24 through 12.26, for the voltages 425, 700, and 960 kV,
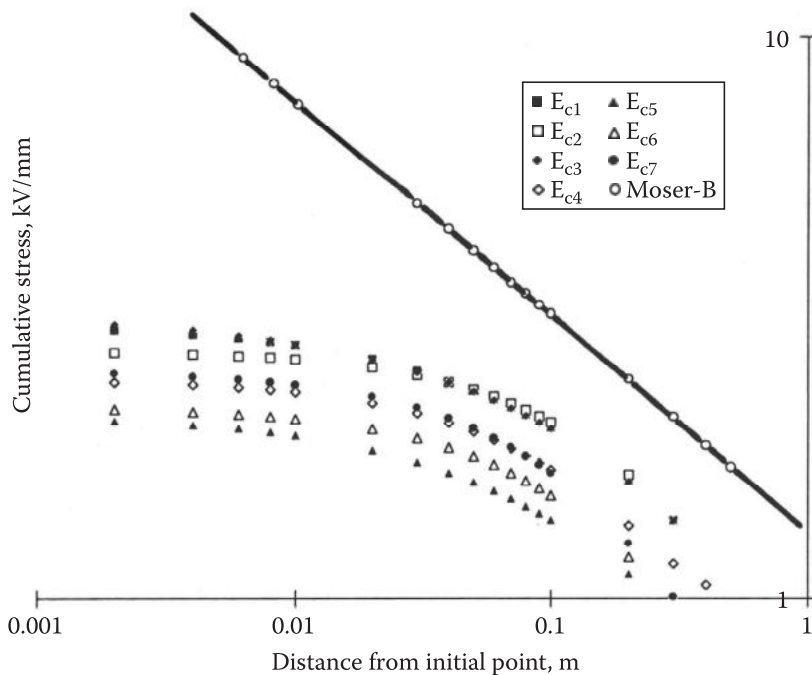

FIGURE 12.24 Curves of cumulative stress at 425 kV—Moser criterion. E_{c1}–E_{c8} refer to cumulative stress curves from field calculation sites 1–7, shown in Figure 12.21. The straight line represents the Moser criterion for Bulk oil.
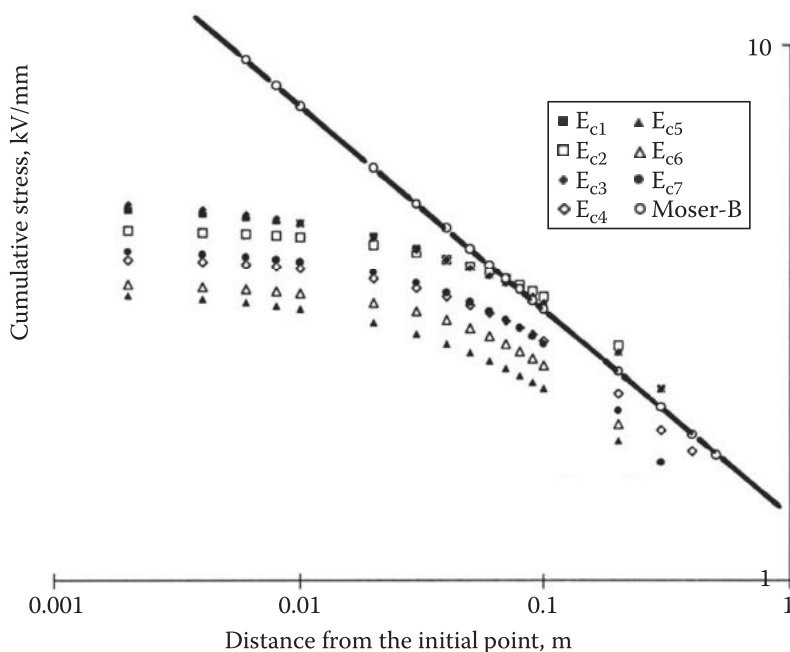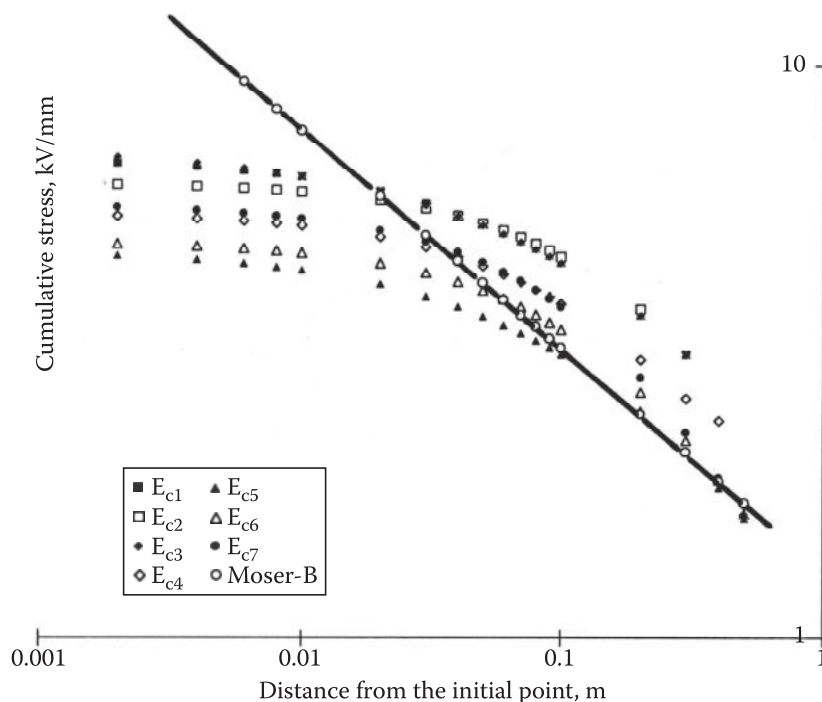

FIGURE 12.25 Curves of cumulative stress at 700 kV—Moser criterion. E_{c1}–E_{c8} refer to cumulative stress curves from field calculation sites 1–7, shown in Figure 12.21. The straight line represents the Moser criterion for Bulk oil.

FIGURE 12.26   Curves of cumulative stress at 960 kV—Moser criterion. E_{c1}–E_{c8} refer to cumulative stress curves from field calculation sites 1–7, shown in Figure 12.21. The straight line represents the Moser criterion for Bulk oil.

respectively. The cumulative stress curves are compared with the straight line corresponding to the Moser criterion (Moser, 1979; Nelson, 1989): a cumulative stress curve remaining below the Moser criterion straight line is a good indication that no breakdown is likely to occur along the corresponding path. The following observations can be made:

- At the voltage level of 425 kV (Figure 12.24), all the cumulative stress curves remain below the Moser criterion line. The bushing shield should withstand this voltage level.
- At the voltage level of 700 kV (Figure 12.25), only the curves of cumulative stress originating from the bushing shield electrode intercept the Moser criterion line. Breakdown may occur from the bushing shield electrode.
- At the voltage level of 960 kV (Figure 12.26), all cumulative stress curves intercept the Moser criterion line. Breakdown may occur along any of the paths analyzed, although the probability is higher at the bushing shield electrode.

It is obvious from the earlier results that the cumulative stress can only provide a qualitative assessment of the likelihood that a specific path would result in breakdown of the oil gap at a given voltage level.

12.3.3.3 Probability of Breakdown

With the distribution function of the probability to initiate the breakdown of the oil gap from an elementary volume discussed previously, the probability that the breakdown will be initiated from a particular region within the oil gap can be readily evaluated by the following:

- Subdivide the region of interest into N_p hypothetical paths, initiated from the highly stressed electrode and crossing the oil gap.
- Subdivide the path into N_v elementary volumes of 2×10^{-2} cm^3, initiating from an elementary surface of 0.1 cm^2, at the highly stressed electrode.

Probability of initiating breakdown from a specific path: It is equivalent to the Moser criterion of cumulative stress, with the N_v elementary oil volumes aligning along the hypothetical breakdown path. The resultant probability of initiating the breakdown from the N_v elementary volumes is

$$P_p\left(u\right)=1-\prod_{N_v}\left[1-p_i\left(u\right)\right] \tag{12.9}$$

where

    $P_p(u)$ is the probability to initiate breakdown from the oil volume containing N_v elementary oil volumes
    $p_i(u)$ is the probability to initiate breakdown from the ith elementary volume in the assumed breakdown path

Figure 12.27 presents the probabilities of initiating breakdown from the same paths used in the evaluation of the cumulative stress and for values of the applied voltages varying between 400 and 1000 kV. These probabilities are generally low, varying between 10^{-5} and 10^{-6}, and do not allow a direct conclusion on the dielectric performance of the oil interval. However, like the Moser cumulative stress, one can determine which breakdown path is critical to the dielectric performance of the oil gap. In the present case, the paths originating from the points of calculation 1–3 are more critical than all the other paths evaluated.

Probability of initiating breakdown from an equigradient contour: In the particular case where the HV test setup has an axial symmetry, the points located on the contour obtained by rotating the electrode around its axis, have the same gradient, forming an equigradient contour at the electrode surface. The probability to initiate the breakdown is the same for all the paths originating from the same equigradient contour at the electrode. Their combined effect is a higher probability to initiate the breakdown from the equigradient contour. Noting that the breakdown path is originated from an elementary surface of 0.1 cm² on the equigradient contour of 0.1 cm wide at the electrode, one gets

$$P_c\left(u\right)=1-\prod_{N_s}\left[1-P_{pi}\left(u\right)\right] \tag{12.10}$$

where N_s is the number of paths initiating from the equigradient contour.

Figure 12.28 presents the probability to initiate breakdown from an equigradient contour passing by the same points of calculation 1–9 in Figure 12.12. One can see that these probabilities are in the order of 10^{-4} to 3×10^{-3} for the range of applied voltage between 400 and 1000 kV. The large number of
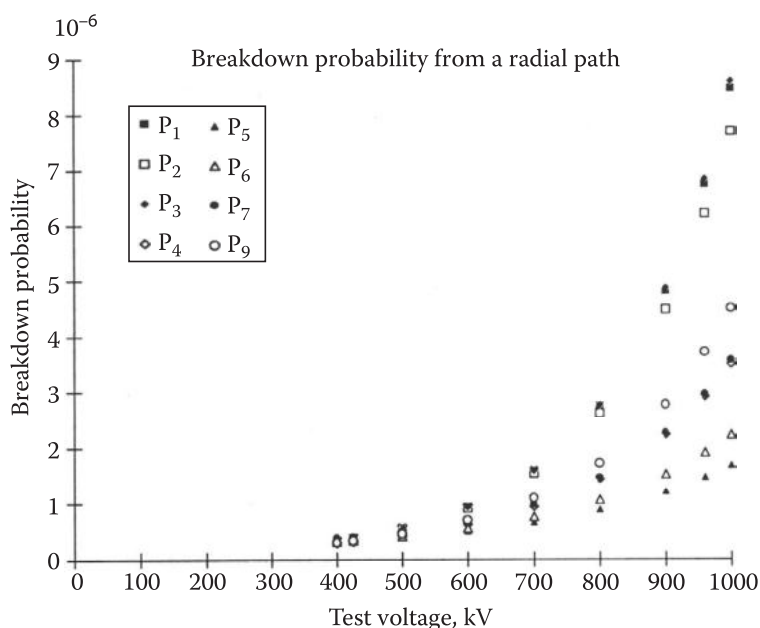

FIGURE 12.27 Variation of the probability of initiating breakdown from a specific path with the test voltage. P_1–P_9 refer to the breakdown paths initiating from field calculation sites 1–8, shown in Figure 12.21.
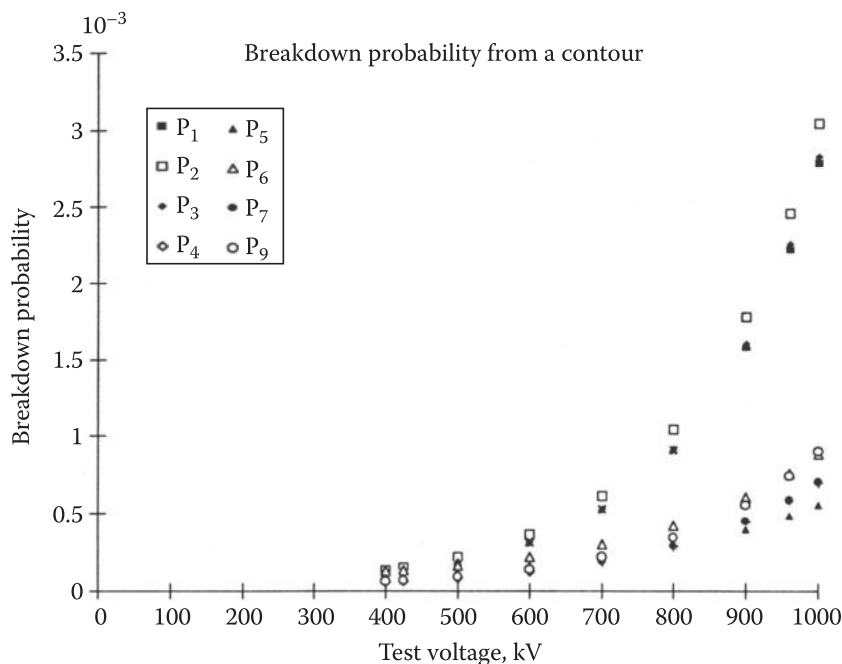
FIGURE 12.28 Variation of the probability of initiating breakdown from an equigradient contour with the test voltage. P_1–P_9 refer to the breakdown paths initiating from field calculation sites 1–8, shown in Figure 12.21.

breakdown paths originating from an equigradient contour at the electrode surface effectively increases and accentuates the probability to initiate the breakdown from the bushing shield–turret assembly, as compared with the other equigradient contours within the test cell. However, as in the case of breakdown probability from a specific path, the relatively low probabilities do not provide a clear indication regarding the dielectric performances of the test gap.

Probability of initiating the breakdown from a component: Noting that an electrode component (bushing shield electrode, HV connection, termination electrode) is composed of a number N_c of equigradient contours, one can evaluate the probability to initiate the breakdown from a specific component according to

$$P_s\left(u\right)=1-\prod_{N_c}\left[1-P_{ci}\left(u\right)\right] \tag{12.11}$$

where N_c is the number of equigradient contours contained in a component.

Figure 12.29 presents the probabilities of initiating breakdown from the bushing shield electrode, assuming the same probability for the contours forming a given component.

The following observations can be made:

- At the voltage of 425 kV, all components of the HV circuit present relatively low probabilities to initiate breakdown, below 2%. No breakdown is expected at this voltage level.

- At the voltage of 700 kV, the probability to initiate the breakdown from the bushing shield electrode is 7% compared to probabilities less than 2% from the other components. The breakdown is unlikely at this voltage. However, if breakdown occurs, it should be initiated from the bushing shield electrode.

- At 960 kV, all components of the HV circuit have a finite probability to initiate the breakdown, although the probability of initiating breakdown from the bushing shield electrode reaches 25% compared with a probability less 10% from any other component.

- The probabilities to initiate breakdown from a component fall in the range of values with more practical meaning, which allows a direct assessment of the adequacy of the dielectric performance of the related component.
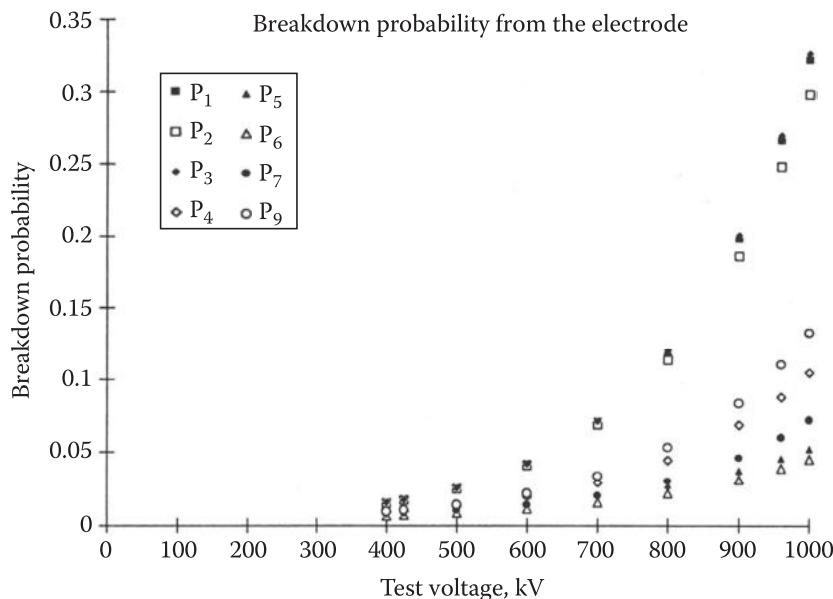
FIGURE 12.29 Variation of the probability of initiating breakdown from a component with the test voltage. P_1–P_3 Breakdown from the bushing shield electrode assuming constant field equal to that of point 1–3, P_4, P_9 Breakdown from the connecting conductor assuming constant field equal to that at point 4 and 9. P_5–P_7: Breakdown from the termination electrode assuming constant field equal to that at points 5–7.

12.4 Audible Noise from Power Transformers

The energization of power transformers generates acoustic noise due to vibration in the transformer core and in the cooling system. The noise generated may be sufficiently high to affect the local environment and have an impact on the choice of the location of the substation. Two mechanisms are responsible for the noise produced by the transformer core: the elongation of the core under magnetostriction effect and the transverse vibration of the core due to magnetic attraction. Both effects are independent of the polarity of the magnetic flux, and therefore, the transformer core vibrates essentially at twice the power supply frequency.

Figure 12.30 shows the octave-band frequency spectra of the AN generated by a 325/25 kV–275 MVA transformer in different modes of operation. One can see that the core vibration (curve *a*), measured
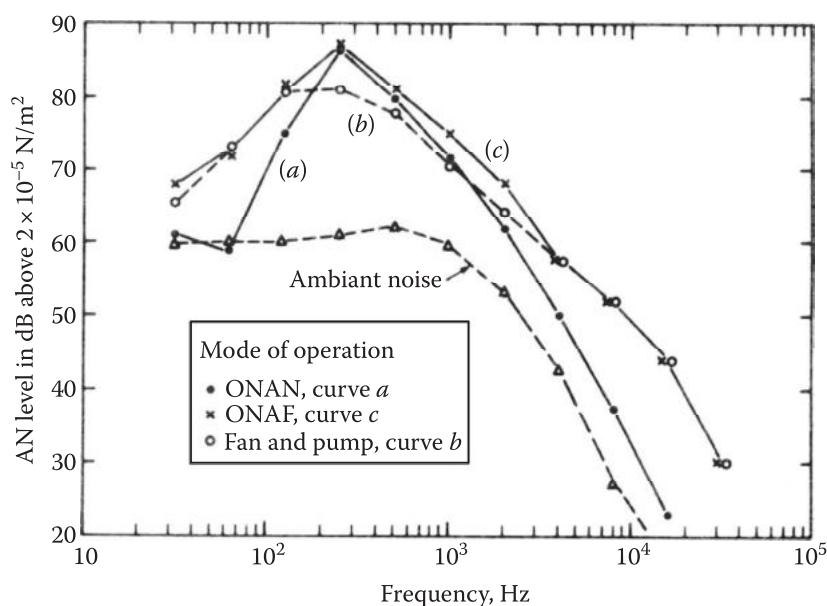

FIGURE 12.30 AN spectra from power transformer. (a) Noise from core vibration. (b) Noise from cooling system. (c) Resultant noise spectrum. (From Trinh, N.G. and Ménard, Y., Audible noise generated by power transformers of a substation—Its influence on the urban noise, Paper A76 473-9, presented at the *IEEE PES Summer Meeting*, Portland, OR, 1976.)

during the ONAN operation, has a frequency spectrum composed essentially of power frequency and its harmonics, with a maximal noise level at 240 Hz. The noise from the cooling system, pumps and fans, has a broader spectrum (curve *b*).

12.4.1 Transformer Audible Noise Characteristics

The AN characteristics of power transformers are determined by the average noise level obtained from a number of A-weighted measurements taken at regular intervals, 0.9 m around the major sound-producing surfaces of the transformer, and should comply with the limits set by national and international standards. The position of the microphone should be at 0.3 m from the major sound-producing surface and at least 1.8 m from any portion of the cooling system. The height of the microphone should be at midheight for small transformers and at 1/3 and 2/3 of the height of large power transformers (NEMA, 1973). Figure 12.31 shows the typical measurements of the AN made around a transformer of 425/25 kV–275 MVA. The noise level varies between 80 and 90 dBA.
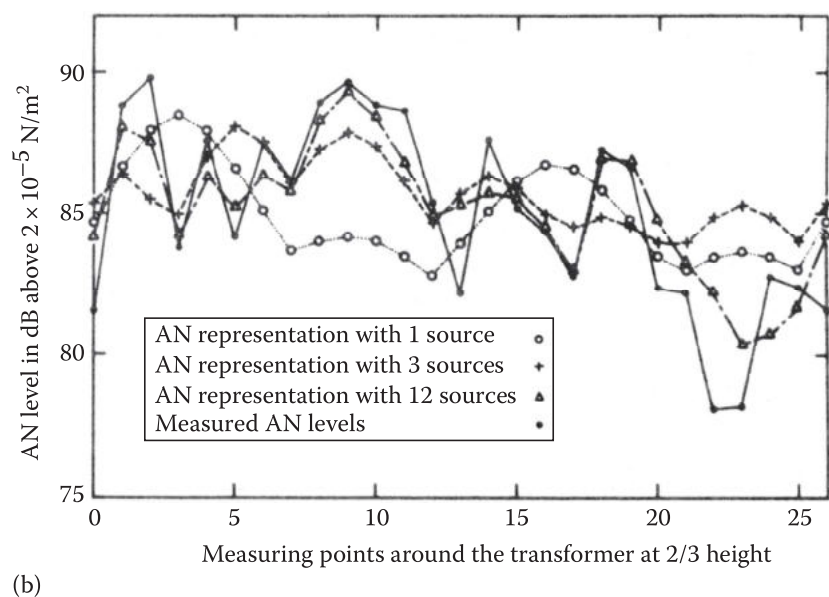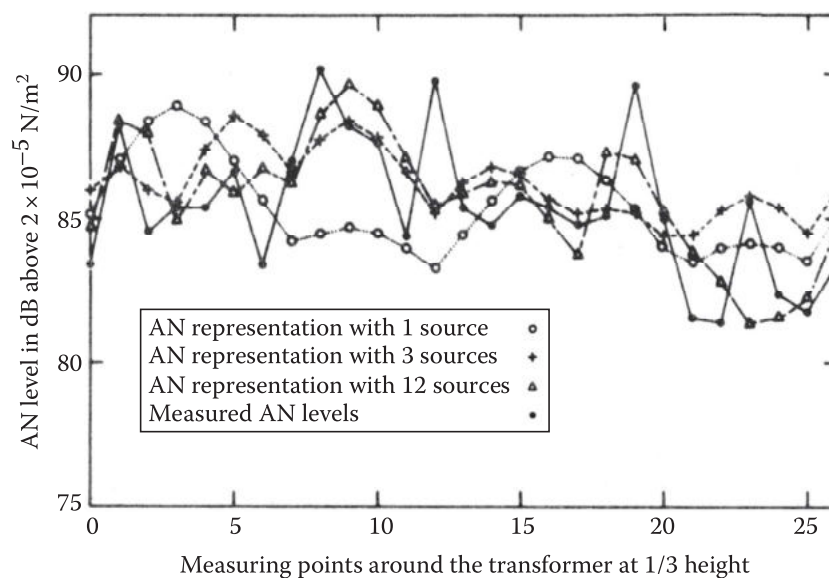

(a)

(b)

FIGURE 12.31 Acoustic characteristics of a power transformer of 325/25 kV–275 MVA. (a) measured at 1/3 height (b) measured at 2/3 height. (From Trinh, N.G. and Ménard, Y., Audible noise generated by power transformers of a substation—Its influence on the urban noise, Paper A76 473-9, presented at the *IEEE PES Summer Meeting*, Portland, OR, 1976.)

12.4.2 Representation of the Audible Noise from Power Transformers

The earlier AN characteristics of power transformer do not lend themselves to a more detailed analysis. There is an incentive to define an acoustic representation of the power transformer that would reproduce the same AN characteristics and facilitate the analysis of a transformer noise. A logical approach consists of representing the power transformer by a number of point sources located within the transformer. The number of the noise sources and their position are arbitrary, with the highest number of noise sources not exceeding the number of measurements made. Their acoustic power is determined from the measurements as described in the following.

Referring to Figure 12.32, the sound pressure $P(x, y, z)$ at any point M is given by

$$P = \sqrt{\rho_0 c \sum_1^N \left[\frac{W_i}{4\pi r_i^2} + K \frac{W_i}{4\pi r_{im}^2} \right]} \qquad (12.12)$$

where

r_i and r_{im} are distances from the measuring point M to the point source S_i and its image S_{im} with respect to the ground
W_i is the associated generated acoustic power
K is the coefficient of reflection of the ground
ρ_0 is the air density $\rho_0 = 1.293$ kg/m^3
c is the sound velocity in air, $c = 344.2$ m/s

Noting that the sound pressure at the measuring point is related to the measured noise level AN according to

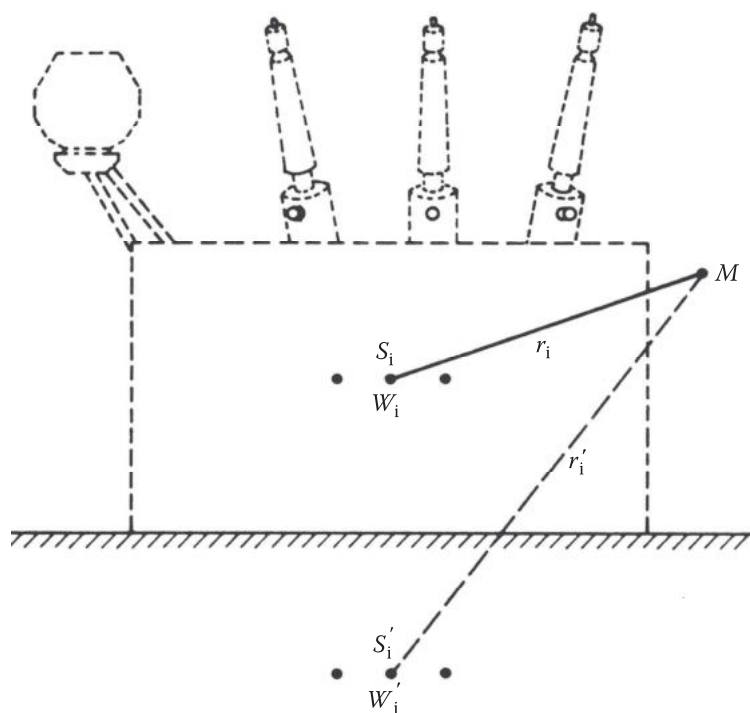$$P_i = 2 \times 10^{-5} \exp\left[\frac{AN_i}{20} \ln 10 \right] \qquad (12.13)$$

FIGURE 12.32   Acoustic representation of a power transformer. (From Trinh, N.G. and Ménard, Y., Audible noise generated by power transformers of a substation—Its influence on the urban noise, Paper A76 473-9, presented at the *IEEE PES Summer Meeting*, Portland, OR, 1976.)

a system of N equations can be obtained for the N_s unknown point sources as

$$\sqrt{r_0 c \sum_1^N \left[\frac{\hat{W_i}}{4\mathrm{p}r_i^2} + K \frac{\hat{W_i}}{4\mathrm{p}r_{im}^2} \right]} = 2 \times 10^{-5} \exp\left[\frac{AN_i}{20} \ln 10 \right] \qquad (12.14)$$

The solution of the preceding system of N linear equations for W_i exists only if $N \geq N_s$, that is, if the number of point source N_s is less than or equal to the number of test points.

Acoustic power of transformer: With the proposed acoustic representation of power transformers, the total acoustic power W generated by a transformer can be readily evaluated according to

$$W = \sum_1^{N_s} W_i \qquad (12.15)$$

where
  W_i is the acoustic power of the ith point source
  N_s the number of point sources representing the power transformer

In the earlier expression, the generated acoustic power is expressed in watts. It can also be expressed in terms of dB above a reference acoustic power $W_0 = 10^{-6}$ W as

$$W \, (\mathrm{dB}) = 10 \log\left[\frac{W}{W_0} \right] \qquad (12.16)$$

Figure 12.33 presents the typical variations of the generated acoustic power W as a function of the VA rating of the transformer obtained from conventional AN test results. The following observations can be made:

- The generated acoustic power W varies with the mode of operation. It approximately doubles when the transformer changes from the ONAN to ONAF mode. This implies that the contribution from the cooling system to the overall noise is comparable to the noise coming from the transformer core. In Figure 12.33, OFAF refers to forced oil, forced air cooling mode.
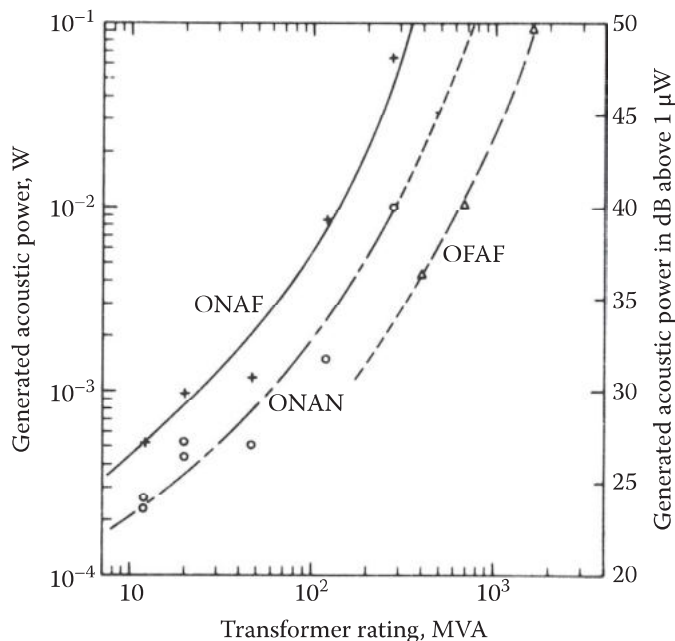

FIGURE 12.33 Variation of the acoustic power with the transformer rating for different modes of operation. (From Trinh, N.G. and Ménard, Y., Audible noise generated by power transformers of a substation—Its influence on the urban noise, Paper A76 473-9, presented at the *IEEE PES Summer Meeting*, Portland, OR, 1976.)

- The acoustic power increases with the VA rating of the transformer at a rate of about 4 dB per doubling of the VA rating. In terms of its absolute value, the generated acoustic power W can be approximately related to the VA rating according to

$$W = A_0 \left(\text{VA} \right)^{1.3} \tag{12.17}$$

where A_0 is a constant, depending on the mode of operation of the transformer.
- Transformers equipped with OFAF (forced oil, forced air) or OFWF (forced oil, forced water) cooling systems have a significantly lower acoustic power, due to their relatively small physical dimensions.

AN level: Once the acoustic power of the N_s sources is determined, the sound pressure P at any point around the transformer can readily be evaluated according to Equation 12.12 and the corresponding AN level according to

$$\text{AN} = 20 \ln \left[\frac{P}{P_{re}} \right] \div \ln 10 \quad \text{with } P_{re} = 2 \times 10^{-5} \text{ N/m}^2 \tag{12.18}$$

Figure 12.31 compares the calculated noise levels with the measurements made around the 325/25 kV–275 MVA transformer. As expected, the agreement improves with increased number of point sources used to represent the acoustic characteristics of the transformer.

12.4.3 Audible Noise in Far Field

It has been shown previously that a large number of point sources may be required to adequately represent the acoustic characteristics of a power transformer. The situation is different when one is interested only in the noise level at large distance from the transformer. With the representation of noise generation by point sources located within the transformer, a distance of several times the main transformer dimension could be considered as far field. Figure 12.34 compares the noise variations in the far field along the main axis of the transformer calculated with different acoustic representations of the transformer. No significant difference is observed among the calculated results beyond a few tens of meters from the transformer. This simplifies considerably the evaluation of acoustic impact of power transformers in a substation on the urban noise environment.

12.5 Standard HV Testing of Power Transformers

A number of tests are prescribed by international standards, ANSI and IEC, to verify the adequacy of power transformers and, in particular, their insulation with respect to the various stresses. For ac voltage, this implies *applied potential* and *induced voltage* tests, and for impulse voltage, it includes *standard impulse, chopped wave,* and *switching impulse* tests. Detailed test prescription and procedures are given in national and international standards (ANSI C57) (IEC 60076-3). These are briefly outlined in the following.

12.5.1 Test with AC Voltage

12.5.1.1 Applied Potential Test

It is carried out on transformers with full (ungraded) insulation. The power frequency test voltage is applied to the terminals of one winding at the time, with the other winding terminals maintained at ground potential.
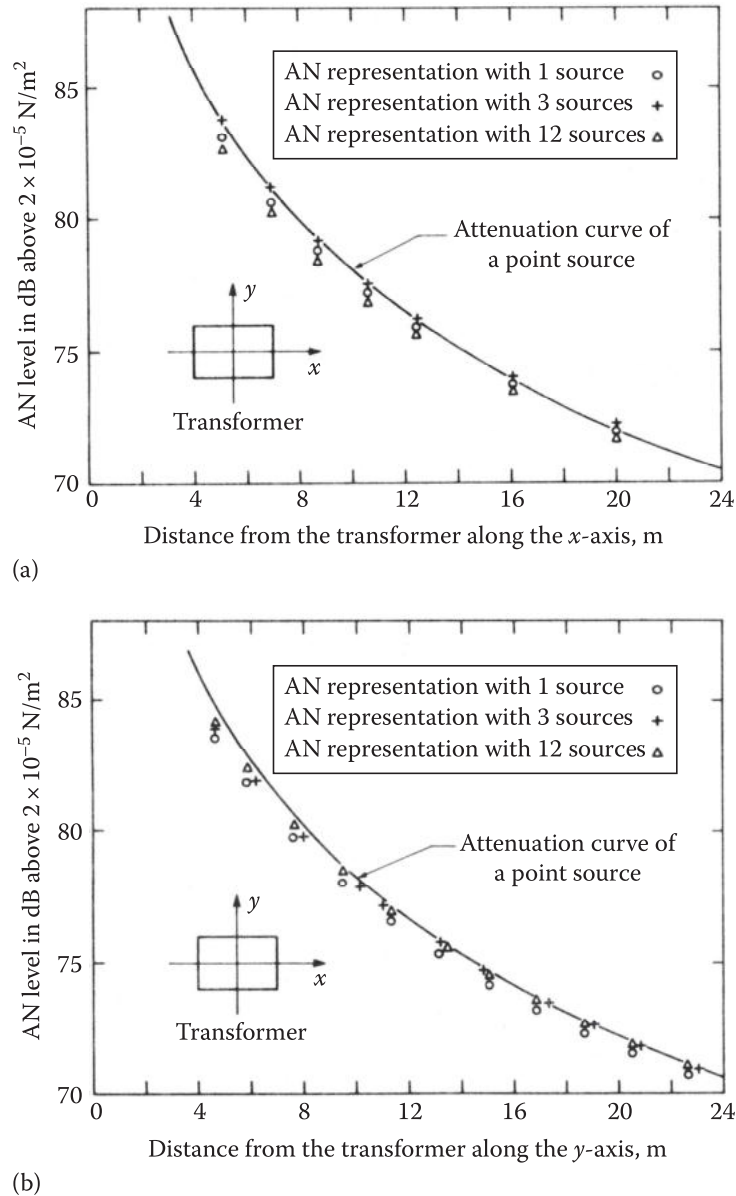
(a)

(b)

FIGURE 12.34 Far-field behavior of AN from power transformer. (a) Variation along the transformer x-axis. (b) Variation along the transformer y-axis. (From Trinh, N.G. and Ménard, Y., Audible noise generated by power transformers of a substation—Its influence on the urban noise, Paper A76 473-9, presented at the *IEEE PES Summer Meeting*, Portland, OR, 1976.)

12.5.1.2 Induced Voltage Test

It is carried out under ac voltage at a multiple of power frequency, to avoid core saturation. The applied voltage is 1.73 p.u. for 7200 cycles, followed by a period of 1 h at 1.5 p.u., during which a PD is monitored and constitutes the base for acceptance.

Measurement of PDs: Figure 12.35 shows the typical circuit for measuring PDs during induced voltage test. It is noticed that in this case, the test voltage is generated by the power transformer itself, its low-voltage winding being energized from the high-frequency ac voltage source. The PD measuring equipment is connected across the HV winding via a series-connected coupling capacitor C_k, which isolates it from the low-frequency HV. It is particularly interesting to note that PDs in voids are sensitive to voltage changes. As a result, a test carried out at a frequency n times the power frequency is equivalent to a test at power frequency n times longer. Two methods for evaluation of PDs are currently followed: measurement of the apparent charge and measurement of the radio influence voltage (RIV), with the former method gaining wider acceptance in recent years. A detailed discussion of the two PD measurement methods is presented in Chapter 14.
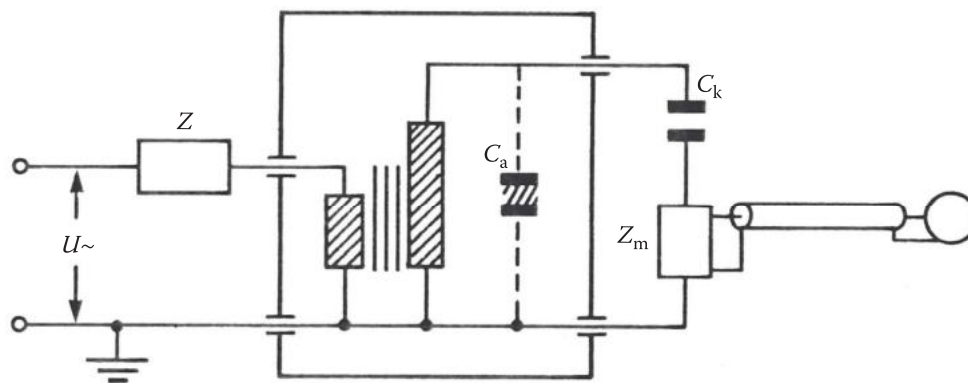
FIGURE 12.35 Circuit for PD measurement during induced voltage test on power transformers.
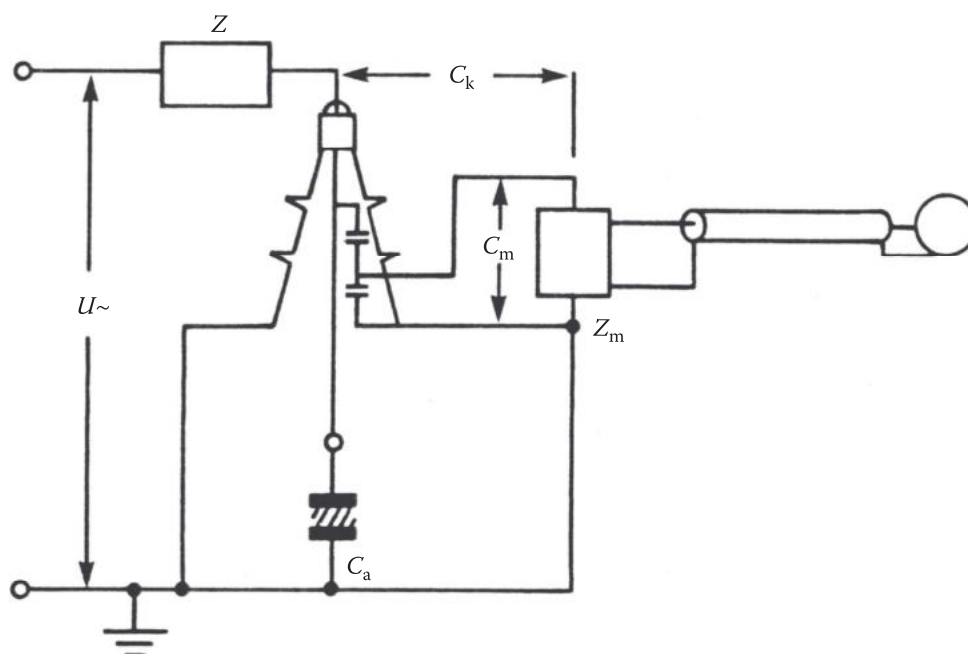

FIGURE 12.36 Circuit for PD measurement using a bushing capacitive tap. (From IEC Publication 60060-2, *High Voltage Testing Techniques, Part 2: Measuring Systems*, 2nd edn., IEC, Geneva, Switzerland, 1994a.)

In testing power transformers, advantage may also be taken of the availability on the bushing of a capacitive tap, which can serve as a coupling capacitor to the PD measuring instrument, as illustrated in the circuit shown in Figure 12.36. This is particularly useful in on-site PD measurement of power transformers.

Location of PD sites: The development of PDs may be accompanied by the generation of acoustic noise, in the form of acoustic pulses, whose frequency spectrum extends up to the ultrasonic range of several kHz. Acoustic pulses propagate across the insulation to impinge on the transformer tank, where they can be detected by means of ultrasonic detectors. The acoustic signals are delayed with respect to the electrical pulse by the traveling time of the acoustic wave from the PD site to the detectors, usually in the range of milliseconds. With several detectors fixed at different locations on the transformer tank and using the electrical PD signal to trigger the measurement of acoustic pulses, it is possible to locate the site of the PDs by means of triangulation.

12.5.2 Impulse Tests

HV impulse generators are used to generate lightning and switching impulses for testing of power transformers. The inductive nature of the transformer and shunt reactors requires particular considerations, principally to obtain the appropriate impulse wave shape, as discussed in the following.

12.5.2.1 Standard Impulse

Reference is made to the circuit of Figure 12.37, which shows the standard circuit for generating a double exponential impulse voltage, to which an inductive load L is connected. The curve of Figure 12.37 shows the variations of the required capacitance of the impulse generator to produce a time to half value of t_{50} of 50 μs (Train, 1981).

It is noticed that the smaller is the load inductance L, the larger will be the capacitance C_g of the impulse generator. Furthermore, for an inductive load of about 7 mH, it will not be possible to obtain an impulse with a time t_{50} of 50 μs. Such a limitation is due to the series-connected front resistor R_f with the inductive load L, which has a unit-step response according to

$$u_L\left(t\right)=u_o\exp\left[-\frac{R_f}{L}t\right] \tag{12.19}$$

It is obvious that the time to half value is determined by the circuit time constant $\tau = L/R_f$, independent of the capacitance of the generator. Reducing the resistance R_f will increase the time to half value of the impulse. However, a small value of R_f will make the circuit oscillate due to the stray inductance of the circuit and sets a lower limit for R_f.

For very low-impedance transformers, some standards allow the addition of a small resistance, 400 Ω or less, in series with the ground terminal, to increase the effective time to half value of the impulse. However, the voltage across the inductive load is considerably reduced and its wave shape significantly modified.

Another circuit that can be used in testing of low-impedance transformers is shown in Figure 12.38, where an inductance L_d is connected in parallel with the front resistor to bypass it after the peak voltage
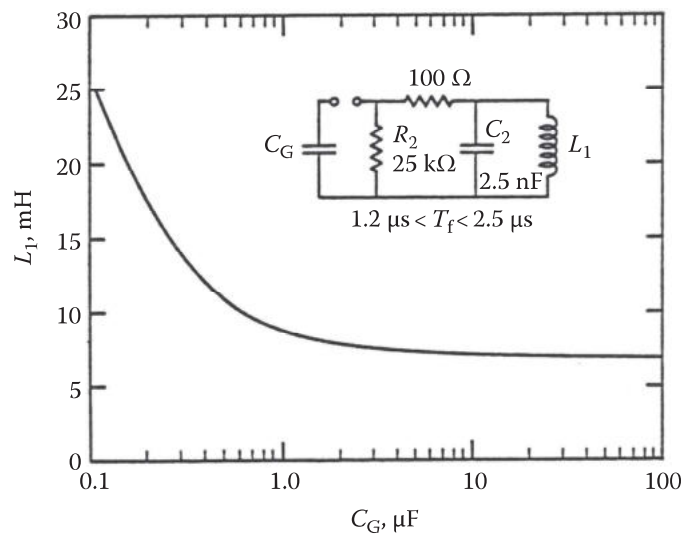

FIGURE 12.37 Variations of the required capacitance of the impulse generator to produce a double exponential impulse with a time to half value of 50 μs for different inductive loads.
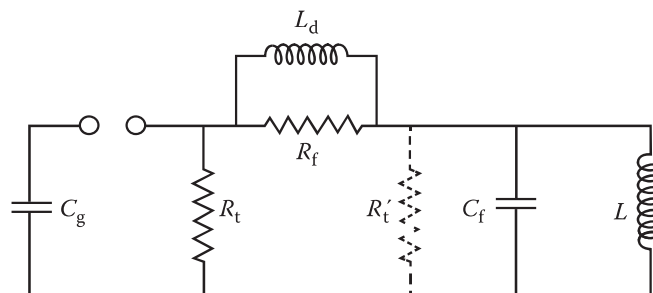

FIGURE 12.38 Circuit for testing low-impedance transformers.

is reached. The time to half value of the test impulse voltage is controlled by the natural oscillating frequency of the circuit:

$$\mathbf{w} = \frac{1}{\sqrt{(L + L_{\mathrm{d}})C_{\mathrm{g}}}} \tag{12.20}$$

and damped by the tail resistor R_{t} (Figure 12.38). The main drawback of this approach is the high energy required by the impulse generator, which may reach several hundreds of kJ.

12.5.2.2 Switching Impulse

The performance of an impulse generator can be conveniently analyzed by means of the single-stage equivalent circuit shown in Figure 12.39a, where C_{g} is the total capacitance of the generator; R_{f} and R_{t} are the wave front and tail resistances, respectively. C_{f} is the total wave front capacitance and L is the inductance of the test object, which, in the case of a transformer, is equal to the magnetizing inductance, since switching surge tests are normally produced on transformers, which have their nonimpulsed terminals open-circuited.

Figure 12.39b shows the required characteristics of the switching impulse for testing power transformer (IEC Standard 60071-1, 1993): the time-to-peak, $T_{\mathrm{p}} \geq 100$ µs. The time T_{90} is defined as the time during which the voltage transient exceeds 90% of the peak value, which should be greater than 200 µs to ensure that the insulation is adequately stressed. T_0 is the time to the first voltage zero on the tail of the wave and shall not be less than 1000 µs.

An analysis of the circuit in Figure 12.38 by Train (Train, 1981) has shown that the Laplace transform of the voltage across the inductance is given by

$$u_{\mathrm{s}} = \frac{U_{\mathrm{c}}}{R_{\mathrm{f}}C_{\mathrm{f}}} \frac{s}{s^3 + s^2 K_1 + s K_2 + K_3} \tag{12.21}$$

where U_{c} is the charging voltage of the impulse generator, and

$$K_1 = \frac{(R_{\mathrm{t}} + R_{\mathrm{f}}) + (R_{\mathrm{t}} C_{\mathrm{g}}/C_{\mathrm{f}})}{C_{\mathrm{g}} R_{\mathrm{t}} R_{\mathrm{f}}} \quad K_2 = \frac{1 + (C_{\mathrm{g}} R_{\mathrm{t}} R_{\mathrm{f}}/L)}{C_{\mathrm{g}} C_{\mathrm{f}} R_{\mathrm{t}} R_{\mathrm{f}}} \quad \text{and} \quad K_3 = \frac{R_{\mathrm{t}} + R_{\mathrm{f}}}{L C_{\mathrm{f}} C_{\mathrm{g}} R_{\mathrm{t}} R_{\mathrm{f}}}$$

Appropriate charts are also produced for the selection of various circuit parameters so that the switching impulse will meet the specified characteristics. Figure 12.40 permits the test engineer to rapidly evaluate the value of the wave front capacitance required for any value of the inductance L of the test object and the impulse generator capacitance C_{g}. The figure also shows the circuit efficiency. The values selected must lie to the right of line a–b; otherwise, the time T_{90} will be less than 200 µs. Also, the
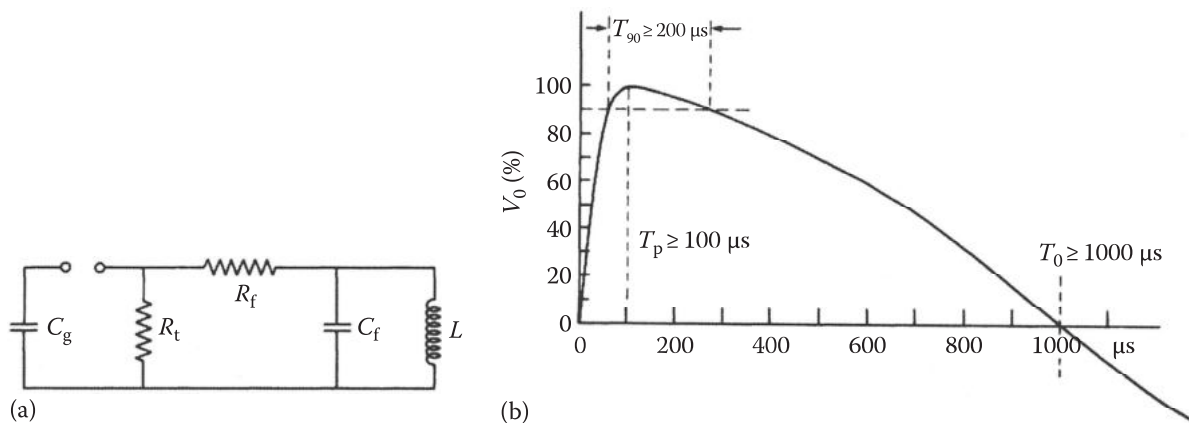

FIGURE 12.39 Equivalent circuit and required wave shape for switching impulse test on shunt reactors and power transformers. (a) Equivalent test circuit. (b) Standard switching impulse requirements. (From Train, D., *IEEE Trans. Power Appar. Syst.*, PAS-100(6), 3125, 1981.)
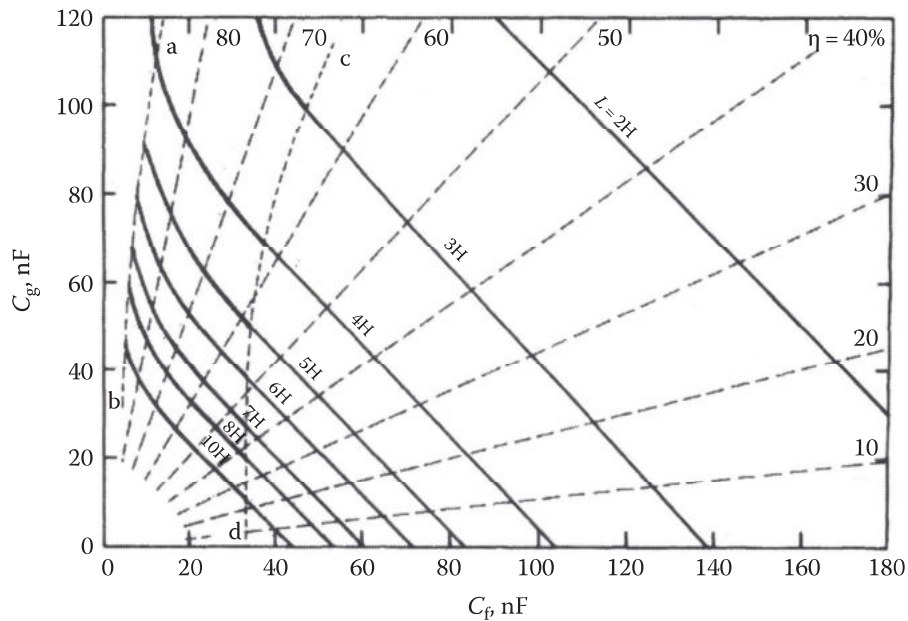
FIGURE 12.40 Test circuit characteristics for the selection of the wave front capacitance C_f. (From Train, D., *IEEE Trans. Power Appar. Syst.*, PAS-100(6), 3125, 1981.)

values selected must lie to the left of line c–d; otherwise, the overshoot will exceed the 90% level. Thus, the effective working zone lies between the lines a–b and c–d.

Having found the value of the wave front capacitance, the wave front resistance R_f can be selected from Figure 12.41, which shows the variations of T_p with the time constant T_{rf} defined as

$$T_{rf} = R_f C_{eq} = R_f \frac{C_g C_f}{C_g + C_f} \tag{12.22}$$

where C_{eq} is the equivalent capacitance:

$$C_{eq} = \frac{C_g C_f}{C_g + C_f}.$$

For a given value of T_p, one can obtain the corresponding value of the time constant T_{rf} and calculate the appropriate value of R_f; for example, for $T_p = 100$ μs, the time constant T_{rf} is 20 μs.
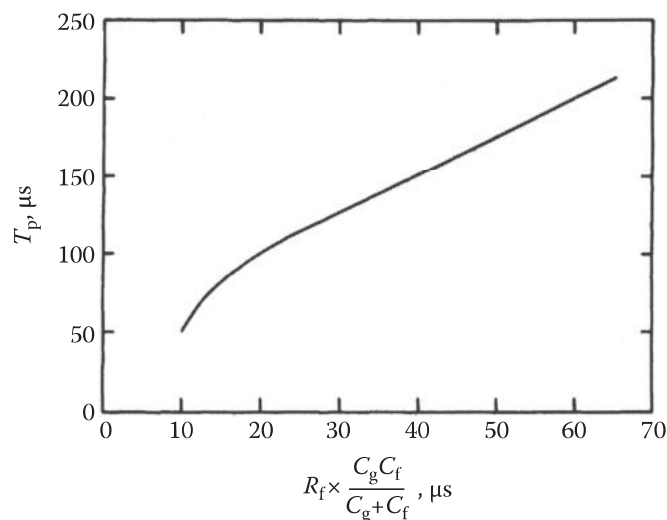

FIGURE 12.41 Influence of the wave front time constant, T_{rf}, on the time-to-peak, T_p. (From Train, D., *IEEE Trans. Power Appar. Syst.*, PAS-100(6), 3125, 1981.)
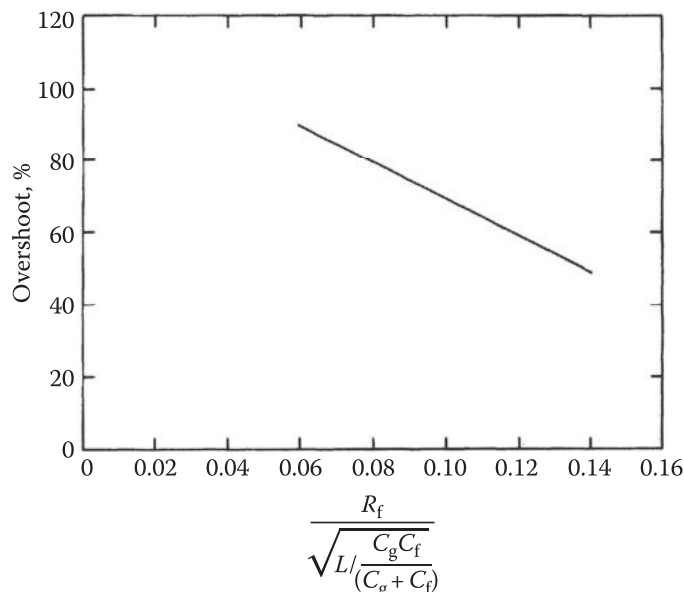
FIGURE 12.42 Influence of the damping factor on the overswing of the generated switching impulse. (From Train, D., *IEEE Trans. Power Appar. Syst.*, PAS-100(6), 3125, 1981.)

Figure 12.42 shows the effect of the circuit damping factor, $a = R_f / \sqrt{L/C_{eq}} = R_f / \sqrt{L\left(C_g + C_f\right)/C_g C_f}$, on the overswing of the generated switching impulse, expressed as a percentage of the maximum test voltage at T_p. The overswing should be less than 90%. A too high value of the overswing may require increasing the wave front resistance R_f and, hence, a longer time-to-peak T_p.

Finally, Figure 12.43 shows the influence of the ratio $C_g/\left(C_g + C_f\right)$ on the time T_{90} during which the voltage transient remains above the 90% level. It should be pointed out that using the results of Figure 12.40 and Figure 12.43, values of T_{90} in the range of 200–256 μs are obtained.

As described earlier, the switching impulse test is made by discharging the impulse generator into the HV winding of an open-circuited transformer. The load inductance seen by the impulse generator is equal to the magnetizing inductance of the transformer and may be very high, usually above 100 H.
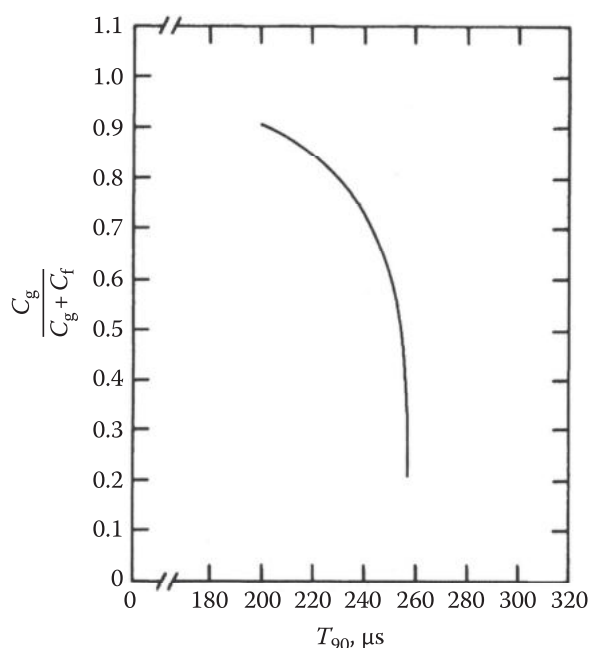

FIGURE 12.43 Influence of the ratio $C_g/\left(C_g + C_f\right)$ on the time T_{90}. (From Train, D., *IEEE Trans. Power Appar. Syst.*, PAS-100(6), 3125, 1981.)

The equivalent circuit shown in Figure 12.39 can still be used to evaluate the performance of the test circuit, however, with appropriate change in the values of

- The front capacitance: $C_f = C_f' + C_t$, with C_f' as the external load capacitance and C_t as the surge capacitance of the transformer winding
- The inductance of the test object: $L = L_m \gg L_1 + L_2$, with L_1 and L_2 as the leakage inductances of the primary and secondary windings, respectively

Typical waveforms obtained during switching impulse tests on transformers are illustrated in Figure 12.44 and summarized in Figure 12.44d. In this figure, curve 1 indicates the waveform normally obtained. T_0 is very long in the absence of core saturation, typically 4000–5000 μs. In addition, the time T_{90} is also very long compared to the minimum required value of 200 μs. This results in prolonged overstressing of the insulation.

Magnetic saturation of the core frequently occurs, and the voltage will drop very rapidly as shown by the curve 1a of Figure 12.44c and d. When higher voltages are applied, core saturation will occur earlier as shown in curve 2 of Figure 12.44d. It is therefore impossible to have identical oscillograms at reduced and full test values. The core saturation can be minimized by magnetically biasing the core in the reverse

(a)   1425 kV 500 μs/div.

(b)   1000 kV 500 μs/div.
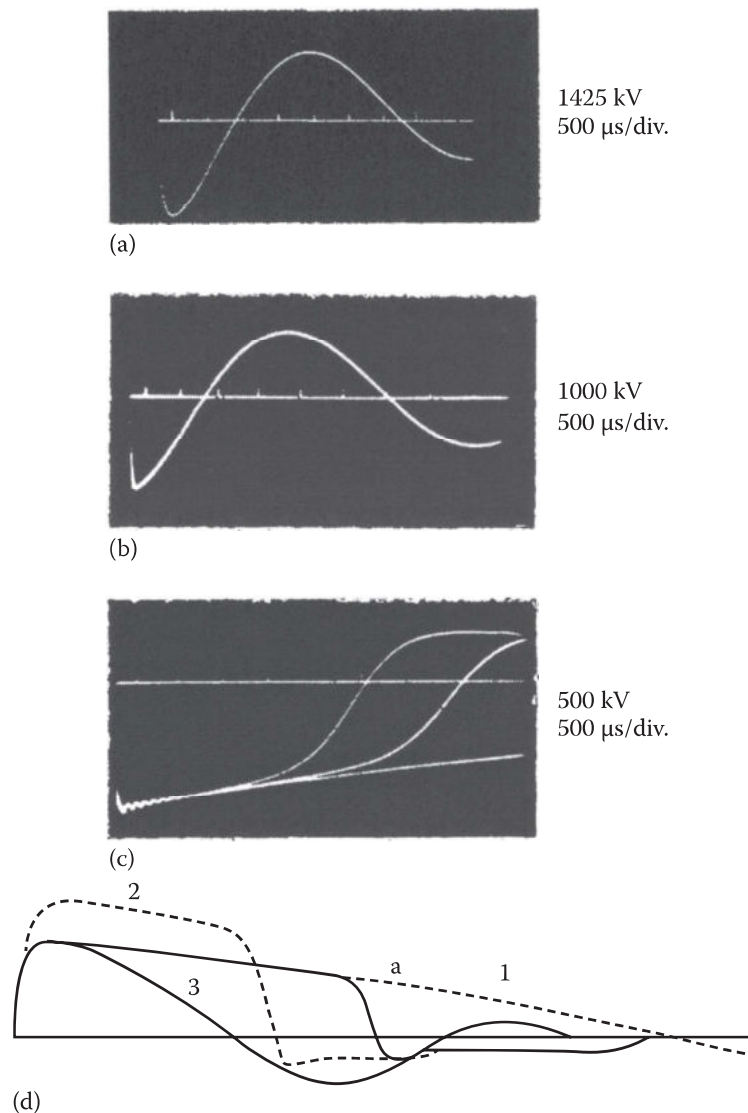
(c)   500 kV 500 μs/div.

(d)

FIGURE 12.44 Typical waveforms obtained during switching impulse tests on power transformers. (a), (b) and (c) Switching impulse wave forms at different voltage levels. (d) Schematic description of the effect of voltage level on impulse waveform. (From Train, D., *IEEE Trans. Power Appar. Syst.*, PAS-100(6), 3125, 1981.)

direction before applying the test voltages. This is usually obtained by either circulating a dc current through the winding or applying an impulse voltage of opposite polarity.

The duration of the test voltage on the transformer can be reduced if a low-inductance reactor is connected in parallel with the HV winding of the transformer. Curve 3 of Figure 12.44d shows the waveform that can be obtained with such an arrangement. A practical application of this approach may take advantage of the fact that

- Voltages are transferred according to the turn ratio under switching impulse conditions
- Most power transformers are provided with tertiary winding, having voltage ratings in the range of less than 20 kV

A compact air core, low-inductance coil can be used for this purpose, for example, a 735 kV transformer having a 9.6 kV tertiary winding has a turn ratio of 44.2; an inductance of 5 mH, connected to the tertiary winding, will have an effective value of 9.8 H when transferred to the HV winding.

Finally, the effective surge capacitance as seen by the impulse generator is not necessarily the capacitance of one phase only, since the other two phases may have voltage induced in them, depending on the arrangement of the tertiary windings. The surge capacitance can be determined from energy considerations by assuming that an equivalent capacitance stores the same amount of energy at the full test voltage. Figure 12.45 gives the equivalent capacitances for various arrangements of the tertiary windings.
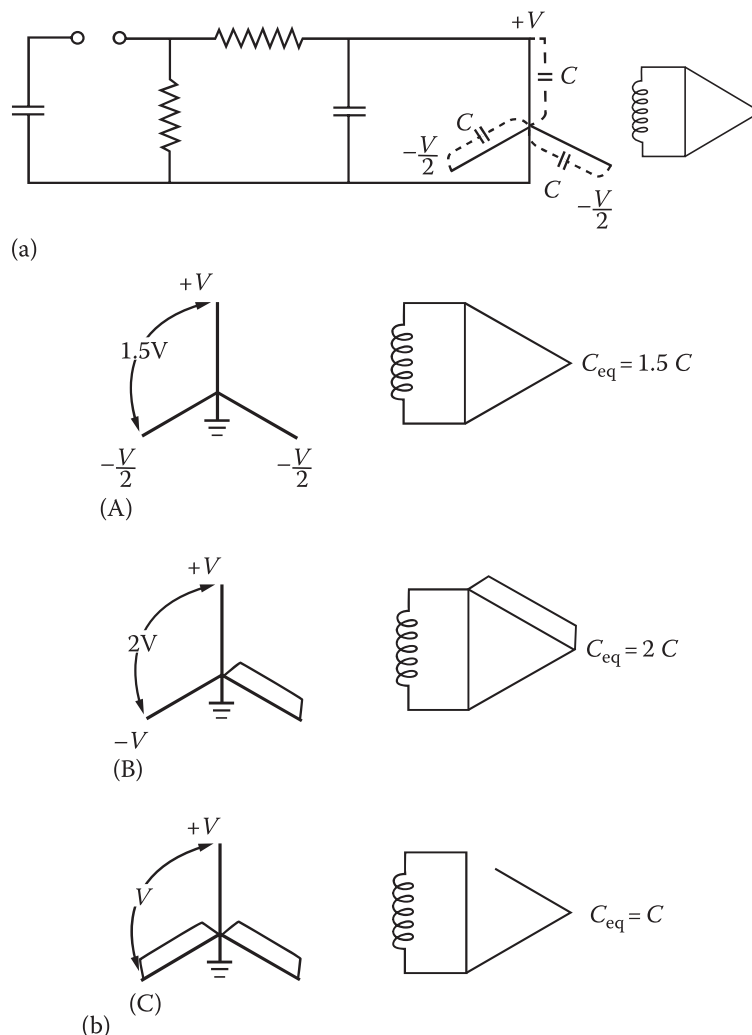

FIGURE 12.45 Equivalent surge capacitances for various arrangements of the tertiary windings. (a) Equivalent circuit. (b) Typical arrangements of the tertiary windings. (From Train, D., *IEEE Trans. Power Appar. Syst.*, PAS-100(6), 3125, 1981.)

12.5.2.3 Chopped Wave

It is produced by connecting a spark gap, usually sphere gap, across the winding tested. By adjusting the distance between the sphere electrodes, the gap will flashover, producing an impulse wave chopped at the appropriate time. Natural flashover voltage of spark gaps may have a dispersion in the flashover voltage and, hence, results in variations of the time to chop in the order of microseconds. This is unacceptable for testing of power transformers, which requires a variation of less than 0.1 μs in the time to chop, to obtain reproducible oscillograms for fault detection. A solution to this problem is in the use of triggered spark gaps, which may be connected in series to meet the required test voltage. Details of this solution are given in Chapter 14.

12.5.3 Detection of Failure during Impulse Tests

Dielectric tests on power transformers sometimes result in failure of the transformer insulation. However, due to the relatively small energy of the test source, these failures do not always result in a complete collapse of the test voltage, but are limited to local breakdown of the winding insulation: turn-to-turn or layer-to-layer failures, with partial collapse in the test voltage. Partial failure of the winding also changes its impedance and, hence, affects the impulse current as measured in the ground circuit. Detection of failures occurring in dielectric tests is currently done by comparing oscillograms of the test voltages and currents made at reduced and full voltage and looking for minute changes in the recorded waveforms. Figure 12.46 compares such oscillograms of voltage and current for the case of a partial failure of the test winding and illustrates this approach.
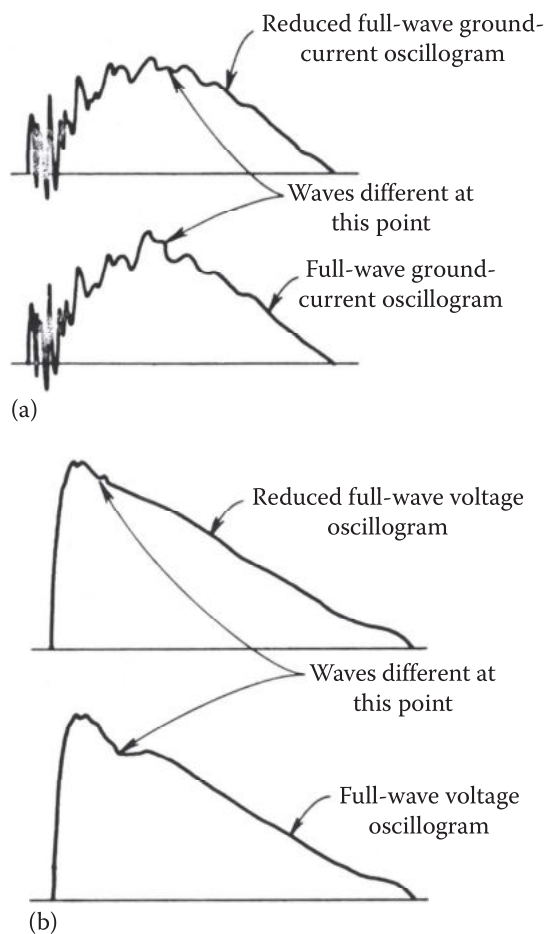

FIGURE 12.46 Comparison of impulse voltage oscillograms and ground currents to identify partial failure of transformer winding in dielectric tests. (a) Current signals. (b) Voltage signals. (From Bean, R.L. et al., *Transformers for the Electric Power Industry*, McGraw-Hill Book Co., New York, 1959.)

Practical experience shows that voltage oscillograms are sensitive to detect most of the disturbances, while oscillograms of ground current are sensitive to certain types of failure. Disturbances occurring during tests with chopped wave are more difficult to detect from the oscillograms. For these reasons, the procedure in all standard impulse tests is

- To apply a reduced full wave test, between 50% and 70% of the test level, at the start of the impulse tests
- To perform the full wave test at the end

Any partial failure occurs during the tests; it will usually appear as a difference in the oscillograms at reduced and full wave voltages.

Digital transient recorder: Important progress has been made in recent years by the introduction of digital transient recorders sufficiently performing for the measurement of fast transient signals. The recorded digital data offer the advantage that they can be processed to provide information otherwise impossible with analog signal:

- Reconstruction of the impulse signal deformed by the HV measuring system (Malewski, 1982)
- Determination of the transfer function of the test specimen, which can then be used to detect any change in the transfer function, resulting from partial failure during dielectric test (Malewski and Poulin, 1988; Freyhult and Carlson, 1991)

12.6 Aging and Incipient Faults

Operating power transformers subject their insulation to aging and development of incipient faults, which eventually can cause failure.

12.6.1 Aging Mechanism

Several aging processes are present in power transformers, namely, thermal, electrical, and environmental aging. They will be discussed in the following.

12.6.1.1 Thermal Aging

When oil–paper insulation is subjected to thermal stress, irreversible damage may be produced in both the oil and paper components of the insulation. The overall effect is a reduction of the mechanical and dielectric performance of the insulation with time.

Arrhenius relation: The life of varnish cloth subjected to a constant thermal stress, investigated by Montsinger in 1930 (Montsinger, 1930), was among the first studies of thermal aging. In this study, the aging state of the insulation was characterized by the residual tensile strength of the paper. The time required for the insulation to reach a given aging state follows an empirical equation

$$T = A\exp\left(-m\theta\right) \tag{12.23}$$

where
  T is the life time
  A is the initial state of the insulation
  m is a constant
  θ is the temperature in °C

Montsinger found that while the initial tensile strength was characteristic of the insulation system, the parameter m was relatively constant and amounts to $m = 0.088$ for the various insulation systems evaluated.

This results in the now familiar *8 degrees* rule, which states that *the thermal life of an insulation system is reduced by half for each 8°C increase in the operating temperature* (values between 7°C and 10°C have been used in actual practice).

In 1948, Dakin proposed the Arrhenius's chemical rate theory to explain thermal degradation (Dakin, 1948), by noting that the physical changes observed during thermal aging are reflections of internal chemical changes. Thermal aging of paper breaks the chemical bonds of the cellulose molecules, which results in a lower *DP* and a loss of mechanical properties, for example, the paper becomes brittle as a result of the reduced tensile strength. A more descriptive expression of the insulation life was derived:

$$T = A\exp\left(\frac{B}{\theta}\right) \tag{12.24}$$

where

T is the life time
θ is the temperature in K
A and B are constants determined by the activation energy of the particular chemical reaction responsible for thermal aging

Taking the logarithm of both sides yields

$$\ln T = \ln A + \frac{B}{\theta} \tag{12.25}$$

Thus, if one plots the logarithm of the insulation life against the reciprocal of the absolute temperature, the resulting graph is a straight line, often known as the Arrhenius life curve as illustrated in Figure 12.47, which compares the experimental results obtained by Dakin, Clark, and Montsinger (Dakin, 1948).

12.6.1.2 Electrical Aging

Oil–paper insulation subjected to a relatively uniform field has a well-defined dielectric strength, typically 30 kV/mm under ac voltage and 110 kV/mm under lightning impulses. When exposed to a constant electric field over a long period of time, the insulation will age and gradually loses its dielectric strength. The electrical life *T* of the insulation system varies according to the empirical *inverse power law* (Nelson, 1972; Kiersztyn, 1981):

$$T = A\frac{1}{U^n} \tag{12.26}$$

where

U is the applied voltage in p.u.
A is the nominal life expectation of the insulation system at 1 p.u.
the exponent n has a value between 6 and 12

Taking the logarithm of both sides in the earlier Equation 12.26 yields

$$\ln T = \ln A - n\ln U \tag{12.27}$$

which indicates a linear relationship between the logarithms of the life expectation *T* and the applied voltage *U*.

Attempts to formulate a theory for electrical aging (Kiersztyn, 1981) have not been conclusive. The reason appears to be that failure of the insulation system at HVs may not follow the same mechanism
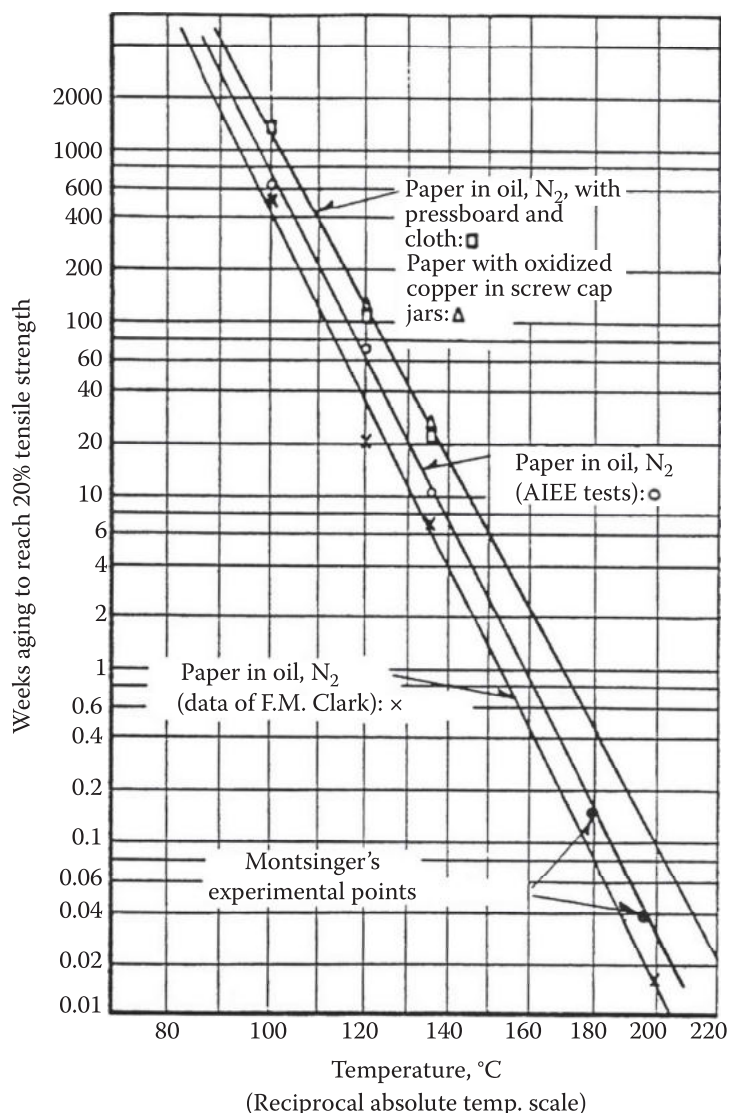
FIGURE 12.47 Thermal aging—Arrhenius curves. (From Dakin, T.W., *AIEE Trans.*, 67(Part I), 113, 1948.)

active at lower voltages. Different breakdown mechanisms have effectively been identified in oil–paper insulation and discussed in Chapter 6:

- The direct breakdown by streamers burst at relatively short time under high field.
- Breakdown initiated by particle contamination at lower field intensities.
- Incipient faults developing at operating field intensities and involving intense PDs developing either in the bulk oil volume or at the oil–paper interface. One of the mechanisms for PD development in oil is via the formation of gas bubbles (Kao and McMath, 1970). Due to the difference in the dielectric constants of gas and oil, gas bubbles are subjected to higher field intensity than the surrounding oil, by a factor equal to their relative dielectric constants, typically 2.2. This local field enhancement, combined with the lower ionizing potential of gases, makes the bubbles the weak link in oil and oil–paper insulation, particularly favorable to PD development. The phenomenon is strongly affected by the gas content in the oil, since higher gas content favors the formation of gas bubbles.

12.6.1.3 Environmental Aging

During normal operation, the insulation of power transformers may experience environmental changes, which affect their dielectric performance. The most common of these changes is due to ingress of

moisture and air. Particles may also be generated or accidentally introduced. Both aspects are well recognized today by utilities and manufacturers (Boisdon et al., 1994).

Moisture increases the rate of degradation (Fournié, 1990). The effect may be partly attributed to the fact that water is released from paper during thermal aging and helps to further enhance the process (Fabre and Pichon, 1960).

Carbon particles result from oil and paper decomposition by PDs or carbonization at hot spots in the insulation system, for example, winding joints and core, and may be generated over the service life of the transformer.

Environmental aging is rarely the direct cause of failure of the insulation; it generally enhances other active aging processes such as thermal and electrical aging. It also triggers a number of changes in quality control, manufacturing processes, and maintenance practices; all contribute to minimize its impact and improve the dielectric performance of the equipment. These aspects will be discussed in the following.

Oxygen and air: The presence of oxygen (or air) causes oxidation of the transformer oil and accelerates the degradation of oil–paper insulation in power transformers. The process may be attributed to the oxidation by-products of the oil (Shroff and Stannett, 1985). The paper degradation rate may be tenfold higher in the presence of oil when compared to chlorine-impregnating liquids. The process also consumes oxygen so that, unless there is a constant supply of oxygen, the effect will eventually die out. Laboratory tests on reduced-scale transformer models (Fournié, 1990) show that the area of the air–oil interface has a definite effect on the aging rate. Replacing air by nitrogen also reduces the aging process by as much as 30% over the temperature range of 110°C–140°C. These results tend to indicate that the influence of oxygen is more pronounced in free-breathing transformers than in sealed units, due to the continuous diffusion of oxygen from ambient air into the oil–paper insulation. However, the diffusion process is complex and difficult to evaluate. Aging is estimated to be 1.6–2.5 times faster in free-breathing transformers than in sealed units (Bouvier, 1977; Murray et al., 1982).

12.6.1.4 Decomposition By-Products

Hot spots, PDs, electric arc, etc., due to their higher temperatures, can degrade the insulating oil to a higher degree and produce decomposition by-products that are specific to the insulating fluid:

- Low-level PDs produce large amounts of hydrogen H_2 with a small amount of methane CH_4.
- Overheating of the oil produces ethylene C_2H_4, while arcing in oil generates acetylene C_2H_2.
- By-products associated with PDs and hot spots involving H_2O, CO_2, CO, and carbon, and recently furans (furfuraldehydes), are related to paper degradation.

12.6.2 Assessment of the Actual State of the Insulation

From the application point of view, the most straightforward way to determine the aging state of an insulation system is from its residual dielectric performance. However, this approach has two major drawbacks: the necessity of performing HV tests on-site and the risk of damaging the equipment in doing so, even at reduced test levels. For these reasons, assessment of the aging state of the oil–paper insulation is generally obtained by

- Physical–chemical tests on the oil and paper components
- Nondestructive dielectric tests on the equipment, for example, measurement of power loss, PDs, and more recently transfer function of the windings

12.6.2.1 Measurement of Bulk Parameters

Capacitance and insulation loss factor tan δ, sensitive to thermal aging, and PD level, that may lead to incipient faults, are currently used to evaluate the insulation state of HV transformers. Although feasible in terms of methods of measurement and test equipment, on-site measurement of insulation

loss factor tan δ and PDs requires temporary removal of the equipment from the system, a situation not always acceptable to utilities, which have to deal with the unavailability of the transformer under investigation.

Online monitoring of power losses and PDs is a viable alternative. It requires that measuring devices, such as capacitive coupling and current probe, be added to the equipment. It is a formidable task unless it has been foreseen from the moment the equipment is purchased, a condition not always met in practice. As a result, the most frequently used methods to assess the actual state of the insulation system rely on the measurement of the decomposition by-products that can be obtained from samples of the insulating oil used.

12.6.2.2 Measurement of Physical–Chemical Characteristics of the Insulation Components

Aging of the insulation changes the physical–chemical properties of the insulation and produces decomposition by-products that can be detected by measurements made on the components of the insulation: oil and paper.

Characterization of oil: Aging of transformer oil is caused mainly by oxidation, which gradually degrades the oil, eventually making it unsuitable for service (Lamarre et al., 1987). Its dielectric and physical properties, such as breakdown strength, conductivity, dissipation factor, and interfacial tension, are affected by the oxygen-containing compounds with functional groups such as aldehydes, ketones, alcohols, phenols, peroxides, and carboxylic acids, which are more polar than the parent hydrocarbons (Lamarre et al., 1987). The degree of oxidation of transformer oil is usually determined by its soluble acidity, peroxide contents, and interfacial tension.

Oxidation of transformer oil is an autocatalytic phenomenon involving hydroperoxides that can be prevented by adding inhibitors, typically DBPC or DBP, to decompose the peroxide (Lamarre et al., 1987). However, in this process, the inhibitors are gradually destroyed, and their effect will therefore cease as soon as all the added inhibitors are destroyed. Sharp increases in the soluble acidity and polar compounds accompanied by a sharp drop in the interfacial tension occur when the DBPC is depleted. Sludge formation begins shortly after, accompanied by a reduction in the dissolved copper and followed by saturation of the oil with oxidation by-products.

Current practices aiming at keeping the oil free of soluble acidity would require reclaiming before complete depletion of the inhibitors (Lamarre et al., 1987) to avoid irreversible degradation of the oil due to the nonacid compounds, which are not eliminated by the reclaiming process. Removal of sludge by filtration (Lamarre et al., 1988) temporarily restores the oil that, however, takes less time to become oxidized.

Characterization of paper: As dry Kraft paper is heated above 100°C, its chemical bonds are readily broken, reducing the *DP*, which corresponds to the average number of glucose rings in the cellulose molecule. This is a direct measure of the aging state of the paper since it corresponds to the mechanical strength of the paper. This direct approach has a drawback in that it requires access to critical locations in the paper insulation inside the transformer. As a result, alternate means have been developed to measure *DP* indirectly by evaluating the changes in physical–chemical and dielectric properties of the oil–paper insulation.

CO and CO_2 dissolved in oil are most often measured since a direct correlation exists between their contents and the *DP* of the paper insulation. Figure 12.48 shows the variations in the residual tensile strength and *DP* as a function of the content of CO and CO_2 dissolved in the oil (Yoshida et al., 1987). One notices the strong correlation between the gas content and the *DP* of the paper, as the two curves almost coincide with one another. However, CO and CO_2 are not exclusive to paper; as a result, there has been an increasing interest to find new tracers, uniquely related to the degradation of paper.

Furans, being such candidates, are gaining importance in evaluating paper insulation aging. Figure 12.49 shows variations in the furfuraldehyde content of paper as a function of *DP* (Burton et al., 1984; Shroff and Stannett, 1985). It can be seen that a monotonic relationship exists, which allows the degree of aging of the paper to be estimated by measuring the furan content in the oil.
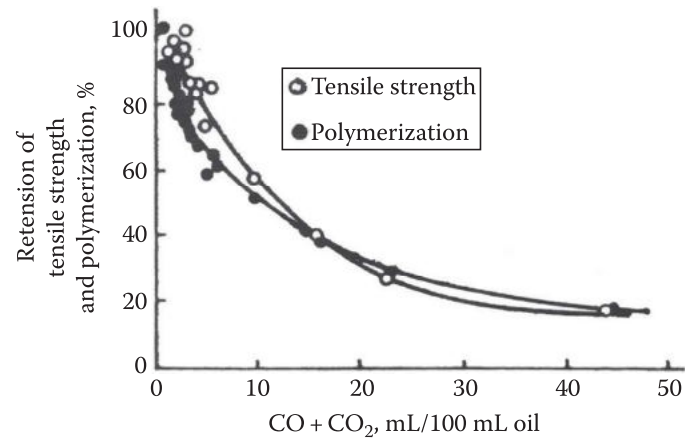
FIGURE 12.48 Correlation between the content of dissolved CO and CO_2 in oil and the *DP* of Kraft paper. (From Yoshida, H. et al., *IEEE Trans. Electr. Insul.*, EI-22(6), 795, December 1987.)
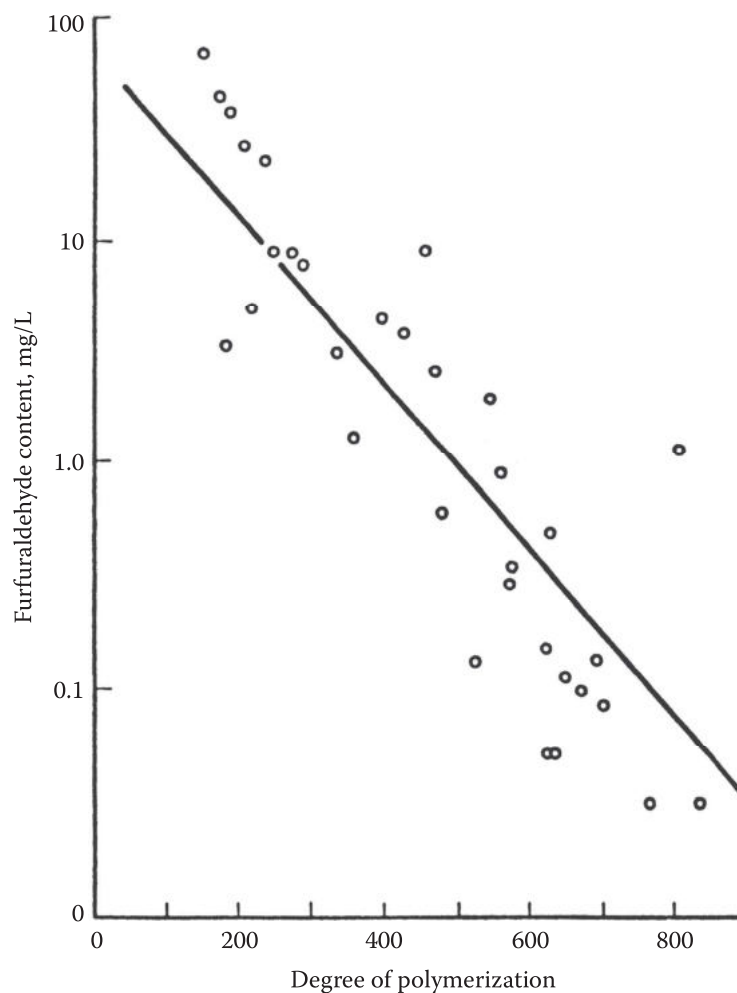

FIGURE 12.49 Correlation between the furan content dissolved in oil and the *DP* of the Kraft paper. (From Shroff, D.H. and Stannett, A.W., *IEE Proc.*, 132(Part C, 6), 312, November 1985.)

Correlation of the dielectric parameters to aging of the paper insulation has not been as successful. This is illustrated by the results in Figure 12.50, which shows variations in the dissipation factor tan δ of the oil with *DP*. Although a general increase in tan δ was observed with a lower *DP*, the dispersion of the results does not allow a clear correlation between the two parameters (Shroff and Stannett, 1985).

Characterization of oil–paper insulation: The tacit assumption here is that there is a correspondence between the aging state of the insulation system as a whole and that of its two constituent components.
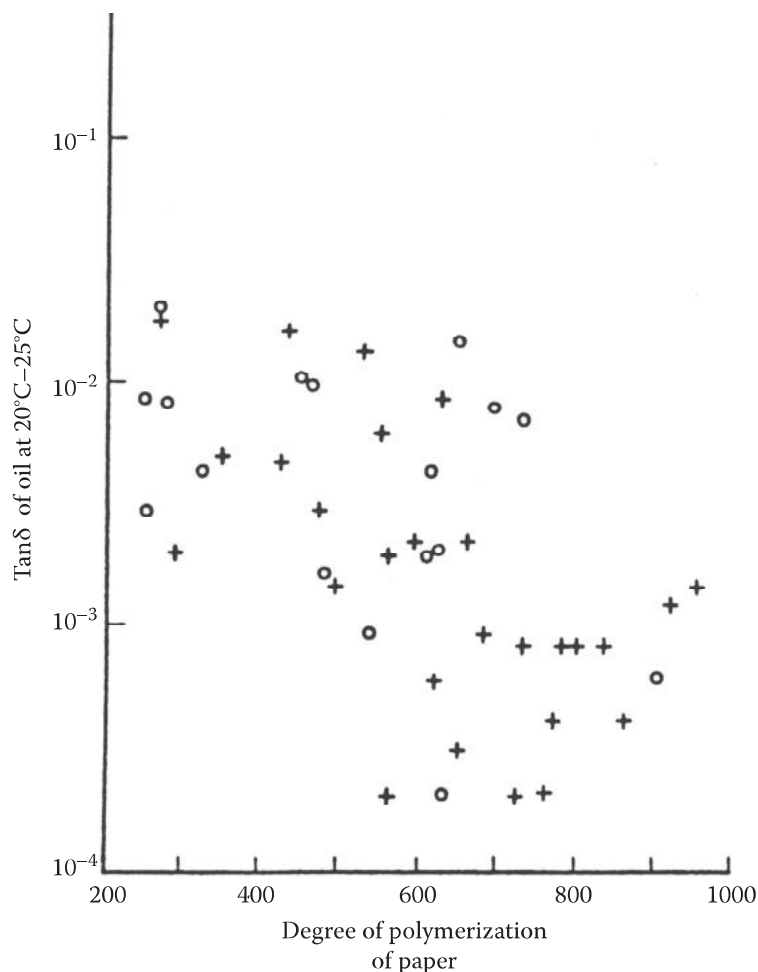
FIGURE 12.50 Correlation between power loss factor tanδ of oil–paper insulation and the *DP* of the Kraft paper. (From Shroff, D.H. and Stannett, A.W., *IEE Proc.*, 132(Part C, 6), 312, November 1985.)

While this assumption seems reasonable, the actual relationship between the various aging states is still to be determined for each individual insulation system. This is illustrated by the results in Figure 12.51, which compares the variations in the residual tensile strength, *DP*, and the dielectric breakdown strength of insulating paper retrieved from power transformers as a function of their time in service (Yoshida et al., 1987). It can be seen that while significant changes occurred in both the tensile strength and *DP* of the paper, only a marginal reduction in its breakdown strength was observed over the 30 years of time period.

12.6.2.3 Nondestructive Tests

PD detection and tan δ measurements provide alternative means of directly evaluating the aging state of the transformer insulation. However, the correlation with the dielectric insulation state and, hence, the remaining life of the paper insulation remains difficult and so far has not been established.

12.6.2.4 End of Life

Because of the presence of different aging processes active simultaneously during the service life of power transformers, there is not a unique definition for end of life of the insulation, but each aging process may define an end of life for a component of the insulation system.

Oil: Complete oxidation of the oil is usually assumed when the soluble acidity reaches saturation, corresponding to an acidity index of 0.2 mg KOH/g oil. However, it is of current practice to delay the oxidation of the oil by the addition of inhibiting additives such as DBPC. The useful life of the oil corresponds to the depletion time of the inhibitors (DBPC). The oil is then due for reclaiming, although oxidation is still below saturation.
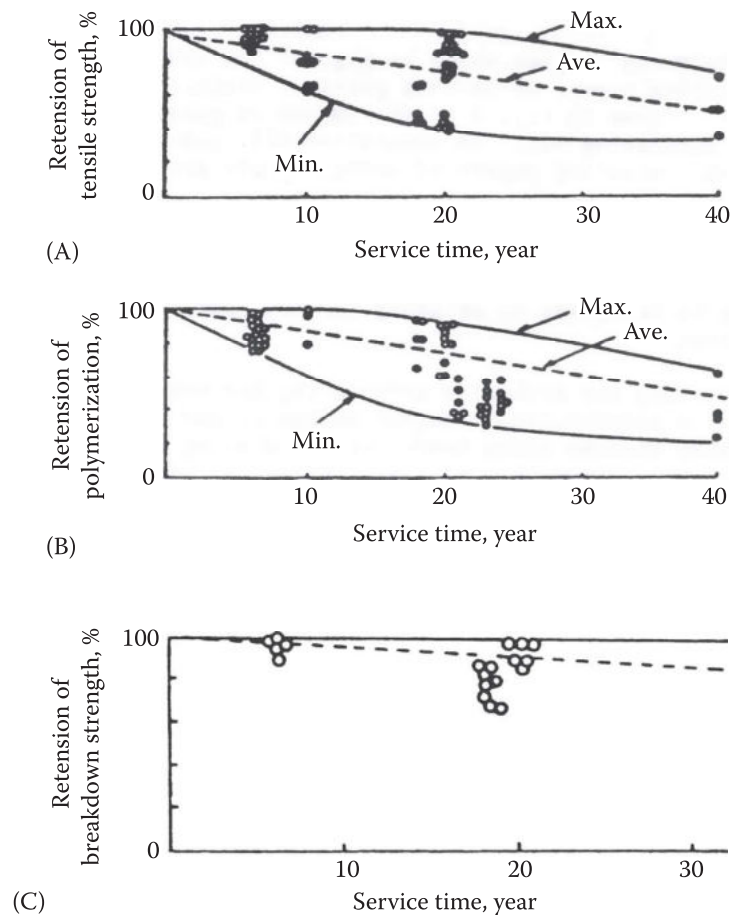
FIGURE 12.51 Variations of the residual performance with time in service. (A) Residual tensile strength to traction. (B) Residual degree of polymerization *DP* and (C) Residual dielectric performance of the oil-paper insulation of a transformer. (From Yoshida, H. et al., *IEEE Trans. Electr. Insul.*, EI-22(6), 795, December 1987.)

This is illustrated by the results of an accelerated oxidation test in Figures 12.52 and 12.53, showing variations in soluble acidity and peroxide contents of naphthenic and paraffinic oils as a function of oxidation time (Lamarre et al., 1987). Abrupt changes in the soluble acidity and peroxide contents were observed at the end of the induction period when the DBPC inhibitor was used up, followed shortly afterwards by the formation of sludge before oxidation reaches saturation.

Paper: For paper insulation, end of life is generally defined as the degradation stage when the paper has lost half of its mechanical strength, often measured by the tensile strength. Alternately, the end of life of paper insulation can also be related to its limit *DP*, typically 100–250. Figure 12.54 shows variations in tensile strength as a function of the *DP* of Kraft paper in free-breathing and nitrogen-blanketed transformers (Dakin, 1948). It can be seen that a linear relationship exists between these two parameters, and as the paper ages, the tensile strength is reduced proportionally with *DP* to a critical value of $DP_l = 100$–250 (Shroff and Stannett, 1985), where abrupt changes in the tensile strength are observed. The limit value DP_l corresponds to a fully aged paper, which has lost all its mechanical properties. Although there is no equivalent reclaiming process available for the paper, utilities can still extend the useful life of aged power transformers by moving them to locations with less operating stresses in the system.

Insulation system: The service life of power transformers is not a well-defined parameter, in part due to the lack of correspondence between the molecular structure of cellulose and its mechanical properties, on one hand, and the electrical properties of the oil–paper insulation on the other. Very few data actually are available on the dielectric performance of power transformers with aged insulation (Trinh et al., 1984; Campbell, 1991). Operating experiences have provided examples of transformers that are kept in operation even if their paper insulation has become brittle, normally an indication of aging beyond all reasonable limits. In practical terms, utilities would rather continue to operate the equipment until the
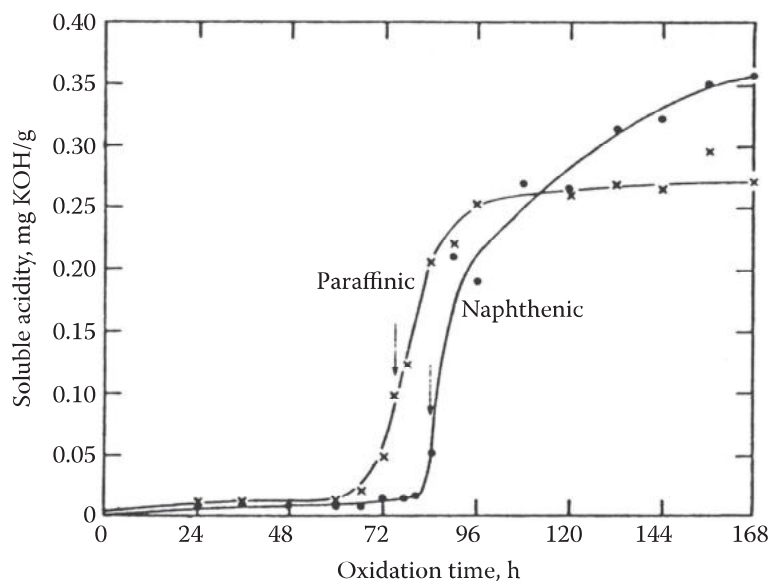
FIGURE 12.52 Variations of soluble acidity in naphthenic and paraffinic oils as a function of oxidation time. (From Lamarre, C. et al., *IEEE Trans. Electr. Insul.*, EI-22(1), 57, February 1987a; Lamarre, C. et al., Antioxidant functionality in liquid and solid materials, in *CIGRE Symposium*, Report No. 900-05, Vienna, Austria, May 1987b.)

FIGURE 12.53 Variations of peroxide content in naphthenic and paraffinic oils as a function of oxidation time. (From Lamarre, C. et al., *IEEE Trans. Electr. Insul.*, EI-22(1), 57, February 1987a; Lamarre, C. et al., Antioxidant functionality in liquid and solid materials, in *CIGRE Symposium*, Report No. 900-05, Vienna, Austria, May 1987b.)
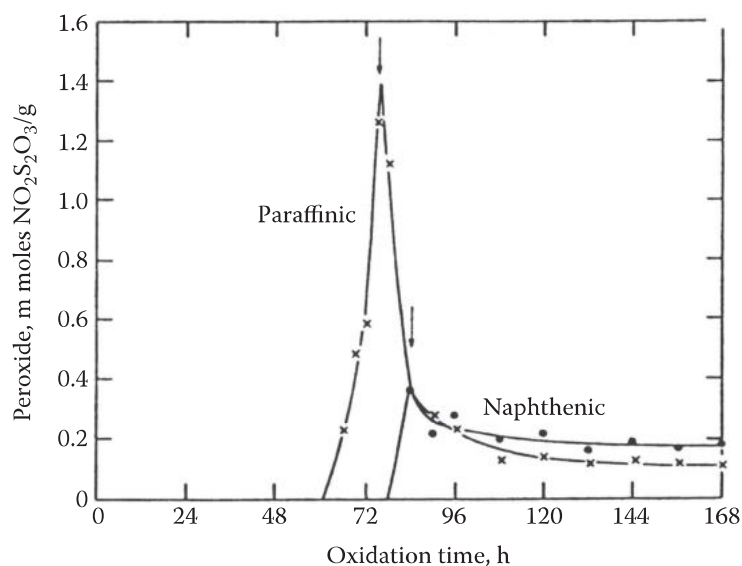
costs of maintenance, energy losses, and forced outages become excessive. Canadian utilities usually consider a normal service life somewhere between 35 and 50 years. The difference may be related to the operating conditions of the equipment. In Europe, transformers are operated closer to their maximum rating when compared to Canadian practice.

12.7 Considerations for Operating and Maintenance

Operating and maintenance of oil–paper-insulated transformers consist essentially of attempting to keep the insulation in conditions as close as possible to those prevailing at its commissioning and to detect or prevent the development of PDs and incipient faults. Detailed procedures are generally developed by utilities from recommendations of manufacturers and their own operating experience. We are presenting in the following a few aspects that may need particular consideration.
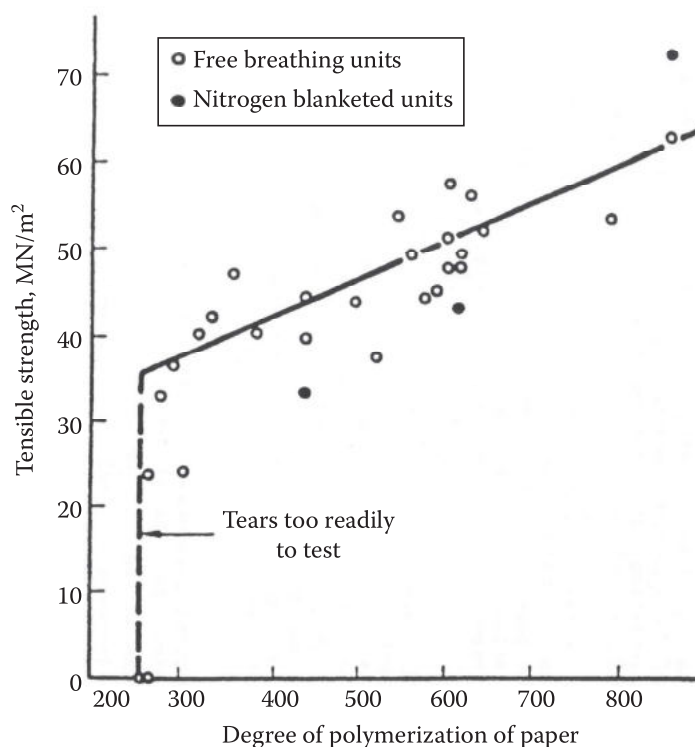
FIGURE 12.54 Variations of withstand to traction of Kraft paper as a function of the *DP* of the paper. (From Shroff, D.H. and Stannett, A.W., *IEE Proc.*, 132(Part C, 6), 312, November 1985.)

12.7.1 Operating

Commissioning: Large power transformers are delivered to the site, emptied of its oils, and, sometimes, with its bushings removed for transportation. Particular care must be taken to minimize the risk of disturbing the dielectric integrity of the transformer insulation by on-site works. Among these, oil filling of the transformer can be improved by continuous monitoring of oil quality and, in particular, its particle content during the filling process. After filling of the transformer, a closed loop circulation of the oil is maintained, accompanied by filtering and monitoring the particle content in order to remove the residual particle contamination in the oil.

Figure 12.55 from Palmer and Sharpley (1969) shows the improvement in particle contamination obtained by such a procedure for oil filling of a transformer. Notice the marked increase in the particle content following oil filling, associated with the detachment of particles from the insulation, which is gradually filtered out during the 168 h of continuous filtering.

Cumulative aging: The well-defined mechanism of thermal aging in oil–paper insulation allows the establishment of the loading conditions for power transformers, based on the evaluation of life loss in tensile strength of the paper. Detailed recommendations for loading of power transformers are given in national and international standards (ANSI Standard C57.92). Table 12.9 summarizes typical operating conditions for power transformers, and their life expectation under constant temperature, assuming a loss of 80% of the tensile strength of paper.

Elaborate methods for the determination of the dynamic loading condition for power transformers are given in standards (ANSI C.57-92). They are elaborated by calculating the time that a transformer can operate under a given loading condition to limit the life loss to less than 1% of its life expectation. It assumes that

- The temperature at the beginning of the overload immediately rises to the value it will eventually have at the end of the overload
- The temperature will immediately drop back to the original value at the end of the overload
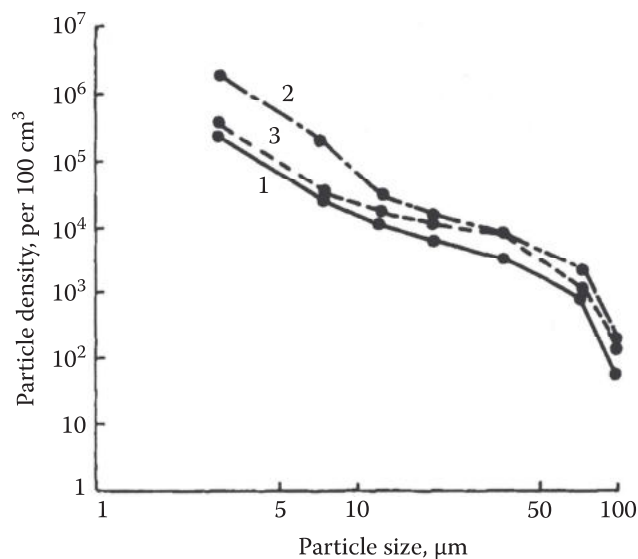
FIGURE 12.55 Variation of the particle content in transformer oil at initial oil filling: 1—before entering the transformer; 2—after filling; 3—after 168 h filtration. (From Palmer, S. and Sharpley, W.A., *Proc. IEE*, 116(12), 2029, December 1969.)

TABLE 12.9

Typical Operating Conditions and Life Expectation of Power Transformers

Parameters	Values
Average daily ambient temperature	30°C
Average winding temperature rise at full load	55
Average daily winding temperature	85
Differential between average winding and hottest spot	10
Hottest spot daily average temperature at full load	95
Maximum ambient temperature	40
Maximum hot spot temperature	105
Life expectation at constant temperature of 95°C	32,000 h
Life expectation at constant temperature of 115°C	2,900

Source: ANSI C57.92, *Guide for Loading Mineral Oil Immersed Power Transformers.*

The general procedure for determining the loss of life at any given overload is as follows:

1. From the test data on the transformer, the oil and copper-to-oil temperatures at the initial normal load and also the final temperature if the overload continues indefinitely.
2. Calculate the time constant τ from the physical data: weight of copper and oil, volume of oil, etc.
3. Calculate the actual oil rise at the end of the overload period, taking into account the time constant determined in step 2.
4. Calculate the hottest spot temperature.

The standard provides appropriate graphs and tables to determine the time that the transformer can operate under overload condition, without using up more than 1% of the life of the transformer.

Low temperature: Power transformers operate over a wide range of ambient temperatures, from −40°C to 50°C. Under conditions of very low temperatures, paraffin in the oil can form wax and disturb the operation of power transformers at start-up. In addition, the increased viscosity of the oil at low temperatures favors the development of hot spots within the insulation, which can occur under steady state and

transient loading conditions (Aubin and Langhame, 1992). At low ambient temperatures, hot spots developing under steady-state loading conditions remain below the limit temperature of 110°C. However, those developing under transient overload conditions can exceed the limit temperature after 4 h under overload.

Operating transformers and shunt reactors in extremely cold climate regions may require particular considerations (Lampe, 1985), including the following:

- Use of naphthenic oils with low viscosity to avoid formation of wax.
- Avoid start-up at low temperatures. When this is not possible, start-up can be made at reduced load, to allow the oil getting heated sufficiently before subjecting to full load conditions.
- Leave shunt reactors that must be switched on and off on the system as long as possible.
- Avoid tap changer operation below −25°C unless the tap changers are designed for low-temperature operations.

12.7.2 Maintenance

Maintenance practices comprise a set of measures adopted by the utility, in accordance with the recommended practices from national and international standards and equipment manufacturers, to ensure appropriate follow-up of the state of the insulation system in order to take a decision regarding the suitability of its continuing in service. The essential item in all maintenance practices is a logbook or computer file to keep record of all major works and changes in the recorded parameters, starting from the day the equipment is commissioned, serving as reference levels. The actual practices vary with each utility. We discuss in the following considerations regarding maintenance of power transformers.

12.7.2.1 Routine Maintenance

This consists of verifying the operating conditions of the equipment in accordance with the recommendations from the manufacturers. It corresponds generally to visual inspection and keeping record of the operating parameters: oil level, temperature, humidity, gas relays, and apparent state of insulators.

12.7.2.2 Diagnostic Maintenance

The diagnostic maintenance comprises a number of data sampling: oil sampling for gas in oil, various physical–chemical analyses, and on-site measurements on the equipment temporarily removed from service to detect changes in tan δ, winding capacitances, hipot tests, etc. Most of these tests, however, are at relatively low voltages, less than 50 kV, so that their value is more in detecting trends of variations in the parameters monitored based on adequate record keeping rather than in evaluating the current state of the insulation system.

Measurements in oil: Assessment of oil quality is the most common diagnostic used in practice, probably because oil is the most accessible component. Oil samples taken from operating transformers can be analyzed for dissolved gases, water content, DBPC content, interfacial tension, soluble acidity (neutralization number), conductivity, dissipation factor tan δ, dielectric strength, particle content, furan content, and polarization. Most of these measurements are related to the state of the oil; a few also provide information on the state of the paper and the insulation system as a whole.

Measurements of the *DBPC* content, the interfacial tension, and the neutralization number can provide information on the degree of oil oxidation (Yoshida et al., 1987). The dielectric degradation of the oil can be evaluated by measuring the conductivity, the dissipation factor, and the dielectric strength of oil samples.

Humidity: In a sealed insulation system, the ingress of humidity is well controlled, and any increase in the humidity level would require investigation regarding the source of humidity ingress. In a free-breathing insulation system having contact with the ambient air in the conservator, humidity is removed from the ambient air by silica gel, which needs to be regularly changed to keep its efficiency. The ingression of humidity in the oil–paper insulation is followed by a redistribution of water content between the

insulation components and, often, leads to a higher concentration of humidity in the paper than in the oil, which complicates the drying process.

Particles: Regular control of particle content in oil allows detecting anomalies within the insulation, which generate particle contamination. Particle contamination can be measured and the nature of the particles determined. Carbon particles are indicative of PD activities or the presence of hot spots. Efficiency of the control depends on the sampling point and good record-keeping procedure.

Gas-in-oil analysis: It is the most common method used to evaluate the insulation aging state. It provides information on the oil degradation from the presence of specific by-products, methane (CH_4), acetylene (C_2H_2), ethylene (C_2H_4), etc. (IEC Standard 60599, 1978; IEEE Standard C57.104-1991), and, to some extent, on the paper degradation in relation to the concentrations of CO, CO_2, and *furan or furfuraldehyde*. Although the decomposition by-products are common to these high-energy processes, the rate amounts of the by-products formed are specific to the individual process. This property of decomposition by-products provides a convenient means to detect, identify, and, to a certain degree, assess the severity of the aging process (Duval and De Pablo, 2001; Duval, 2002) and is included in the IEC standard for analysis of dissolved gas in transformer oil. It suffices to evaluate the relative gas ratios defined according to

$$\%CH_4 = \frac{\%CH_4}{\%CH_4 + \%C_2H_2 + \%C_2H_4} \quad (\text{Methane})$$

$$\%C_2H_4 = \frac{\%C_2H_4}{\%CH_4 + \%C_2H_2 + \%C_2H_4} \quad (\text{Ethylene})$$

and

$$\%C_2H_2 = \frac{\%C_2H_2}{\%CH_4 + \%C_2H_2 + \%C_2H_4} \quad (\text{Acetylene})$$

The results are reported on a triangular chart shown in Figure 12.56 to identify the nature of the fault and its relative severity. Examples of diagnostics obtained with dissolved gases are illustrated in Figure 12.57.

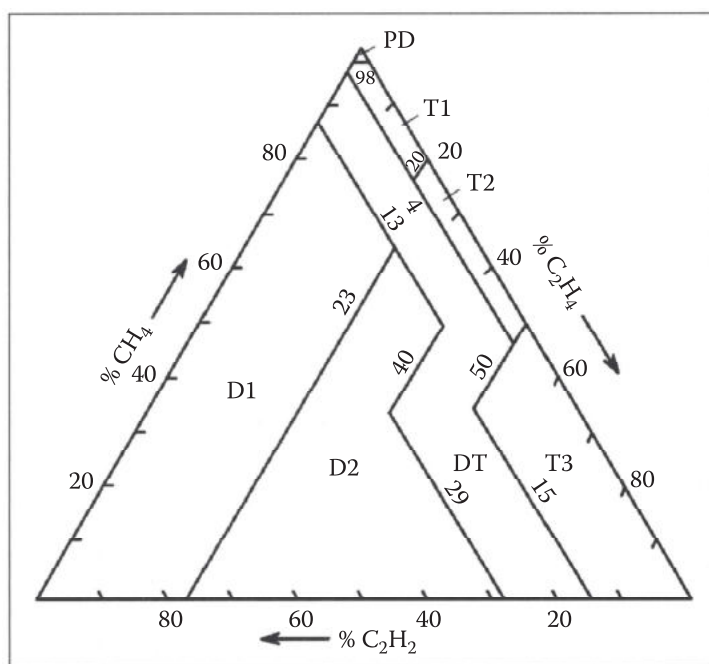**FIGURE 12.56** Triangular chart for diagnostics of incipient faults in power transformers: T—thermal faults, D—discharges, and DT—mixtures of thermal and electrical failures. (From Duval, M., *IEEE Electr. Insul. Mag.*, 18(3), 8, May/June 2002.)
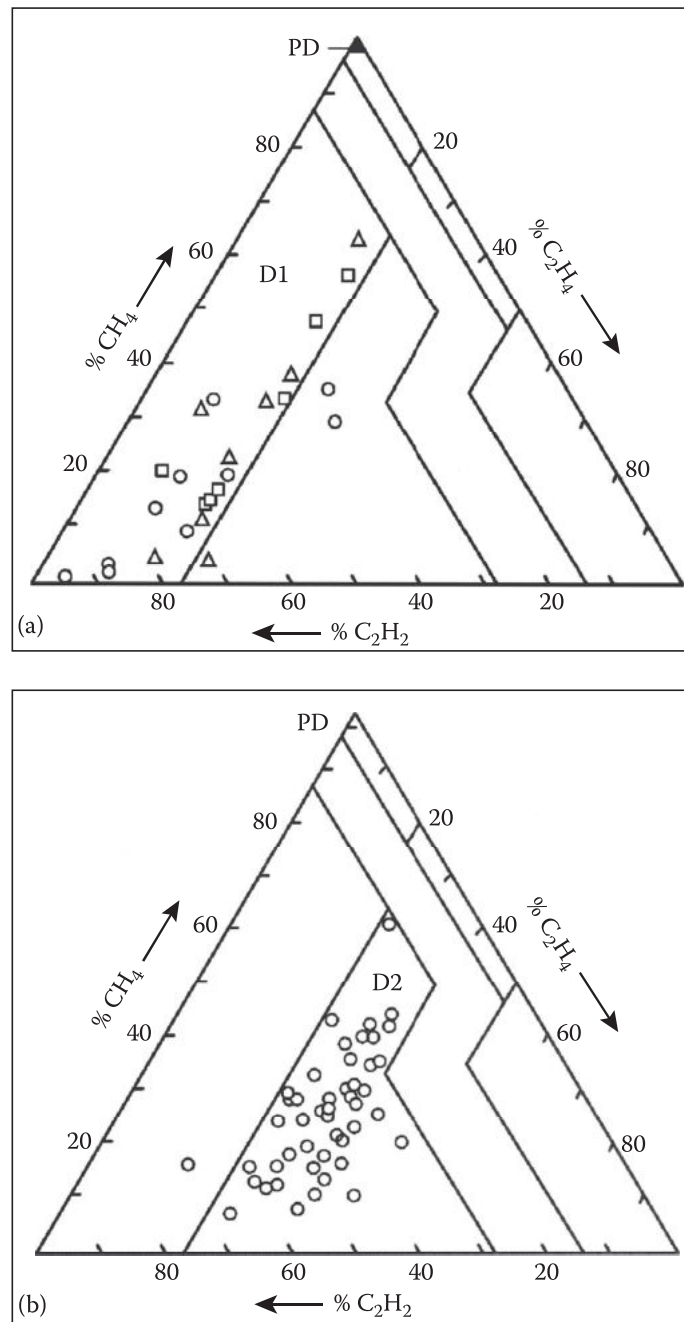
FIGURE 12.57 Examples of a dissolved gas analysis for diagnostics of incipient faults in power transformers. (a) Discharges of low energy - zone D_1. (b) Discharges of high energy - zone D_2. (From Duval, M., *IEEE Electr. Insul. Mag.*, 18(3), 8, May/June 2002.)

Additional diagnostics, comprising the measurement of moisture, particle content, and dielectric strength of the oil, are generally made to complete the analysis of the actual state of insulating oil.

The relative amounts of the dissolved gases generated can help identify the aging processes involved, thermal degradation, PDs, or arcing (Fallou, 1970; Duval, 1974). Variations of the gas content with time can be indicative of progression of the aging process. Finally, environmental aging can be estimated from water, air, nitrogen, and oxygen contents. It should be noted, however, that the interpretation of the results must take account of whether the oil–paper insulated is hermetically sealed or in constant contact with ambient air (Kant and Miyamoto, 1995; Duval and de Pablo, 2001).

Assessment of the paper: Assessment of the aging state of paper, when accessible, can be made by direct measurement of the *DP* and the mechanical strength: tensile, tear, burst, or double-fold. The latter parameters can all be correlated to *DP* and provide useful data on the aging state of the paper. Moisture

content in the paper is known to enhance its aging. Its measurement in transformer insulation has been difficult, although significant development is being achieved in this field.

12.7.2.3 Monitoring

A number of parameters have been identified and used to continuously monitor transformer insulation. Hydrogen generation is currently monitored, while potential for a multigas monitoring system exists; its use on operating transformer has not been widespread. Temperature and hot spot monitoring has been investigated by the Canadian Electrical Association (CEA), and a thermal life integrator has been developed but their use in power transformers has been limited, partly due to the reliability problem of the fiber optic system installed for temperature monitoring. PD detection, by both electrical and acoustic signals, has been explored.

12.7.2.4 On-Site Evaluation

Nondestructive on-site tests are not always possible, mainly because of the necessity to temporarily remove an important piece of equipment from the power system and the needs for special test equipment, which can be brought on-site. However, they can be planned ahead, taking advantage of scheduled revision work or subsequent repair or major overhaul work on the equipment. Different nondestructive tests can be made on-site: PD and power loss measurements, evaluation of the impedance transfer function, etc., which provide an insight to the insulation state of the equipment.

Measurements of PD and power loss: Nondestructive evaluation of the state of the oil–paper insulation system (equipment) can be done by measuring the PD level and dissipation factor tan δ. *PD* measurements are sensitive to local discharge activity, an early indication of local deterioration, and are part of the quality control of power transformers during acceptance tests. Monitoring or repeating the *PD* measurements at regular intervals may allow early detection of incipient faults prior to failure of the equipment. Location of the discharge site is also possible. The difficulty with this approach is the rapid transition of incipient faults to failure, leaving little time for advance notice of the runaway situation. Measurement of the dissipation factor tan δ can be a good indication of the aging condition, but its correlation with the paper degradation and oil oxidation has not been reliable due to the sensitivity of tan δ to other parameters, such as excessive moisture and contamination of the oil.

REFERENCES

ANSI C57.92. *Guide for Loading Mineral Oil Immersed Power Transformers*, 1981.

Aubin, J. and Y. Langhame. Effect of oil viscosity on transformer loading capability in low ambient temperatures. *IEEE Transactions on Power Delivery* PWRD-7(2): 516, 1992.

Bartnikas, R. and K.D. Srivastava. *Elements of Cable Engineering*. Waterloo, Ontario, Canada: Stanford Educational Press, June 1980.

Bean, R.L., Chackan Jr, N., Moore, H.R., and E.C. Wentz. *Transformers for the Electric Power Industry*. New York: McGraw-Hill Book Co., 1959.

Boisdon, C., Carballeira, M., Guinic, PH., and J. Pottevin. On-site conditioning of power transformers—Its control and impact on the dielectric withstand. CIGRE, Report No. 12-101, Paris, France, August 1994.

Bouvier, B. Papier et papier imprégné, *Techniques de l'ingénieur* D-280 : 1–26, 1977.

Burton, P.J., Graham, J., Hall, A.C., Laver, J.A., and A.J. Olivier. Développements récents au CEGB pour l'amélioration de la prévision et de la surveillance des performances des transformateurs. CIGRE, Report No. 12-09, Paris, France, 1984.

Campbell, M. Factory testing of thermally aged HVDC converter transformers. Montréal, Québec, Canada: Canadian Electrical Association, Report No. ST-270, December 1991.

Crine, J.P. and C. Vincent. Influence of ultrasonic homogenization on particle counts and dielectric strength measurements of transformer oil. *IEEE Transactions on Electrical Insulation* EI-23(4): 751–755, August 1988.

Dakin, T.W. Electrical insulation deterioration treated as a chemical rate phenomena. *AIEE Transactions* 67(Part I): 113–122, 1948.

Duval, M. Fault gases formed in oil-filled breathing EHV power transformers—The interpretation of gas analysis data. IEEE Paper No. C 74 476-8, 1974; In: *IEEE Summer Meeting*, Anaheim, CA, July 14–19, 1974.

Duval, M. A review of faults detectable by gas-in-oil analysis in transformers. *IEEE Electrical Insulation Magazine* 18(3): 8–17, May/June 2002.

Duval, M. and A. de Pablo. Interpretation of gas-in-oil analysis using new IEC publication 60599 and IEC TC 10 databases. *IEEE Electrical Insulation Magazine* 17(2): 31–41, March/April 2001.

Fabre, J. and A. Pichon. Deterioration process and products of paper in oil, application to transformers. CIGRE, Report No. 137, Paris, France, 1960.

Fallou, B. Synthèse des travaux effectués au LCIE sur le complexe papier-huile. *Revue Générale d'Électricité* 79(8): 645–661, September 1970.

Fournié, R. *Les isolants en électrotechnique—Essais, Mécanismes de dégradation, Application industrielles.* Paris, France: Edition Eyrolles, 1990.

Freyhult, T. and A. Carlson. Improved reliability of 800 kV transformers. In: *CIGRE Symposium*, Montréal, Québec, Canada, 1991.

Grimmer, E.J. and W.L. Teague. An improved core form transformer winding. *AIEE Transactions* 70: 962, 1951.

IEC Standard 60060-2. *High Voltage Testing Techniques, Part 2: Measuring Systems*, 2nd edn. Geneva, Switzerland: IEC, 1994.

IEC Standard 60071-1. Insulation Coordination, Part 1: Definitions, Principle and Rules. Geneva, Switzerland: IEC, 1993.

IEC Standard 60076-3. *Power Transformer, Part 3: Insulation Levels and Dielectric Tests*. Geneva, Switzerland: IEC, 1994.

IEC Standard 60599. *Interpretation of the Analysis of Gases in Transformers and Other Oil-filled Electrical Equipment in Service*, 1978.

IEEE Transformer Committee. *IEEE Guide for Transformer Loading*, IEEE Transformer Committee.

IEEE Standard C57.104. *IEEE Guide for the Detection and Determination of Generated Gases in Oil-Immersed Transformers and their Relation to the Serviceability of the Equipment*. IEEE Transformer Committee, 1991.

Kan, H. and T. Miyamoto. Proposals for an improvement in transformer diagnosis using dissolved gas analysis (DGA). *IEEE Electrical Insulation Magazine* 11(6): 15–26, November/December 1995.

Kao, K.C. and J.P. McMath. Time-dependent pressure effect in liquid dielectrics. *IEEE Transactions on Electrical Insulation* EI-5(3): 64–68, September 1970.

Kiersztyn, S.E. Formal theoretical foundation of electrical aging of dielectrics. *IEEE Transactions on Power Apparatus and Systems* PAS-100(11): 4333–4338, November 1981.

Lamarre, C., Crine, J.P., and M. Duval. Influence of oxidation on the electrical properties of inhibited naphthenic and paraffinic transformer oils. *IEEE Transactions on Electrical Insulation* EI-22(1): 57–62, February 1987a.

Lamarre, C., Crine, J.P., and H. St-Onge. Antioxidant functionality in liquid and solid materials. In: *CIGRE Symposium*, Report No. 900-05, Vienna, Austria, May 1987b.

Lamarre, C., Duval, M., and J.P. Crine. Optimum reclamation time for insulating oils. In: *55th Annual DOBLE Conference*, April 11–15, 1988, pp. 10-6.1/10-6.15.

Lampe, W. power transformers and shunt reactors for arctic regions. IEEE Transactions, Paper 85-SM 374-4, Vancouver, British Columbia, Canada, 1985.

Malewski, R. Digital techniques in high voltage measurements. *IEEE Trans.* PAS-101: 4508–4517, December 1982.

Malewski, R. and B. Poulin. Impulse testing of power transformers using the transfer function method. *IEEE Transactions on Power Delivery* PWRD-3(2): 476–489, 1988.

Miners, K. Particles and Moisture Effect on Dielectric Strength of Transformer Oil using VDE electrodes. *IEEE Trans.* PAS-101: 751–756, March 1982.

Montsinger, V.M. Loading transformers by temperature. *AIEE Transactions* 49: 776–792, 1930.

Mori, S. Development of gas-insulated transformer in Japan. In: *IERE Workshop on Gas-Insulated Substations*, Toronto, Ontario, Canada, October 1990, pp. 8–20.

Moser, H.P. *Transformerboard*. Rapperswil, Switzerland: Scientia Electrica, 1979.

Mukaiyama, Y., Nonaka, F., Tagaki, I., Higaki, M., Endo, K., Sakamoto, T., Hiraishi, K., and K. Kawashima. Development of a perfluorocarbon liquid immersed prototype large power transformer with compressed SF_6 gas insulation. *IEEE Transactions on Power Delivery* PWRD-6(3): 1108–1116, 1991.

Murray, D.W., McDonald, J.M., White, A.M., and P.G. Wright. The Effect of Basestock Composition on Lubricant Oxidation Performance. Petroleum Review, Paper IP 82-002, pp. 36–40, February 1982.

Narbut, P., Maslin, A.J., and C. Wasserman. Vaporization cooling for power transformer. *AIEE Transactions on Power Apparatus and Systems, Part III B*, 1319–1327, December 1959.

Nelson, J.K. An assessment of the physical basis for the application of design criteria for dielectric structures. *IEEE Transactions on Electrical Insulation* EI-24: 835–847, October 1989.

Nelson, W. Graphical analysis of accelerated life test data with the inverse power law model. *IEEE Trans.*, EI-21(1): 2–11, February 1972.

NEMA Standard Publication TR-1. Transformers, regulators and reactors. National Electrical Manufacturer Association, 1973.

Norris, E.T. High voltage power transformer insulation. *Proceedings of IEE* 110(2): 428, February 1963.

Okubo, H., Okamura, K., Ikeda, M., and S. Yanabu. Creepage flashover characteristics of oil-pressboard interfaces and their scale effects. *IEEE Transactions on Power Delivery* PWRD-2(1): 126–132, January 1987.

Oommen, T.V., Moore, H.R., and L.E. Luke. Experience with gas-in-oil analysis made during factory tests on large power transformers. *IEEE Transactions on Power Apparatus and System* PAS-101: 1048–1052, May 1982.

Palmer, S. and W.A. Sharpley. Electric strength of transformer insulation. *Proceedings of IEE* 116(12): 2029, December 1969.

Rouse, T.O. Technical requirements dielectric liquids. In: *Proceedings of the Workshop on Substitute Insulation for Polychlorinated Biphenyls*, EPRI, Palo Alto, CA, April 1987.

Samat, J. and Lacasse, D. Micro-particules dans l'huile de transformateur: conséquence sur la tenue diélectrique. *Revue Alsthom*, (11): 47–58, 1988.

Shroff, D.H. and Stannett, A.W. A review of paper aging in power transformers. *IEE Proceedings* 132(Part C, 6): 312–319, November 1985.

Singer, H., Steinbigler, H., and Weiss, P. A charge simulation method for the calculation of high voltage fields. *IEEE Transactions on Power Apparatus and System* PAS-93: 1660–1668, September/October 1974.

Tokoro, K., Harumoto, Y., Kabayama, Y., Yamauchi, A., Sato, T., and T. Ina. Development of 72 kV 40 MVA gas-vapor cooled transformer. *IEEE Transactions on Power Apparatus and System* PAS-101(11): 4341–4349, November 1982.

Train, D. Switching surge test circuits for high voltage shunt reactors and power transformers. *IEEE Transactions on Power Apparatus and System* PAS-100(6): 3125, 1981.

Trinh, N.G. Electrode design for testing in uniform field gaps. *IEEE Transactions on Power Apparatus and System* PAS-99(3): 1235–1242, May/June 1980.

Trinh, N.G., Olivier, R., Vincent, C., and J. Régis. Effect of impurity particles on transformer oil under normal operating conditions. *IEEE International Symposium on Electrical Insulation*, Boston, pp. 225–228, June 1980.

Trinh, N.G., Aubin, J., and L. Bolduc. Evaluation of the dielectric and short-circuit capabilities of naturally aged power transformers. *IEEE Transactions on Power Apparatus and System* PAS-103(1): 109–120, January 1984.

Trinh, N.G. and Y. Ménard. Audible noise generated by power transformers of a substation—Its influence on the urban noise. Paper A76 473-9, presented at the *IEEE PES Summer Meeting*, Portland, OR, 1976.

Trinh, N.G., Vincent, C., and J. Régis. Electrode area, stressed-volume: Two apparent effects of large-volume oil-insulation. In: *IEEE International Symposium on Electrical Insulation*, Philadelphia, PA, June 6–9, 1982a, pp. 115–118.

Trinh, N.G., Vincent, C., and J. Régis. Statistical dielectric degradation of large-volume oil–insulation. *IEEE Transactions on Power Apparatus and System* PAS-101(10): 3712–3721, October 1982b.

Weber, K.H. and H.S. Endicott. Area effect and its extreme basis for the electric breakdown of transformer oil. *AIEE Transactions* 75: 371–381, June 1956.

Wilson, A.C.M. *Insulating Liquids: Their Use, Manufacture and Properties*. IEE Electrical and Electronic Materials and Devices Series 1. Stevenage, England: Peter Peregrinus Ltd, 1980.

Wilson, W.R. A fundamental factor controlling the unit dielectric strength of oil. *AIEE Transactions* 72(Part III): 68–73, February 1953.

Yoshida, H., Ishioka, Y., Yanari, T., Teranishi, T., and T. Suzuki. Degradation of insulating materials of transformers. *IEEE Transactions on Electrical Insulation* EI-22(6): 795–800, December 1987.